



Institutionen för vattenbyggnad
Chalmers Tekniska Högskola

Department of Hydraulics
Chalmers University of Technology

Physics of Ice and Snow as Affects Thermal Pressure

Lars Bergdahl

Report
Series A:1
ISSN 0348-1050

Göteborg 1977

Address:	Institutionen för vattenbyggnad Chalmers Tekniska Högskola Fack S-402 20 Göteborg 5, Sweden
Telephone:	031/81 01 00

PREFACE

In connection with my work on thermal ice pressure I dealt, by necessity, with ice physics, which proved to be a fascinating field of science. Since my aim was to calculate ice pressure, rather than to study the properties of ice, I tried to maintain a practical attitude to what I learnt, but being a physicist at heart I could not help being engaged in the subject. As a civil engineer, however, I hope that my efforts have brought out something new to the profession.

This is not a book on the physics of ice in general but on those physical properties of ice that affect the development and magnitude of thermal ice pressure. For the purpose of calculating those pressures, all relevant properties had to be quantified whether or not reliable theories or experimental results existed.

The resulting mixture of knowledge and hypothesis makes this partly a book on what should be known rather than on what is known. I hope that this concept will make the book valuable to other engineers dealing with ice and that it may demonstrate to physicists which questions that are of most practical interest.

Of course, there are more engaging books on the subject as for example Pounder: "The Physics of Ice" (1965) which is recommended for reading pleasure and its brilliancy. The most extensive book on ice physics is probably Hobbs: "Ice Physics" (1974) containing nearly 800 informative pages.

I am most grateful to my late tutor, Professor Lennart Rahm, who originally awakened my interest in ice engineering. I also wish to thank my colleagues in the Division of Hydraulics for all their efforts to support my work, and, especially Mrs Göta Bengtsson who typed the manuscript and Mrs Alicja Janiszewska who drew all the figures.

December 1977

Lars Bergdahl

LIST OF CONTENTS

page

	SUMMARY	
	PREFACE	
1	INTRODUCTION	1
1.1	Thermal Ice pressure	1
1.2	Partaking Physical Processes	4
2	STRUCTURE OF ICE	7
2.1	Substance of Water	7
2.2	Crystal Structure of Ice	9
2.3	Ice Terminology	14
2.4	Fresh-Water Ice	15
2.41	Formation of Columnar Ice	16
2.42	Crystal-Axis Orientation	17
2.43	Frazil and Frazil Ice	21
2.44	Snow and Snow Ice	22
2.45	Lake and River Ice Covers	24
2.5	Saline Ice	27
2.51	Sea Water and Ice at Sea	28
2.52	Formation of Columnar Sea Ice	30
2.53	Phase Relations of Columnar Sea Ice	33
2.54	A Structural Model of Columnar Sea Ice	39
2.55	Saline Snow Ice	40
3	DENSITY	41
3.1	Compact Density of Pure Ice	41
3.11	Density of Natural and Artificial Ice	43
3.2	Density of Snow	44
3.3	Density of Sea Ice	46
3.31	Sea-Ice Density Calculated from Phase Relations	46
3.32	Density of Natural Sea Ice	49
3.4	Thermal Expansion of Ice	51
4	THERMAL CONDUCTIVITY	52
4.1	Thermal Conductivity of Fresh-Water Ice	52
4.2	Thermal Conductivity of Columnar Sea Ice	55
4.3	Thermal Conductivity of Snow	58

5	SPECIFIC AND LATENT HEATS	63
5.1	Specific and Latent Heats of Water	63
5.2	Heat Capacity of Fresh-Water Ice	63
5.3	Heat Capacity of Sea Ice	64
5.4	Heat Capacity of Snow and Porous Ice	68
6	TEMPERATURE DIFFUSIVITY	69
6.1	Temperature Diffusivity of Fresh-Water Ice	69
6.2	Temperature Diffusivity of Columnar Sea Ice	71
6.3	Temperature Diffusivity of Snow	73
7	OPTICAL PROPERTIES	77
7.1	Radiation from Black Bodies	77
7.11	Solar Radiation	79
7.12	Emissivity	80
7.2	Refraction	80
7.21	The Optic Axis	81
7.22	Refractive Indices	82
7.23	Polarization Effects	82
7.3	Reflection	83
7.31	Reflection Coefficients of Ice and Snow	84
7.4	Absorption of Solar Radiation	88
7.41	Absorptivity of Ice	90
7.42	Absorptivity of Snow	91
7.43	Generalized Values on the Extinction Coefficient	92
8	ENERGY BALANCE OF AN ICE OR SNOW COVER	94
8.1	Radiation Balance	95
8.2	Heat Transfer	97
8.3	Examples on the Energy Balance	98
9	MECHANICAL PROPERTIES	100
9.1	Structural Considerations	100
9.2	The Role of Temperature	101
9.3	Deformation of Ice	102
9.31	Linear Rheological Models	103
9.32	A Nonlinear Rheological Model	105
9.4	Rheology of Fresh-Water Ice	106
9.41	Elasticity	106
9.42	The Poisson Modulus	108

9.43	Creep	109
9.44	Creep of Single Crystals	111
9.45	Creep of Polycrystalline Ice	114
9.46	Activation Energies for Creep and Self-Diffusion	117
9.47	Elastic Lag	118
9.48	Relaxation Times	120
9.5	Strength of Ice	122
9.51	Crack Initiation and Propagation	122
9.52	Tensile Strength	123
9.53	Compressive Strength	124
9.54	Design Strength	125
9.6	The Scale Effect	126
9.7	Mechanics of Columnar Sea Ice	127
9.71	Strength	128
9.72	Elasticity	131
9.73	Creep	137
9.74	A Rheological Model of Sea Ice	138
	LIST OF TABLES	140
	LIST OF FIGURES	141
	LIST OF NOTATIONS	145
	LIST OF REFERENCES	152

1. INTRODUCTION

This study deals with those physical properties of ice that should be taken into account when calculating thermal ice pressure. In order to give a picture of to which extent the physics of ice is involved in such calculations, a description of the phenomenon is given below, followed by a survey of the different physical processes taking part.

1.1 Thermal Ice Pressure

A very thin sheet of ice has a temperature close to 0°C . When such a sheet grows in thickness, the temperature of its surface decreases due to the low air temperature. The upper layers of the ice contract, but since the temperature at the lower boundary still is 0°C , the contraction causes tensile tension, creep, and cracks in the ice. The growth rate of the ice cover is mostly rather slow, so that, with the exception of the first few centimetres, the ice has time to creep without the formation of tensile cracks, that is, if the ice increases in thickness at a constant temperature of its upper surface.

If, however, at a time when the ice cover already has been formed and has increased in thickness at constant weather conditions, the air temperature suddenly falls considerably, the upper surface of the ice quickly assumes a new temperature of equilibrium, and after some time a new steady state gradient will be established in the ice cover. The upper surface will contract fast, but the lower boundary will keep its length since it is at the constant freezing-point temperature.

Now, the ice is floating on a horizontal water surface, and thus the free bending of the ice cover is restricted. Instead, the effect will be a bending moment in the ice cover, and the stresses will mostly be released in forming deep cracks, see Figure 1.1. If the change of temperature is very slow the ice may deform viscously without the formation of cracks.

2.

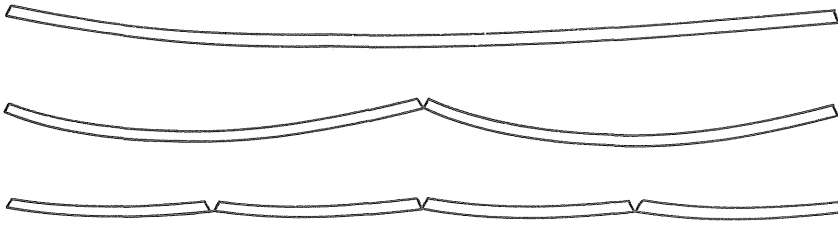


Figure 1.1 The bending and cracking of a floating ice cover due to a fast change of temperature in its upper surface.

The formation of the cracks is often sudden and is followed by a strong wave motion, which is felt if you are standing on the ice. You can also hear the cracks propagating across the ice cover, and it is clearly visible how they are spaced out at intervals of 10 to 20 m. Between these wide parallel cracks, there is a system of thin surface cracks. The cracks will sooner or later be filled by water and drifting snow. Also cracks not extending all through the ice cover will partly be filled by snow and rime. The snow will be packed and recrystallized and the water will freeze in the slots. The freezing will sometimes cause pressure in the ice cover because of the increase of volume from water to ice. This pressure is, however, smaller than the extreme thermal pressures.

Later, if the ice cover is warmed due to mild weather, or water finding its way on to the ice, the upper layers will expand again. Depending on the steepness of the shores, the thickness of the ice and the rate of change of temperature, pressure will develop in the ice, and may be followed by a shove up onto a beach, or folding of the ice cover against banks and in zones of weakness, see Figure 1.2.

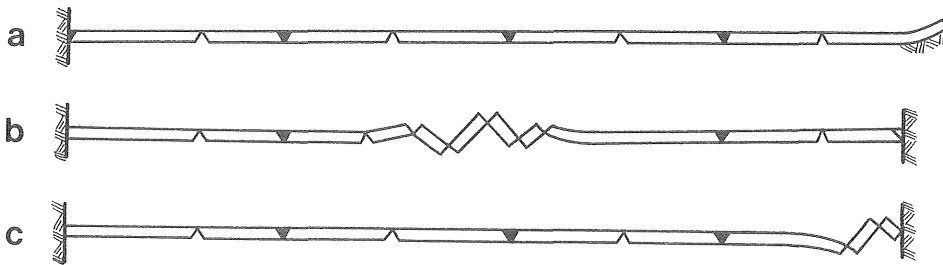


Figure 1.2 Examples of expanding ice covers

- a) shoving up onto a beach
- b) folding out on a lake
- c) folding at a shore.

The magnitude of the ice pressure in the ice cover depends on the rate of change of temperature in the ice, the coefficient of thermal expansion, the rheology of ice, the extent to which the cracks have been filled, the thickness of the ice cover, and the degree of restriction from the shores.

Of course, the rate of change of temperature in an ice cover depends on the change of weather conditions such as wind speed, air temperature, solar radiation, and the depth of the snow cover.

Expected magnitudes of ice pressures due to thermal expansion at a certain lake is thus obviously a function not only of ice and snow properties but also of the local climate, ice conditions and lake configuration.

This study deals with those physical and mechanical properties of ice that should be considered when calculating thermal ice pressures in fresh or saline ice. Techniques to calculate pressures are taken up in another study, "Thermal Ice Pressure in Lake Ice Covers" (Bergdahl 1978) which demonstrates how this is done for defined ambient conditions. Calculated values for five lakes in Sweden between the latitudes $57^{\circ}18'N$ and $68^{\circ}19'N$ are presented in a third study, "Calculated and Expected Thermal Ice Pressures in Five Swedish Lakes" (Bergdahl and Wernersson 1977).

4.

1.2 Partaking Physical Processes

A survey of the different processes considered when calculating ice pressures due to the thermal expansion of an ice cover is given below.

Thermal diffusion

Internal

The equation of thermal diffusion can be used to describe the rate of change of temperature within the ice if appropriate boundary conditions are given.

$$\frac{\partial \theta}{\partial t} = a \frac{\partial^2 \theta}{\partial x^2} + \frac{p(x, t)}{C_p \rho} \quad \dots (1.1)$$

where

- t = time coordinate
- x = vertical coordinate
- θ = temperature at (x, t)
- a = coefficient of thermal diffusion
- C_p = specific heat capacity
- ρ = bulk density
- p = effect source per unit volume at (x, t).

$$a = \lambda / C_p \rho \quad \dots (1.2)$$

where λ = specific heat conductivity

External

Heat is convected away at the upper surface by the air, which can be written

$$q = -A \Delta \theta \quad \dots (1.3)$$

where q = heat flow per unit area

A = coefficient of heat transfer

$\Delta \theta$ = temperature difference between the air and the ice surface

Radiation at the surface and the absorption of short-wave radiation within the ice will add to the external energy exchange. The long-wave radiation absorbed at the surface can simply be included by adding the absorbed radiation to equation (1.3), whereas the short-wave energy flow must be included in equation (1.1) by for example,

$$p = k J \quad \dots (1.4)$$

where p = effect source per unit volume
 k = absorption coefficient
 J = is the intensity of short-wave radiation

A snow cover on the ice will change the external energy flow because of its low thermal conductivity and because of the change in radiation balance and its reflexion of short-wave radiation. Sometimes its weight will cause the ice-cover to sink below the water table, that is, the cover will be flooded with water.

Thermal expansion

Thermal expansion of ice is usually written

$$d\varepsilon = \alpha \cdot d\theta \quad \dots (1.5)$$

where $d\varepsilon$ = expansion per unit length caused by $d\theta$
 α = linear coefficient of thermal expansion
 $d\theta$ = temperature change

Sometimes it is more convenient to use the density as a function of temperature, especially for saline ice where the expansion coefficient is a discontinuous function because of the crystallization of salts, while the density is a continuous function.

Rheology

The mechanics of ice is very complicated and there are several ways of constructing mathematical models for the deformation. For each model the coefficients or moduli must then be evaluated from literature or experiments by curve fitting. A possible four-parameter model is for example,

6.

$$\dot{\epsilon} = \frac{1}{E} \dot{\sigma} + K D (\sigma/E)^n \quad \dots (1.6)$$

where $\dot{\epsilon}$ = rate of deformation, $d\epsilon / dt$

$\dot{\sigma}$ = stress rate, $d\sigma / dt$

E = modulus of elasticity

K, n = coefficients for viscous deformation

D = self diffusion coefficient for the molecules in ice

Nearly all parameters above are functions of ice type and temperature. The absorption coefficient and radiation balance are functions of wave-length too. The coefficient of heat transfer is a function of wind-speed and humidity.

2. STRUCTURE OF ICE

One of the keys to the proper understanding of many ice problems is the crystallography of ice. Its rheology, the scatter in strength, values, the structure of sea ice and the shape of snowflakes can, for example hardly be explained without some insight into the molecular structure of the substance of water. Most of the information in this chapter is taken from Pounder (1965), Hobbs (1974) and Lavrov (1969).

2.1 Substance of Water

As water is one of the most abundant substances on the surface of the earth it has always fascinated men. Although it has a simple chemical formula it has proved to behave anomalous in many ways. It has for example extremely high specific heat capacity and specific latent heat of fusion, its permittivity is abnormally high, and it shows an increase in density when the temperature rises from 0 to +4°C.

The chemical formula of water is mostly written H_2O although in liquid form water mostly appears as groups of molecules, polymers, and thus could be described better by $(H_2O)_n$ where n is of the order of ten. In the vapour state water exists as a monomer $(H_2O)_1$ though many dimers $(H_2O)_2$ still do exist. Natural ice, on the other hand, is crystalline, that is, the molecules are ordered in a regular space lattice.

In the modern theory of valence the water molecule is viewed as consisting of three nuclei surrounded by ten electrons (Hobbs 1974). Two of these electrons circle in the 1s shell around the oxygen nucleus, and the remaining eight electrons are in pairs occupying four orbitals with mixed s and p characteristics. Two of the orbitals are the bonding orbitals directed towards the hydrogen nuclei, the other two orbitals are called the lone-pair orbitals and point in the opposite direction. The four orbitals form a roughly tetrahedral system as is sketched in Figure 2.1.

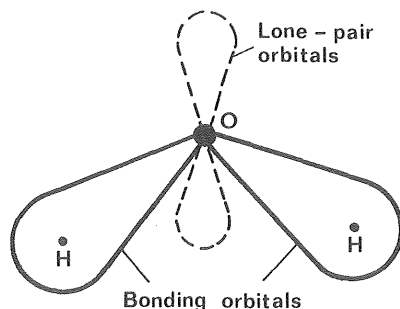


Figure 2.1 Schematic representation of the bonding and lone-pair orbitals in the water molecule. O-oxygen, H-hydrogen atom. The bonding and lone-pair orbitals form a roughly tetrahedral system (Hobbs 1974).

From information in the infrared spectrum of water vapour it has been possible to estimate the bond angle to 104.523° . Using molecular orbital theory all three angles have been estimated: the bond angle to 105° , the angle between the lone-pair orbitals to 120.2° , and the angle between a bond and a lone pair to 107.8° . In a perfect tetrahedral configuration all the angles would be 109.467° .

A consequence of the water molecule not being linear is that it has a negative and a positive side giving it a high dipole moment and permittivity. Also the positive side of one molecule easily attaches to the negative side of another. In this way pairs of molecules, figure 2.2, are formed in the vapour state. In the liquid state other molecules can link to the free ends of the molecule and chains are formed. At high temperature the chains are short but they increase in length as the temperature decreases. Such chains pack very densely and this explains the increase in density of liquid water with decreasing temperature.

At decreasing temperature some water molecules are supposed to have forked chains and eventually five or more monomers group together in a space structure with the central oxygen atom surrounded by four other oxygen atoms, figure 2.3. This last structure is ice-like and it occupies a greater volume than the chain structure. Below $+4^\circ\text{C}$ the change of volume with decreasing temperature is dominated by the formation of space molecules at the cost of chains thus decreasing the density.

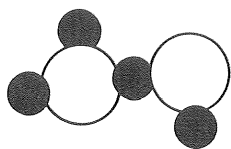


Figure 2.2 A water dimer. Large circles represent oxygen atoms and small circles hydrogen atoms.

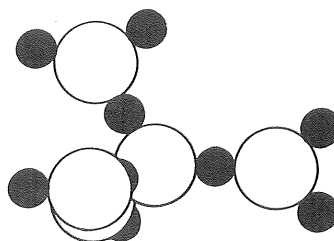


Figure 2.3 An ice-like water polymer. Large circles represent oxygen atoms and small circles hydrogen atoms.

The hydrogen bonds of the water polymers are weak, they are spontaneously broken and reformed all the time, but the mass of bonds represents a high energy and they are the main reason for the high specific heat capacity of liquid water.

The description above of the molecular structure of water is valid inside a water volume. The conditions at a phase interface are different. Here electric double layers are formed so that the outermost layer contains only water monomers. In this way the surface consists of molecular layers of arranged dipoles. This should be of importance to the formation of ice since the first crystals are formed at the surface. Two consequences of the electric double layer are the repulsion between close water droplets and their ability to remain in a supercooled state for a long time.

2.2 Crystal Structure of Ice

In ice each oxygen atom is surrounded by four equally spaced oxygen atoms forming the corners of a nearly perfect tetrahedron, see the dashed lines in figure 2.4. It will serve our purpose to believe one proton to be midway between two adjacent oxygen nuclei. In fact the proton is continuously shifting positions according to a more elaborate theory, see Hobbs (1974) or Pounder (1965), sometimes being closer to one oxygen nucleus sometimes to the other. To form the perfect tetrahedron the angles of the bonds must be 109.5° in all directions as compared to the varying angles in the vapour and liquid states. The

three lowest oxygen atoms in figure 2.4 form an equilateral triangle which makes a part of a so called basal plane.

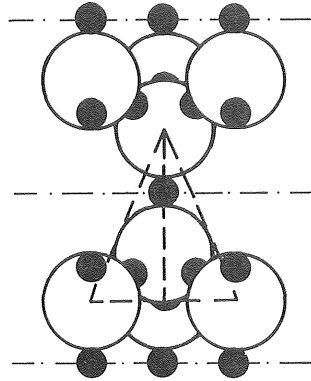


Figure 2.4 Sketch of a part of an ice lattice showing the tetrahedral bond arrangement. Large circles represent oxygen atoms and small circles hydrogen bonds. Dashed lines form a thought tetrahedron.

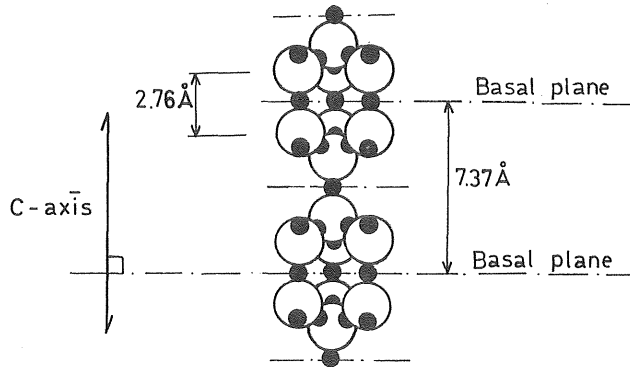


Figure 2.5 A "vertical" strip of tetrahedrons within an ice lattice. The direction perpendicular to the basal planes is called the c-axis. Large circles represent oxygen atoms and small circles hydrogen bonds.

Starting with the group of molecules forming the tetrahedron we can expand the lattice "vertically" as is shown in figure 2.5. There it can be seen that its pattern is repeated at set distances, and that the water molecules are concentrated to certain layers, the basal planes. If the length of the bonds are 2.76 \AA the distance between the basal planes is calculated to 7.37 \AA .

A composition of the tetrahedrons in a "horizontal" plane, the upper part of one of the basal planes in figure 2.5, for example, will result in the hexagonal pattern showing in figure 2.6. This hexagonal symmetry is reflected in the shape of snow flakes and ice particles. In the rime on a window pane this pattern can be observed by anybody. The first ice crystals forming at the surface of freezing water and etchings in a polished ice surface also show their hexagonal character distinctly (Hobbs 1974).

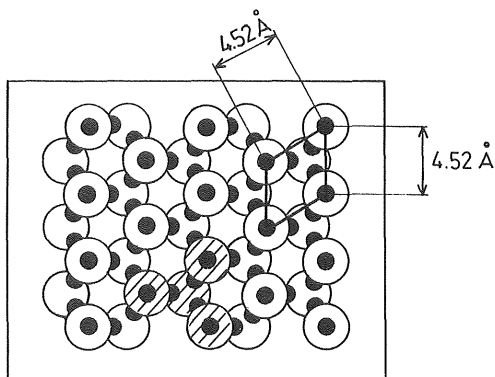


Figure 2.6 A basal plane of ice. Observe that the corners of the hexagons are not on exactly the same level. The shaded group of molecules could be the lowest group in figure 2.5. The diamond is a thought base of a unit prism. Large circles represent oxygen atoms and small circles hydrogen bonds.

The built-up ice crystal has only one axis of symmetry, the c-axis or optical axis, which is perpendicular to the basal planes. Thus ice would be expected to show anisotropy of physical properties. An example of such an anisotropy is that slippage in ice occurs most readily parallel to the basal planes. Slippage along other planes demands stresses that are a magnitude greater. According to Krausz (1968), the basal glide constitutes the main part of

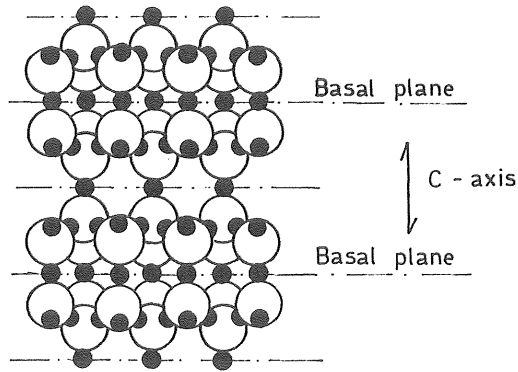


Figure 2.7 A cut along the c-axis across two basal planes in an ice lattice.

the viscous deformation of ice, see figure 2.8. The fact can be explained directly by figure 2.6 and 2.7. A plane that intersects an ice lattice between the basal planes but parallel to these cuts fewer bonds than planes in any other direction.

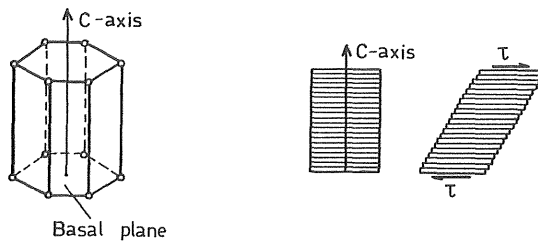


Figure 2.8 A simplified model of a hexagonal prism unit and the process of plastic deformation under shear (Krausz 1968).

A unit lattice or rather a unit prism can be formed with the diamond shown in figure 2.6 as a base and extending between two adjacent basal planes. If the length of a bond is a , the sides of the diamond are $2a \cdot \sin 60^\circ \cdot \cos 19^\circ 28'$, and the height of the prism $2a (1 + \sin 19^\circ 28')$. At the edges of the prism there are 8 molecules which are shared by four neighbouring units each and two which are

wholly within the unit. That is, four water molecules per unit the mass of which is $4 \cdot 2.992 \cdot 10^{-26}$ kg. The volume is then $8a^3 \sin^3 60^\circ \cos^2 19^\circ 28' (1 + \sin 19^\circ 28')$.

Finally the density is

$$\rho = \frac{4 \cdot 2.992 \cdot 10^{-26} \text{ kg}}{8 a^3 \sin^3 60^\circ \cos^2 19^\circ 28' (1 + \sin 19^\circ 28')} \quad \dots (2.1)$$

and if at 0°C $\rho = 916.8 \text{ kg/m}^3$ (Butkovich 1955), the bond length is calculated to 2.76 \AA ($2.76 \cdot 10^{-10} \text{ m}$) and the sides of the diamond are 4.52 \AA and the distance between the basal planes 7.37 \AA .

Distances between points in a crystal, from where the lattice pattern is identical, are sometimes referred to as Burgers vectors. In ice there are thus two Burgers vectors namely 4.52 \AA and 7.37 \AA . The notion is used within the theory of dislocations.

Other forms of solid H_2O do exist as for example a variant with a cubic lattice observed in experiments below -80°C . None of these ice forms can exist at temperatures and pressures naturally occurring on earth. They are stable only at pressures exceeding 0.2 GPa (2000 bar) and therefore they are of no practical interest. See for example Hobbs (1974) for a phase diagram of ice-water.

A crystal lattice is never perfect but contains defects of different types. They may be inclusions of suspended or dissolved impurities as for example salts or air molecules. Other defects are holes, that is, missing atoms, and dislocations, that is, basal planes suddenly interrupted or distorted. The dislocations has recently become of greater interest as they form the basis of a modern theory of deformation and strength of materials. In figure 2.9 two simple types of dislocations are sketched. Lavrov (1969) discusses the most frequent lattice defects in ice. The ice lattice is very selective and it accepts no substitutes for oxygen or hydrogen with the exception of the fluorine ion.

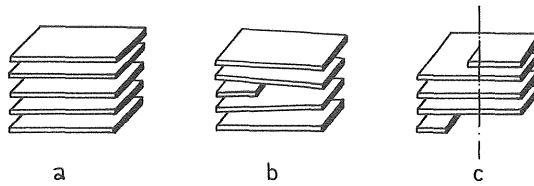


Figure 2.9 Simple types of dislocations:
 a) perfect crystal; b) edge dislocation;
 c) screw dislocation.

The above discussion of the crystal structure refers to the interior of a piece of ice. The surface is by many scientists observed to be liquid-like. Pounder (1965) says that there must exist single water molecules or groups of molecules that are linked to the ice lattice with only one hydrogen bond and thus are free to rotate. Hobbs (1974) and Lavrov (1969) on the other hand explain the liquid-like behaviour of the surface with the preservation of electric double layers even in the solid state.

2.3 Ice Terminology

The terminology used in ice engineering is very confusing. It is therefore necessary to make some definitions in order that we shall agree about the terms used in this book.

Peoples living in close contact with frozen water have many names for its different shapes as ice, frazil, snow, hail and hoar-frost (rime). It would never occur to a Swedish child to name a snowball a piece of ice. In the same way farmers and fishermen of the north make distinction between ice and frazil. In modern engineering literature ice has, however, tended to denote the solid form of water and this has sometimes resulted in confusing tautologies like ice frazil.

The three forms of solid water that we are going to deal with are ice, snow and frazil. By the single term ice is then meant a hard dense matter like, for example, the ice formed on the surface of still fresh water. By frazil is meant small ice crystals formed in super-cooled turbulent water. They can be suspended or gathered in spongy

masses. By snow is meant precipitation in the form of airy crystals depositing loosely and thus forming a layer with very low density.

Ice is often classified according to its genesis. Clear ice is for example formed in a melt of liquid water. The clear ice can further be classified according to crystal shapes and crystal axis orientation. Snow ice is formed from a mixture of snow and water, frazil ice from frazil and water etc. Sometimes also a classification according to the place, where the ice is found, is used. This is not recommendable.

Another very important classification is according to the salinity of the ice into fresh-water ice and sea ice. The term sea ice is not well chosen because it may include all types of ice at sea, for example, ice bergs which have no salinity. A better choice of words would be fresh-water ice and saline ice.

Michel and Ramseier (1971) have proposed a "Classification of River and Lake Ice Based on Its Genesis, Structure and Texture". Their classification, but not always their terms and explanations, will be used in this book, when possible, and their notations P1, S1 etc. will be given below in connection with the description of different types of fresh-water ice.

Other works on ice terminology are a working document by IAHR (Kivisild 1970), International Glossary of Hydrology (WMO 1974), WMO Sea Ice Nomenclature (1970), Illustrated Glossary of Snow and Ice (Armstrong, Roberts, Swithinbank 1966), The Baltic Sea Ice Code (1959), and a draft on Nordic ice terms (Fremling 1975).

2.4 Fresh-Water Ice

Fresh-water ice appears in a few varieties which have different physical properties due to how they were formed. Some of the properties can be explained by the size and shape of crystals other properties by crystal axis orientation. To give some insight, the process of ice-cover formation will be described below.

2.41 Formation of Columnar Ice

When a lake is cooled down in the autumn the whole body of water first attains the temperature $+4^{\circ}\text{C}$ which is the temperature of maximum density of water. During this process the water of the lake mixes easily in the vertical direction and the process is called the autumnal turn-over. As the lake is cooled further the cooled water stays at the surface because of the decreasing density. At calm weather the surface layer rather fast reaches the freezing point while the water at the bottom still can be $+4^{\circ}\text{C}$.

The freeze-up happens mostly a clear and cold night and starts by the growth of ice needles from nuclei of crystallization on the surface of the lake. The nuclei are often small hoar-frost crystals precipitating from the cold air above the water surface. They can be minute discoids or needles. The growing crystals first form a sparse net and thereafter the meshes are grown over by thin clear ice.

When the surface has been frozen over the ice cover increases in thickness by the downward growth of the initial ice crystals, and some of the crystals also grow horizontally at the cost of others. The result of the ice-cover formation is columnar ice with oblong crystals standing in the ice. Many of the crystals at the ice-water interface are extended all through the ice cover, figure 2.10. Their length thus equals the thickness of the ice cover, and their diameter increases with depth. At a depth of 0.3 to 0.6 m the diameter is frequently 0.05 - 0.15 m.

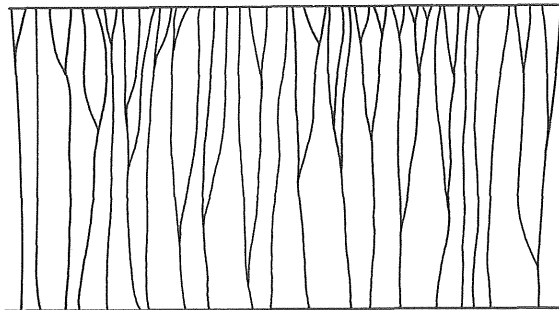


Figure 2.10

A vertical section through columnar ice with drawn crystal boundaries. As some crystals with favourable crystal-axis orientation encroach on others there are fewer but courser crystals at the underside of the ice cover.

The formed ice is called clear ice because of its transparency, black ice because it looks dark from above or columnar ice because of its structure. Impurities in the water are concentrated at the crystal boundaries, and in the spring when the ice is warmed by the sun most of the radiation is absorbed in the crystal boundaries causing the melting to start there. Shortly before the break up, the ice cover therefore has deteriorated to densely packed but loosely connected candle-like ice crystals. Such ice is called candled ice.

At windy weather the initially formed ice consists of frazil or small discoid crystals which form slush at the surface. This situation is rather unusual, however, as generally a strong wind brings up warm water from deep layers in the lake. Sometimes the lake is also snowed over before it has frozen, and the initial ice is then, of course, formed from snow slush. When the slush has frozen the increase in thickness proceed by the growth of the crystals down through the water as described above.

2.42 Crystal-Axis Orientation

The crystal-axis orientation in a columnar ice cover is important to know because the rheological properties in c-axis direction are different to those along the basal plane. As an example slippage in ice crystals mostly occurs in the basal planes, figure 2.8.

The size of the crystals also influence the mechanical properties as many crystal boundaries per unit volume give rise to more flexible ice than few boundaries. In columnar ice horizontal c-axes imply narrow crystals and vertical c-axes comparatively large crystals.

There has been a very long discussion on the reasons why there is different crystal-axis orientation in lake ice covers. Sometimes it has even been observed that one winter a whole lake ice cover has mostly vertically oriented crystals, and the next winter on the same lake there are mostly horizontally oriented crystals. Below is an account for the results from this discussion, which explains seemingly contradictory information on ice crystal orientation.

Primary ice P1 Calm surface. Temperature gradient in the water:

The primary ice skin formed at the surface of a water reservoir or lake at calm weather will either have randomly oriented crystals or crystals with vertical c-axes. Vertical c-axes will dominate if there is a temperature gradient in the water close to the surface because nuclei with vertical axes will be able to grow fast over the cold surface, while tilted nuclei cannot develop along their basal planes, because these will tend to grow down into the warmer underlying water. Instead the tilted crystals show up as long needles formed along the intersection between their basal planes and the surface. The dominating vertically oriented crystals are large (5-20 mm) to extra large (> 20 mm) and it is not uncommon with giant (~ 1 m) crystals.

Primary ice P2 Calm surface. No temperature gradient in the water:

Random accis orientation in the primary ice skin will occur when there is no thermal gradient in the water close to the surface. The nuclei of crystallization can then develop in all directions and no crystals are favoured. The crystal size ranges from medium (1-5 mm) to extra large (> 20 mm).

The description of the formation of the primary ice layer is in concord with Shumskii (1955), Brill (1957), Hobbs (1974), Cherepanov and Kamyashinkova (1971). Michel and Ramseier (1971) writes that the rate of cooling or thermal gradient in the air influences the crystal orientation, which it does only indirectly by creating either a gradient in the water surface or a homogeneous supercooled layer of some depth. The crystal size may however be influenced by the rate of cooling. A high rate implies many nuclei per unit area while a low rate implies relatively fewer.

Primary ice P3 Thin frazil-ice cover and P4 Thin snow-ice cover:

If the freeze up starts in agitated water by the formation of frazil at the surface or if the lake is snowed over, the primary ice layer will of course have a random crystal orientation. The crystal size will in both cases be fine (< 1 mm) to medium (1-5 mm), the shape equiaxed, but the frazil-ice crystals will be angular while the snow-ice crystals will be rounded.

The ice cover increases in thickness by the downward growth of the primary ice crystals. The formed clear ice is called columnar ice and its crystals can extend all through the ice cover, see figure 2.10. The diameter of the columns tend to increase with depth since some crystals are cut off from the water by a process called geometrical selection. In this process crystals with tilted c-axes will mostly wedge out crystals with vertical c-axes, see figure 2.11. If, however, most crystals in the primary ice skin have vertical c-axes this orientation will be maintained all through the ice cover. The mechanism has partly been explained by Perey and Pounder (Pounder 1965) and a complete theory has been given by Ketcham and Hobbs (Hobbs 1974).

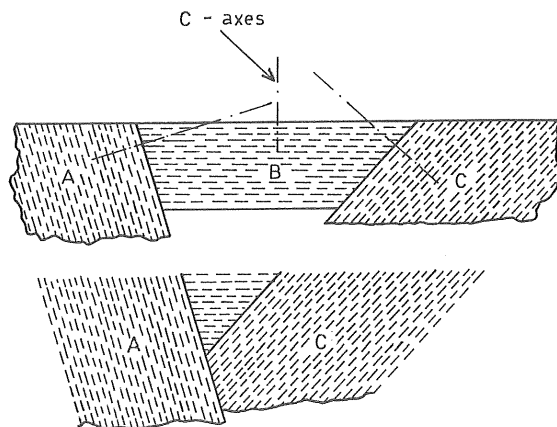


Figure 2.11. Preferred growth of crystals with inclined optic axes, resulting in gradual extinction of a vertically oriented crystal. The lower sketch shows a later stage in freezing.

Secondary ice S1 Columnar ice. Preferred vertical orientation of c-axis:

If the primary ice has crystals with preferred vertical orientation, P1, the secondary columnar ice will have the same crystal orientation. The geometric selection is slow and the crystal diameter will grow only slightly with depth. The diameter of the crystals is usually large (5-20 mm) to extra large (> 20 mm) with irregularly shaped grains.

The length of crystals depends on the relative orientation of adjacent crystals but can vary from large to the length equivalent to the thickness of the columnar ice layer. See figure 2.10.

Secondary ice S2 Columnar ice. Preferred horizontal orientation of c-axis:

If the primary ice has a random crystal orientation (types P2, P3 and P4) the size of crystals will increase more rapidly with depth than for S1. The crystal orientation changes continuously with depth becoming preferred horizontal after 5 to 20 cm of growth. The initial crystal size would be the same as for the primary ice increasing to large (5-20 mm) and possibly extra large (> 20 mm) at the bottom of the columnar layer.

A lake ice cover can also contain other types of ice as for example in perennially frozen arctic lakes where the columns can consist of giant crystals with the c-axes horizontally and nearly parallel (S3). When ice is growing by crystallizing on an object or vertical ice surface the c-axes will mostly be parallel to the surface. For example ice re-freezing in a bore hole will consist of needle-like crystals pointing at the centre of the hole with their c-axes perpendicular to the needles. In Sweden perennial ice is of no practical interest and the other type of ice does not influence the over-all characteristics of an ice cover. When making laboratory experiments it is often formed on the walls of research basins which should be observed (Brill 1957, Muguruma and Kikuchi 1963).

Most reports on the orientation of crystals in lake ice covers are consistent with the account above as for examples descriptions given by Knight (1963) or wind tunnel experiments made by Lyons and Stoyber (1963). The latter scientists found that vertical c-axes dominated when the wind speed was less than 1.5 m/s and at 2.7 m/s horizontal axes.

Sometimes a thin ice consisted by vertically oriented crystals may be broken up into small discoids by a strong wind. The discoids are then pushed together and made to tilt by the wind so that an ice cover with mainly horizontal oriented ice of a crystal size of the order of 0.01 cm is formed.

Also the observations by Muguruma and Kikuchi (1963) on Peter's Lake, Alaska, agree with the description above. They suggest that at normal weather conditions ice with horizontal c-axes is formed and that vertically oriented ice is formed when the wind breaks such thin ice and pushes it together. By normal weather they mean windy weather.

2.43 Frazil and Frazil Ice

When the turbulence in the water is too intensive the formation of a surface ice sheet is prevented, and if the mass of water is supercooled minute ice crystals form at the surface but swirl down and become suspended. This is particular common in rapids, but can also be observed in waves, especially on shores and in shallow areas. The formed crystals grow from colloidal particles to small discoids and spikes that cluster together to porous aggregates. Such suspended ice is called frazil.

In turbulent stretches anchor frazil is developed, that is, the frazil sticks to stones or scraps on the bottom and also to the iron-parts of intakes and turbomachinery. Sometimes it can clog a river or a power-station very fast if the concentration of suspended frazil is high. Motala Ström in Sweden is for example said to have "stopped its pace 1708". The flow of that river is $42 \text{ m}^3/\text{s}$. When going full tilt, passing frazil and supercooled water through its turbines, it can be a matter of seconds for a turbine to be completely choked if the frazil starts to stick to the machinery. Another problem of anchor frazil is that it can lift stones or scrap-iron from the bottom and bring it into turbines or pumps where it damages the equipment.

Secondary ice S4 Frazil ice: In river stretches with a low pace the frazil "sediments" to the surface and forms frazil slush, eventually stopped by some obstacle it may create a hanging dam. The mixture of water and frazil is cooled from above and the water in the pores freezes. A solid ice mass, frazil ice (S4), is formed. The crystal shape is equiaxed to tabular ranging from fine ($< 1 \text{ mm}$) to medium (1-5 mm) sized. The crystal boundaries are irregular, and the crystallographic orientation is random.

When investigating into the deformation and strength of ice as a material, it is often convenient to work with ice specimens that contains

a lot of crystals, in order that the specimens be considered equal and homogeneous. To this purpose frazil ice is well fitted. Many experiments have also been done with artificial frazil ice made from saw dust or splintered ice. See chapter 9: Mechanical Properties. In this respect frazil ice is important, while it plays a minor role for thermal ice pressure.

2.44 Snow and Snow Ice

In connection to thermal ice pressure snow is of interest by two reasons. First, because snow is a good insulator which effectively prevents temperature variations in the air to reach the underlying ice or ground. Secondly, because snow ice is very common on lakes in temperate areas, why it is necessary to know the properties of snow ice as well as of columnar ice. The occurrence of natural snow ice is given in the next paragraph 2.45. Below a very short summary of some features of snow and hail is given. For an elaborate description of the precipitation of snow it is referred to Hobbs (1974).

Snow is formed in clouds by the crystallization of vapour on nuclei of crystallization. The process results in light snowflakes. Hail, on the other hand, is formed by the collision of supercooled water droplets that freezes when combining to bigger drops. This results in hailstones or, if the original particles were snowflakes, in graupels. Raindrops can also freeze and this results in ice pellets. Hailstones and graupels are translucent or milky. Pellets are transparent. Ordinary snow covers can, however, be considered to consist of only snow since hail constitutes a very small fraction of the accumulated solid precipitation.

Snowflakes are hexagonal crystals and their shapes are legion. Some typical shapes are hexagonal plates, six-pointed stellar crystals, solid or hollow columns with hexagonal crosssection, needles, spacial dendrites and capped columns see figure 2.12. These basic shapes are varied in innumerable ways and actually not two snowflakes are equal.

The basic forms of solid precipitation depend on the weather conditions, and due to which form is most numerous the deposited snow cover show different features. This is important for avalanche forecasting. See for example Mellor (1965) or Seligman (1936).

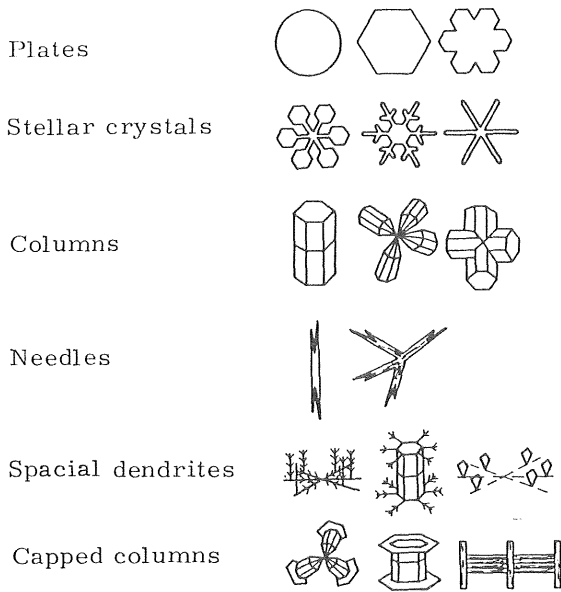


Figure 2. 12. Some typical forms of snowflakes.

It also influences the bulk density and thus the thermal conductivity of a snow cover. These variations are, however, of minor importance for thermal ice pressure as compaction and metamorphosis have greater influence. In glaciers the snow is eventually compacted to glacial ice; opaque ice with high density.

Snow_ice_T1. Frequently snow fields are flooded by water, see paragraph 2.45. The mixture of snow and water then freezes to snow ice, whose crystal size ranges from fine (< 1 mm) to medium (1-5 mm). The shape is round to angular depending on the age of the snow, and the crystals are equiaxed having random orientation. If the snow is soaked but drained again before freezing drained snow ice (T2) is formed. The drained ice has very low density.

The mechanical properties of artificial snow ice has been extensively studied, because of its fine grain and homogeneity which gives good reproductability of experiments.

2.45 Lake and River Ice Covers

Natural ice covers almost never have a simple structure, and have to be very simplified to fit any mathematical model for calculation of thermal pressures or even for simple observation purposes. Below is a comprehensive review of the variations that can be expected, freely after Fremling (a). See also Ager (1960), Lazier and Metge (1972).

On a lake the ice cover can be constituted (from top to bottom) by snow, snow ice, slush and columnar ice. The snow can be moist and compacted or dry and loose, the snow ice and slush can contain little or lots of air, the columnar ice can show different crystal structure as described earlier, and it can also hold various amounts of air bubbles.

The ice cover also vary from place to place on the lake, for example because of uneven accumulation of snow. At the inlet and outlet and in straits the ice cover is affected by currents, and it may also be flooded at the inlet. Along the shores the cover is bent and cracked and sometimes flooded because of the rise and fall of the water level. This is very pronounced in reservoirs especially if they are regulated daily. To these variations comes thermal cracks and ice folds. Along an ice fold the ice cover is treacherous with tilted ice blocks, newly formed columnar ice, water, slush, and snow ice. In Sweden it is also very common to plough winter roads on the ice which also causes complications. Some winters a road for lorries has been prepared across the Bothnian Bay between Sweden and Finland. The distance is approximately 100 km.

The quality of the ice also varies with time. In early winter, when there is little solar radiation the columnar ice is solid and strong. In late winter the columnar ice is candled by the sunshine, and although it maintains its depth it consists largely of water and loose crystals. On the other hand, if it is covered by snow or snow ice it is shielded from the sun and will maintain its strength till the snow or snow ice has disappeared. The snow ice is also affected by solar radiation so that it melts at its crystal boundaries. The result of this is loose granular ice (corn snow ice).

In rivers ice conditions are still more complicated. In slow reaches the conditions can resemble the conditions on a lake. In rapids and narrow reaches, however, a lot of frazil ice is produced and carried downstream creating hanging dams or accumulating as anchor frazil. Water levels will then rise and stretches of ice covers will lift from its supports on the banks and shove onto each other, be broken into pieces and eventually be carried downstream causing ice jams anew. The water level will rise again and the process is restarted and will go on till the river is completely ice covered, the runoff decreases, or the cold weather ceases. In spring the problems will start all over and they are especially pronounced for rivers flowing into colder climate as in the northern Soviet-Union, Canada and Alaska. The problem of thermal ice pressure is however of comparatively little importance in such rivers. Uzuner and Kennedy (1974) have treated these problems quantitatively. A description of the ice conditions in a Swedish unregulated river, the Torne Älv, is given by SMHI (1961).

The layers of snow slush and snow ice in the lake ice cover arise because the ice is pressed down by the load from the snow. Water will then find its way through cracks and holes up onto the ice cover and it will usually rise capillary in the snow to a level higher than the water table, thereby increasing the weight of the snow. The sinking stops when the vertical equilibrium is restored. See figure 2.13.

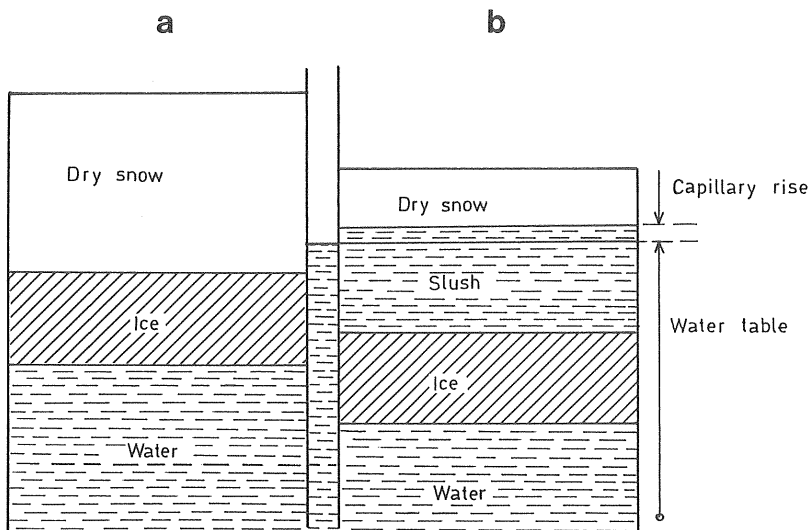


Figure 2.13. A vertical section through an ice cover before (a) and after (b) water has leaked onto it.

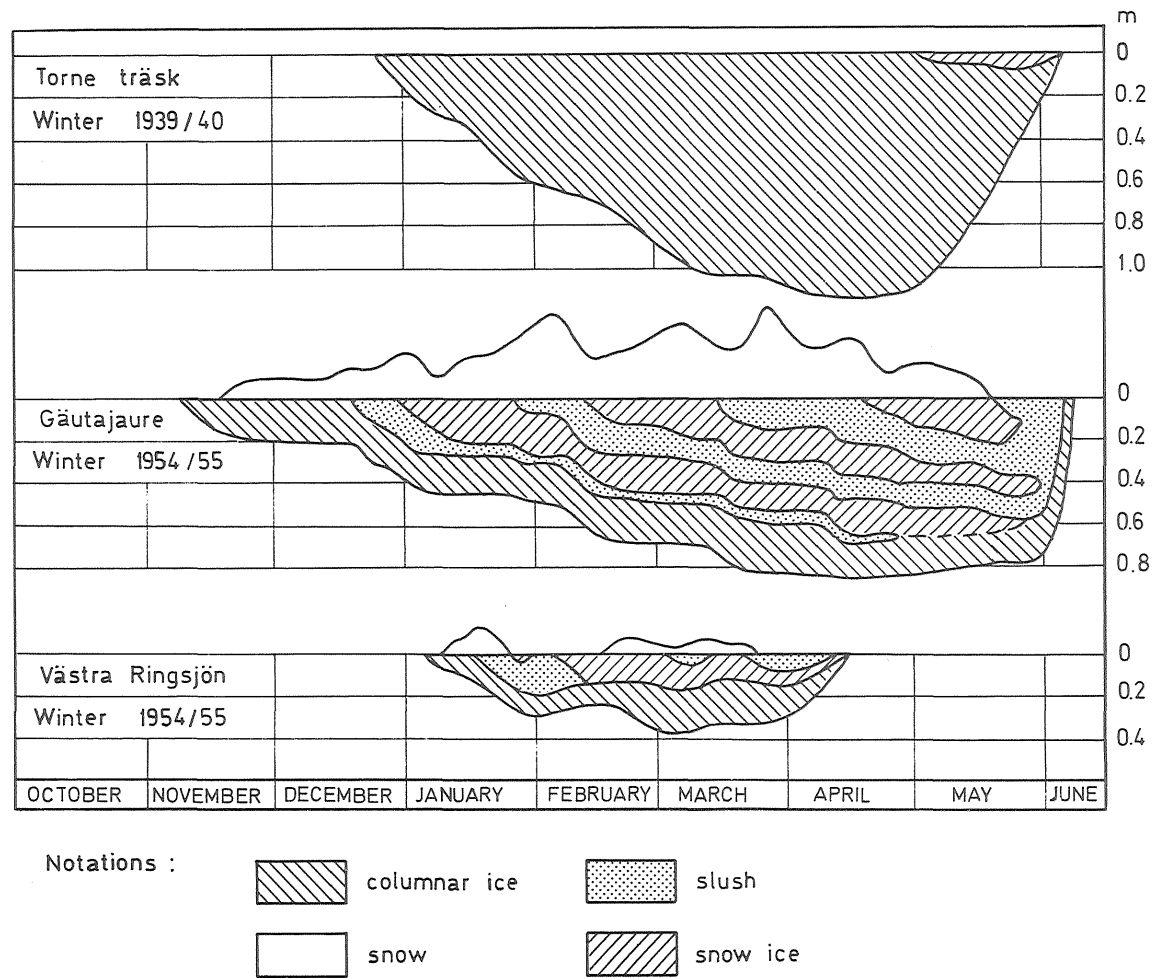


Figure 2.14 Examples of the growth and decay of lake ice covers. (After Fremling 1968).

The slush, that is, the mixture of water and snow, freezes to snow ice from above and the columnar ice is warmed to 0°C . After some time the ice cover will thus be constituted by snow, snow ice, slush and columnar ice. Often there can be several heavy snow falls in a winter which creates an ice cover with repeated layers of snow ice and slush.

Three examples of the growth and decay of lake ice covers are given in figure 2.14. Torne Träsk the winter of 1939/40 and Gäutajaure 1954/55 are extreme examples of ice conditions. Torne Träsk with over 1 m solid columnar ice without snow and Gäutajaure with three double-layers of slush and snow ice on top of a rather thin (0.1 m) columnar ice layer.

2.5 Saline Ice

When ice forms in a weak solution the formed solid will be of pure H_2O because the ice lattice is very selective and hardly accepts substitutes for hydrogen and oxygen atoms. The temperature for the formation of ice is also lowered under 0°C . The hexagonal character of the ice crystal is unaffected by the presence of the salts, but because of the exclusion of the salts from the ice lattice, pockets of concentrated solution is trapped within the ice structure, which gives rise to bulk properties very different from those of fresh-water ice.

The great amount of void volume in saline ice show up in low strength and pronounced viscous behaviour at a high temperature. The fact that the brine in the voids makes up closed systems with the surrounding ice show up in the peculiar behaviour that saline ice decreases its bulk density with increasing temperature. Other results are the lack of a distinct point of freezing and melting, the drainage of the ice caused by temperature gradients and the great variation of thermal "constants" with temperature.

Taking all these facts into account it is not easy to tell directly how they will affect thermal ice pressure, although one astounding conclusion can be drawn. In saline ice falling temperatures give rise to pressures and rising temperatures will release the pressures. This has been observed by Malmgren (1927). See e. g. Peschanskii (1971). The magnitudes of the pressures are however difficult to judge. On one hand the strong dependence of volume on temperature indicates very big pressures, on the other hand the ice is a lot weaker than fresh-water ice and the temperature response of the ice is a lot slower because of the very high heat capacity.

2.51 Sea Water and Ice at Sea.

The salinity of sea water varies between 34 and 38 ‰ in the oceans. In coastal areas and landlocked adjacent seas the variation can be greater. However, the relative proportions of different salts are nearly constant regardless of the absolute concentration. The major constituents of the solution are listed in table 2.15. The concentrations are expressed in kg per kg of solution, the total salinity in this example being 34.48 ‰, which is often taken as a standard figure. See for example Dietrich and Kalle (1967). For the purpose of explaining sea ice properties, it is enough to take the three major constituents of table 2.15 into account.

Table 2.15. Composition of salts of sea water of the salinity 34.48 ‰

Salt	NaCl	MgCl ₂	Na ₂ SO ₄	CaCl ₂	KCl	NaHCO ₃	Other	Total
‰	23.48	4.98	3.92	1.10	0.66	0.19	0.15	34.48

It should be warned that the density of sea water and brine cannot be directly expressed as the density of water plus the weight of the included salts. See Chapter 3.3 Density of Sea Ice. The reason for this is that the ions affect the structure of the liquid water and also some ions are hydrated. Another important effect is that standard sea water does not have a point of maximum density and that the tempe-

perature for the first formation of ice is depressed below 0°C . The density maximum temperature and "freezing-point" temperature are approximately linear functions of salinity for $S < 50$ ‰ and are shown in figure 2.16.

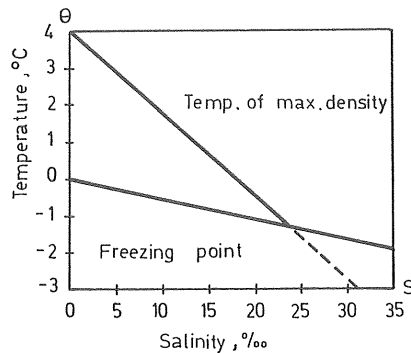


Figure 2.16 The temperature of maximum density and the "freezing-point" temperature as functions of salinity.

It is seen that at salinities greater than 24.7 ‰ the density maximum is below the freezing point. In ice engineering this salinity could be considered the limit between brackish and salt water, because the conditions for ice formation are very different if the salinity is greater than or smaller than this value. In a sea with salt water of homogeneous salinity the whole body of water must be cooled to the freezing-point temperature before ice can form at the surface. In brackish water the conditions are very much like those in lakes, that is, first the body of water is turned over and an inversed temperature gradient is created with the coldest water on top.

Because of this lack of density maximum sea ice can only form in areas with long cold winters as the Arctic and Southern Ocean or in areas with brackish surface water like the Baltic and the Black Sea.

In the Southern Ocean and especially in the Weddell Sea the freezing out of salt and the cooling of the surface water results in very heavy water, salinity 34.62 ‰ and temperature -1.9°C . This water sinks to the bottom, and while warmer water comes in from the

north, the bottom water spreads to the north on the ocean floor. This is actually part of the mechanism of ventilation of the world ocean. The sinking water has a high content of oxygen and is fundamental to the life in the sea. Other parts of the ocean playing the same role but on a minor scale are the Sea of Okhotsk, the Greenland and Irminger Seas (Dietrich and Kalle 1967).

In the southern part of Hudson Bay, in the Baltic and in the Black Sea the top layer is brackish and consequently a cover of columnar ice and snow is created very much in the same way as in lakes.

In areas where big rivers flow directly into a cold saline sea, ice is formed at the interface between fresh and saline water. It is of course continuously floating to the surface and can cause problem to smaller vessels.

A lot of the ice in the seas of Arctic and Antarctic regions is of snow origin. The ice bergs in the North Atlantic are calved from the glaciers of Greenland and Spitzbergen. The tabular ice bergs in the Southern Ocean are broken off from the shelf ice surrounding the Antarctic Continent. This glacial ice is, of course, of great importance to the life in the seas of the polar regions and is also a problem to ships and off-shore installations but has little bearing on thermal pressures

2.52 Formation of Columnar Sea Ice

When eventually ice forms at the sea surface it is growing in a deep layer of water with its temperature at the freezing point and homogeneous density. If considerable turbulence is present during freezing, a layer of discoids and granular ice crystals are formed on the surface as a slush. The slush may be several centimetres thick and it freezes together to a fine grain (< 1 mm) ice cover with randomly oriented c-axes. This way of formation of the initial ice cover is frequent in the sea. If the ice cover formation starts at a calm surface the nuclei of crystallization grow to small disks and develop into dendritic (ramified) stars. The crystal orientation in the latter case is predominantly vertical.

As is the case in lakes, columnar ice is formed when the ice cover is increasing its thickness. Crystals with horizontal c-axes are favoured but the process of geometrical selection (Chapter 2.42) is much faster than in fresh water. It is in fact doubted that the geometrical selection is responsible for the strong preference of horizontally oriented crystals. It is for example observed by Lavrov (1969) that if the initial ice skin has vertical c-axes, new crystals with more favourable crystal orientation form spontaneously at the interface. According to Pounder (1965) it is sufficient with 4 ‰ salinity to get a fast selection of crystals. Whatever the reason all saline columnar ice has horizontal c-axes and a grain ranging from fine (< 1 mm) to large (5-20 mm). Very thick ice (> 0.5 m) can contain courser crystals in its lower layers.

Bennington (1963) discusses the reasons for crystal-axis orientation in columnar sea ice thoroughly. The theories put forward are based on the mechanical convection under the interface ice-water and on the assumption of a gradient of supercooling put forward by Shumskij.

Saline columnar ice is characterized by its great inclusions of brine and air. Weeks and Assur (1967) discuss this phenomenon in detail and have also suggested a model for the shape of the voids and how they vary with temperature. Their model will be accounted for below and used subsequently for the calculation of mechanical and thermal properties. First, however, a qualitative description of the formation of the columnar ice will be given.

As told above the crystal lattice itself is very selective, and therefore the formed ice is pure ice, the salt remaining in the water. In the growth front the salinity of the water increases in this way. As the thickening of the ice cover continues the growing basal planes stretch like plates or fingers down into the supercooled water and not until their length is 2 to 3 cm, bridges are formed between the plates. Brine is in this way confined in the ice. The brine voids form vertical strings of beads in the ice cover. They are concentrated to certain basal planes at a distance of 0.5 to 0.6 mm, their diameter is approximately 0.05 mm, and their length approximately 3 cm.

The salinity of the brine in the voids at the moment of confinement can for salt water be considered as equal to the salinity of the sea. The enriched brine in the growth front is denser than the ambient water and will therefore sink. In this way the salinity is kept constant at the interface. The brine in the narrow space between the platelets is, however, slightly more concentrated and the faster the growth the higher the salinity is in the formed brine voids. For brackish water the salinity at the growth front must not necessarily be of the same salinity as the ambient water, because brackish water can be stably layered over colder but less salt water. Consequently the salinity in the brine voids cannot be easily predicted. Still, columnar ice formed in salt water is, of course, more saline than ice formed in brackish water.

The brine volume of saline ice decreases at decreasing temperature because more water freezes and more salt precipitates in the brine pockets. But even at -80°C the ice contains traces of brine. The expansion when the void water freezes explains the expansion of saline ice with decreasing temperature. As will be shown later most peculiarities of saline ice can be explained by the phase changes in the brine voids.

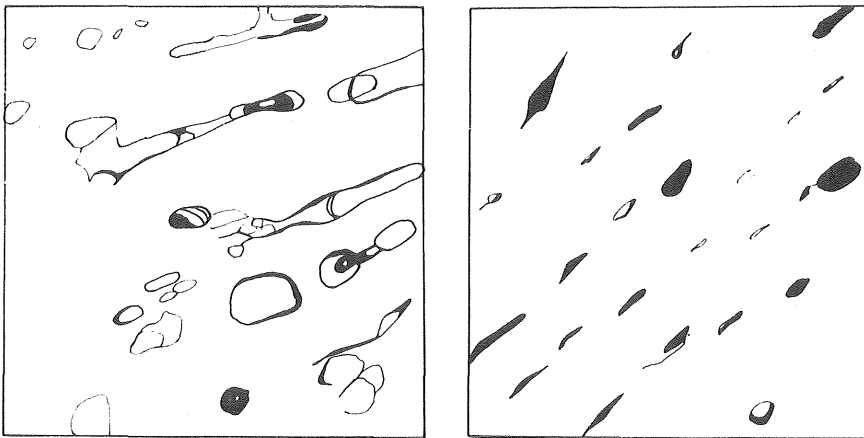


Figure 2.17 Sections through columnar sea ice showing brine pockets at two different temperatures. The right sketch at the lowest temperature.

A sea ice cover contains horizontal layers with greater concentrations of brine voids and air bubbles, which form when the ice cover grows uncommonly rapid. Other mechanisms tend to decrease the salinity of the ice. One is that the brine voids move towards higher temperatures, that is mostly downwards. This fact will be explained in the next paragraph. The draining off is amplified by gravitational drainage. Pounder (1965) says that the voids are interconnected at temperatures over -15°C , which is contradictory to the fact that bulk density changes actually obeys the theories founded on the assumption of a closed system in the ice. The gradient drainage and possibly the gravitational drainage add up so that winter ice has a typical salinity of 4 ‰ and two year old ice of only 1 ‰ although the salinity of newly formed ice can be as high as 20 ‰.

2.53 Phase Relations of Columnar Sea Ice

As is described in paragraph 2.52 columnar sea ice will trap sea water when growing. The trapped sea water brine is the cause of the marked temperature dependence of many properties of columnar sea ice. To calculate these variations as functions of temperature it is necessary to take the phase changes of the two-phase system brine and ice into account. (Assur 1958, Anderson 1960, Schwerdtfeger 1963, Weeks 1963, Pounder 1965, Weeks and Assur 1967, Frankenstein and Garner 1967).

A piece of sea ice with brine pockets can be regarded as a closed system. For simplicity we disregard the existence of air-inclusions in the ice. In such a closed system there is an equilibrium between the brine and the frozen ice. In figure 2.18 the "freezing-point curve" of sea-water brine shows the concentration of brine in equilibrium with ice at different temperatures. For example at -7.6°C , when $\text{Na}_2\text{SO}_4 \cdot 10 \text{H}_2\text{O}$ starts to precipitate, the salinity of the brine at equilibrium is approximately 110 ‰. That is, if the brine in the pockets has a lower salinity, ice will form till the salinity of the brine becomes 110 ‰. On the other hand, if the brine and ice is in equilibrium and the temperature is raised a couple of degrees ice will melt from the walls of the pocket to dilute the brine until the new concentration of equilibrium is reached. Due to gradients of concentration near the walls of the pockets the response is slow in big pockets (Onu 1966).

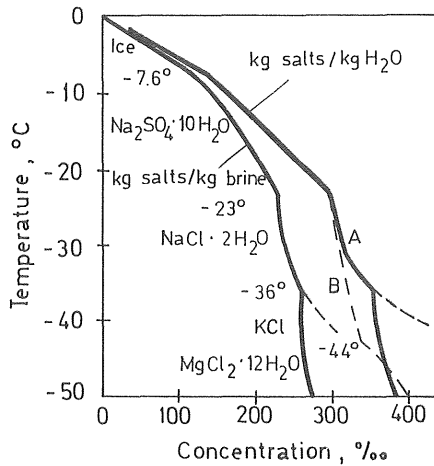


Figure 2.18 "Freezing-point curve" of sea-water brine showing the concentration of brine in equilibrium with ice versus temperature. The various solid salts are listed opposite the segment of the curve in which they are the dominant salt crystallizing. Dashed lines indicate alternate interpretations, or possible alternate paths of crystallization (after Anderson 1960 with changes)

The curve, indicated kg salts/kg H₂O in figure 2.18, describes the ratio between the mass of salts in solution and the mass of solvent in the brine pockets as a function of temperature. This ratio is piece by piece a linear function of temperature which is convenient. The relation between salinity S, mass of salts divided by mass of solution, and the concentration s, mass of salts divided by mass of solvent, can be written

$$s = S / (1-S) \text{ or } S = \frac{s}{1+s} \quad \dots (2.2)$$

Between -7.6°C and the freezing point θ_f where no salts has precipitated the following equation holds

$$s = \alpha_1 \theta \quad -7.6^\circ\text{C} < \theta < \theta_f \quad \dots (2.3)$$

Between -23°C and -7.6°C where Na₂SO₄ · 10 H₂O gradually precipitates other equations must be formulated:

$$\left. \begin{aligned} s + p &= \alpha_1 \theta \\ p &= \alpha_2 (\theta + 7.6) \end{aligned} \right\} -23^\circ\text{C} < \theta < -7.6^\circ\text{C} \quad \dots (2.4)$$

Here p is the mass of precipitated salts divided by the mass of solvent still in liquid form. According to Pounder (1965)

$$\alpha_1 = -0.01848^{\circ}\text{C}^{-1} \quad \text{and} \quad \alpha_2 = -0.01031^{\circ}\text{C}^{-1}.$$

Below -23°C there are alternate ways for crystallization and several salts are precipitating gradually. The number of equations for the description of the phase relations would thus increase successively, but fortunately the phase relations in the ice cause a relatively small change in the bulk properties of sea ice below -23°C . The reason is that at this low temperature the brine voids are rather small. Equation(2.4) will actually do for the calculation of the bulk properties of columnar sea ice down to -30°C , which is a very rare temperature in ice covers whose undersides always are in contact with liquid sea water.

The very first part of the "freezing-point" curve for salinity is in fact the same as the curve of figure 2.16. For low salinity, that is the salinity of ordinary sea water, this curve can also be considered linear. Equation (2.3) gives the freezing point for sea water as

$$\theta_f = \frac{s}{\alpha_1} = \frac{S}{\alpha_1(1-S)} \approx \frac{S}{\alpha_1}; \quad S < 0.050 \quad \dots (2.5)$$

Actually, there is no freezing point of sea ice in the ordinary sence of the word, because at the so called freezing point ice only starts to form and there is a gradual freezing of water in the ice as the temperature decreases. The heat of melting is in this way distributed over a range of temperature so that there is no apparent latent heat of freezing for the closed system but instead a very high specific heat capacity. See chapter 4.

If an oblong brine void is situated along a stationary temperature gradient according to figure 2.19 and the central part has a temperature and salinity in equilibrium with the surrounding ice, the "cold" and "warm" ends will not be in equilibrium. This is because the salt diffuses in the void and so the salinity is nearly homogeneous. The result is that water is freezing at the cold end and that ice is melting at the warm end. This is one of the mechanisms by which already formed ice loses salt.

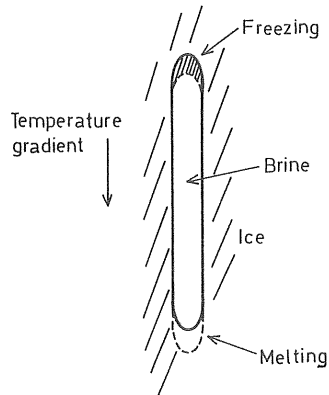


Figure 2.19 Brine migration along the temperature gradient.

From the curves of figure 2.18 the density of sea ice at different salinities or the mass ratios and volume fractions of brine and ice can be calculated. This is done approximately below with the help of the equations (2.3) and (2.4) between -30°C and 0°C .

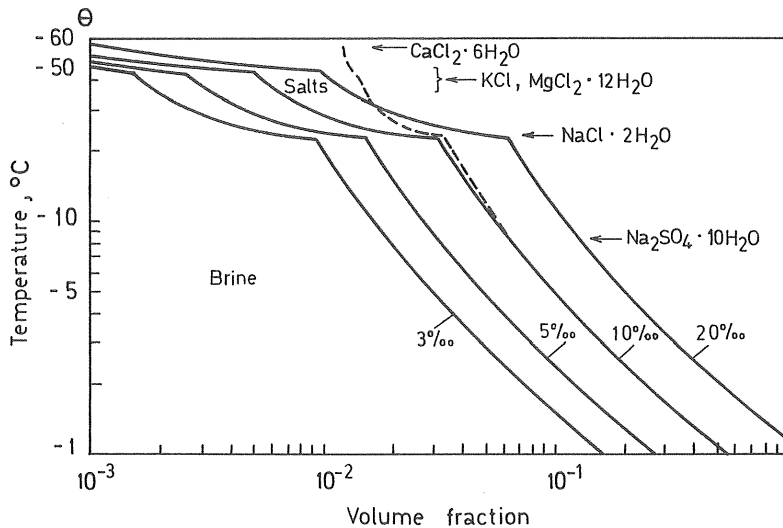


Figure 2.20 Phase relations, by volume, of sea ice of four typical salinities. The salinity decreases with age. The solid salt content is shown only for ice of 10 per mille; it is approximately proportional to salinity. The square root of the abscissa gives the approximate relative strength of the ice, and corresponding relations hold for most other physical properties. After Anderson (1960).

In figure 2.20 the volume fraction of brine is drawn for some typical salinities of sea ice. From this figure it can be seen that at -2°C sea ice with a salinity of 20 ‰ is more than half liquid while at -5°C the same ice is liquid only to $1/5$ by volume. This has, of course, a great influence on the strength of ice and we will look closer at that in chapter 9.

The mass ratios of the phases of columnar sea ice as a function of temperature θ and ice salinity S was calculated by Schwerdtfeger (1963) with the help of equation (2.2) to (2.4). The mass ratios are:

$$\begin{aligned} m_i &= \text{mass of ice (H}_2\text{O) to mass of the system} \\ m_b &= \text{mass of brine} \quad \text{"-} \\ m_p &= \text{mass of precipitated salts} \quad \text{"-} \end{aligned}$$

The sum of the ratios is unity by definition.

For $-7.6^{\circ}\text{C} < \theta < \theta_f$ all the salt is in solution thus

$$m_i + m_b = 1 \quad \dots (2.6)$$

and the salinity of brine S_b is given by

$$S = S_b \cdot m_b \quad \dots (2.7)$$

From equation (2.2) then

$$S = \frac{s_b}{1 + s_b} \cdot m_b \quad \dots (2.8)$$

from which the mass ratios m_b and m_i can be calculated

$$m_b = \frac{(1 + s_b) S}{s_b} \quad \dots (2.9a)$$

$$m_i = 1 - m_b = \frac{s_b - (1 + s_b) S}{s_b} \quad \dots (2.9b)$$

If the densities of brine and ice is known the volume fraction of brine is

$$V_b = \frac{m_b / \rho_b}{m_b / \rho_b + m_i / \rho_i} = \left(1 + \frac{m_i \rho_b}{m_b \rho_i} \right)^{-1} \quad \dots (2.10)$$

For $-23^{\circ}\text{C} < \theta < -7.6^{\circ}\text{C}$ a similar analysis can be made which results in

$$m_b = \frac{S(1 + s_b)}{s_b + p} \quad \dots (2.11a)$$

$$m_p = p \cdot \beta \cdot S / (s_b + p) \quad \dots (2.11b)$$

$$m_i = 1 - m_b - m_p = \frac{s_b + p - S(1 + s_b + p\beta)}{s_b + p} \quad \dots (2.11c)$$

β stands for the mass of the water of hydration in the precipitated $\text{Na}_2\text{SO}_4 \cdot 10 \text{H}_2\text{O}$, $\beta = 2.27$

The volume fraction of brine is consequently

$$V_b = \left\{ 1 + \frac{\rho_b}{m_b} \left(\frac{m_p}{\rho_p} + \frac{m_i}{\rho_i} \right) \right\}^{-1} \quad \dots (2.12)$$

Returning to the freezing point of sea water another interesting fact can be demonstrated. Namely, if it is assumed that there is a free exchange of water between the growing platelets and the sea underneath, the salinity in the brine voids will be equal to the salinity of the sea water S_a . The salinity of the formed ice will then be

$$S = S_a m_{bo} \quad \dots (2.13)$$

where m_{bo} is the mass ratio of brine at trapping.

The freezing point is by equation (2.5)

$$\theta_f = S_a / \alpha_1 \quad \dots (2.14)$$

but the melting point for the ice when it is no longer in contact with the sea water will be higher namely

$$\theta_m = S / \alpha_1 = m_{bo} \cdot S_a / \alpha_1 \quad \dots (2.15)$$

The fraction m_{bo} cannot easily be predicted, but for very fast freezing S can be as high as half the salinity of the ambient water; so that the melting point becomes at least

$$\theta_m = S \cdot \theta_f / S_a \approx \frac{1}{2} \theta_f \quad \dots (2.16)$$

With the aging of the ice there will be still lower salinity and the melting point will be correspondingly raised. The high salinity $S = 1/2 S_a$ also gives that m_{b0} according to (2.13) is as high as 50 %.

The relations calculated in this paragraph will be used subsequently to derive many properties of columnar sea ice, and it is important to bear in mind the assumption that the ice was considered free of air bubbles and that we also did not discuss the possibility that vapour could exist in the system.

2.54 A Structural Model of Columnar Sea Ice

The complicated macrostructure of columnar sea ice, shown in figure 2.17, has been successfully conventionalized to a simple pattern in order to describe the variation of strength with temperature (Assur 1958) and for the calculation of thermal conductivity. (Anderson 1960, Schwerdtfeger 1963)

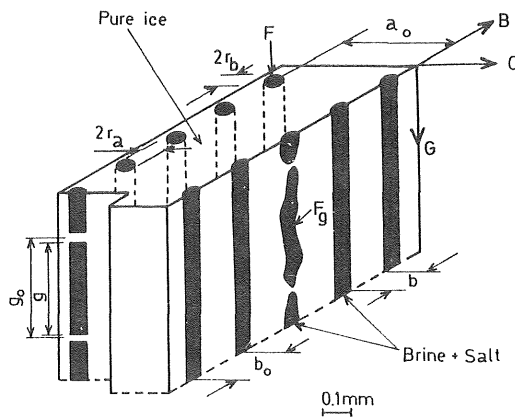


Figure 2.21 An idealized diagram of the shape of the brine inclusions in columnar sea ice and NaCl ice (After Assur 1958).

Taking hold of the characteristic features of the brine inclusions in columnar sea ice an idealized diagram can be made as that in figure 2.21. In the diagram the c-axis of the crystal is horizontal and the G-axis is vertical. Different assumptions of how the shape of the brine voids change with brine volume can be made and will give different relations between bulk properties and temperature. These relations will be described in the chapters on thermal and mechanical properties respectively, where the model will be used.

As mentioned earlier columnar sea ice also contains trapped air bubbles, which are less orderly arranged, compared to the brine voids. When calculating bulk properties of ice the air bubbles will sometimes be taken into account and sometimes be disregarded. The various excuses for this will be explained in due course. Here, it should only be pointed out that stored specimens of saline ice might have been drained off, especially, if they have been stored at an inadequately high temperature. Such a mistake would, of course, offset the intention to verify most of the theories founded on the salinity of the ice, because the void volume of the ice will be related to the original ice salinity and to the storing temperature rather than to the actual salinity of tested specimens.

2.55 Saline Snow Ice

Sea ice covers can be submerged by the load of deep snow in the same way as lake ice covers, see paragraph 2.45. The result is saline slush that freezes to a saline snow ice. This ice must, of course, follow the same phase relations as described above for columnar sea ice, but the distribution, shape and interconnection of the voids are little discussed in literature, why it is difficult to quantify any of its properties. Qualitatively it may be guessed that its great content of air makes it impossible to calculate its volume as a function of temperature.

Saline snow ice will not be discussed further in this book although it is abundant in the Baltic for example. My knowledge of the subject is simply too small.

3. DENSITY

The bulk density of natural ice is very variable due to inclusions of air and brine. As its crystal lattice is very selective the bulk density can, however, always be calculated by means of the densities of its constituents, or rather its content of air and salt can be calculated from measured bulk density values.

The air inclusions in fresh water ice can make the ice at least 5 % easier than compact ice, but the air does not influence the thermal expansion because the air bubbles are very soft compared to the surrounding ice. For the calculation of thermal capacity and conductivity it is, however, important to know the air content because in these respects the air content cannot be neglected.

When calculating thermal expansion of saline ice, the density of the trapped brine must be known. As the brine is enclosed in a system, its density can be given at the equilibrium salinity for each temperature, and thus the brine density in the brine voids is a function of only temperature. An approximate polynomial is given in paragraph 3.31.

3.1 Compact Density of Pure Ice

The density of chemically pure ice without inclusions is usually given as 916.8 kg/m^3 at 0°C , see for example Dorsey (1940). Butkovich (1955) confirmed this by making very accurate measurements of single crystals at -3.5°C . He got the value 917.28 kg/m^3 which extrapolated to 0°C by means of the coefficient of thermal expansion gives 916.82 kg/m^3 .

Butkovich (1957) also measured the density as a function of temperature. His experiments gave that the volume expansion with temperature is linear with good accuracy between -30°C and 0°C . Anderson (1960) proposed a constant volume coefficient of thermal expansion γ of $1.445 \cdot 10^{-4}/\text{K}$ in this interval which gives good agreement also to other scientists results. The volume coefficient, γ , being three times the linear coefficient, α , the latter amounts to $4.82 \cdot 10^{-5}/\text{K}$.

The density as a function of temperature will be given by

$$\rho(\theta) = \rho_0 / (1 + \gamma \theta) \quad \dots (3.1)$$

where $\rho_0 = 916.82 \text{ kg/m}^3$ is the compact density of ice at 0°C , $\rho(\theta)$ the compact density at the temperature θ , and γ the volume coefficient of thermal expansion.

The function 3.1 is plotted in figure 3.1 together with densities calculated from different coefficients of thermal expansion cited by Drouin and Michel (1971). It is seen how well the approximation 3.1 fits to these curves. Curves on the coefficient of thermal expansion itself would have given a false impression of great differences between values.

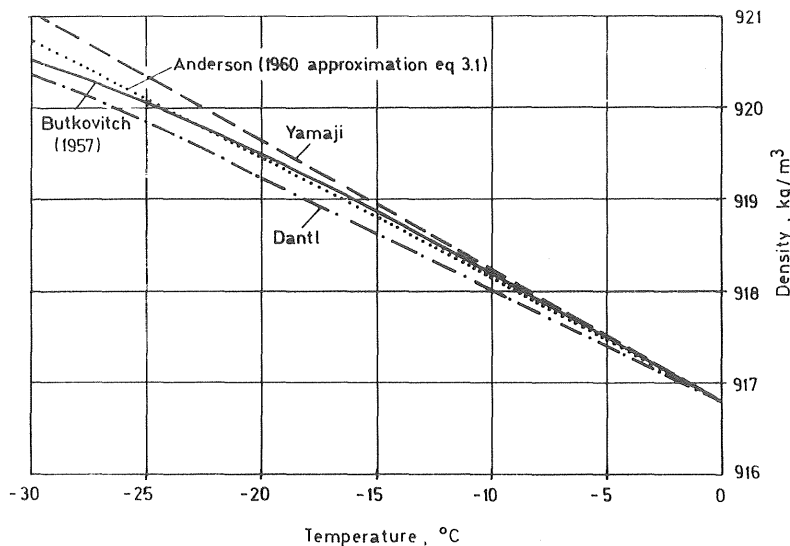


Figure 3.1 Compact density as a function of temperature for fresh-water ice. The functions of Dantl and Yamaji are calculated from information in Drouin and Michel (1971).

Other scientist like Laplace and Post and Jakob and Erk have been interested in the crystal structure of ice (Hobbs 1974). They have measured the linear expansion of single crystals in the crystal-axes directions. If we recall how the lattice distances could be calculated from the meas-

ured density of ice, we can imagine how changes of the distances between the molecules in ice are reflected in a change of crystal dimensions. See chapter 2.2. Ice crystals actually expands anisotropically but in an ice cover the crystal orientation is irregular enough to cancel out these differences.

Although the freezing of water to ice means an increase of volume of 9 %, this does not cause significant horizontal movements or loads in an ice cover, because the increase in volume takes place in the direction of heat transport. Janson (1963) verified this by freezing two open wooden boxes full of water, one box insulated on bottom and walls the other one uninsulated. The first box took a freezing to the bottom. The walls of the other box burst apart.

Water freezing in cracks in the ice is, however, cooled by the surrounding ice and therefore it expands sideways which gives rise to pressure. As the cracks are only a small fraction of the area, the pressure will never be of the same magnitude as extreme thermal pressures. 0.3 MPa would be a common value.

3.11 Density of Natural and Artificial Ice

The bulk density of natural fresh-water ice has been measured by for example Ager (1963 a, b) in a cold room of a temperature of -9.5°C . The specimens were weighed in air and the volume was measured by submerging them in kerosene.

Naturally formed columnar ice (S1 or S2) was found to have a density of between 870 and 920 kg/m^3 . The density of ice formed from water pumped onto a lake ice cover without snow in layers of 1-5 cm was found to vary between $870 - 910 \text{ kg/m}^3$.

Snow ice (T1) formed by pumping or by natural flooding gave values ranging from $870 - 910 \text{ kg/m}^3$ although most values was between 880 and 900 kg/m^3 . If the water penetrates very slowly through the snow cover and the snow has a fine grain, snow ice with a density as low as 870 kg/m^3 can be formed.

If the snow is soaked by water but drained before freezing, the density of the resulting ice (T2) is of the order of 600 kg/m^3 (Michel and Ramseier 1971).

As the compact density of fresh-water ice is always accurately given by equation 3.1, and other impurities than air bubbles have little influence on the bulk density of fresh-water ice, the void content, v , by volume can obviously be calculated by

$$\rho(\theta, v) = \rho(\theta)(1 - v) \quad \dots (3.2)$$

where $\rho(\theta, v)$ is the bulk density and $\rho(\theta)$ is the compact density according to equation 3.1.

3.2 Density of Snow

Snow is a very good thermal insulator because of its light porous structure. Its conductivity is a function of snow density and structure, and therefore it is of interest to see if there is any systematic variation of density due to age or climate. The submergence of ice covers due to snow is of course also dependent of the snow density.

A newly formed snow cover can have a density of 100 kg/m^3 and an old melting snow cover of $400\text{-}600 \text{ kg/m}^3$ due to its high content of liquid water. Even higher values of the density are reached in glacier areas where the snow is gradually compressed to ice.

In Sweden measurements of the depth average density of snow covers have been made at least twice a month during the winters 1909-1928 by SMHI, see figure 3.2. The results from these measurements have been used to estimate the loads from snow on roofs and also the amount of water stored in the snow cover. It can be observed in figure 3.2 that from mid March the density is rising sharply to over 500 kg/m^3 in early April. Probably this is due to a high content of melt water. Such high values should not be used when calculating thermal pressures in an underlying ice cover. Probably the daily variation of air temperature will not reach the ice cover in such occasions.

Drouin and Michel(1971) presents a few values on the density of dry snow from the Quebec area. They do not show any marked dependence on time.

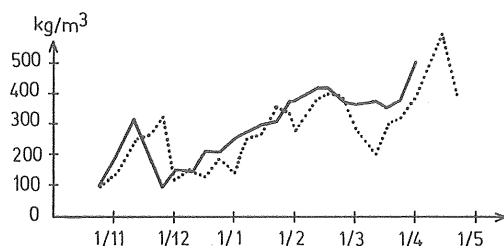


Figure 3.2 The density of the snow cover in the winter of 1915/16, at Gåsbornshyttan; and at Gimo — (Nord and Taasler 1973).

An average over the years of the measured densities at different dates was formed. This average showed a linear increase in density with the date of the year, and if time was given as the age of the snow cover, the density as a function of age became nearly the same for all stations in the country, in spite of the fact that the climate is very different from station to station. A typical diagram on averaged snow densities is shown in figure 3.3. In these investigations one also tried to establish a relationship between snow depth and density but could not find any.

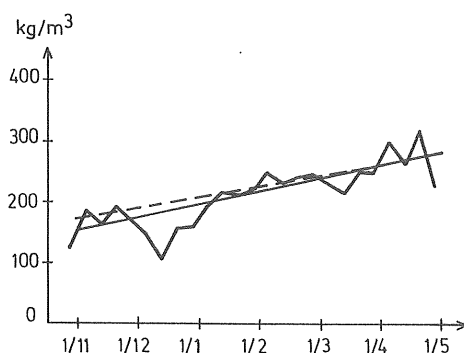


Figure 3.3 Mean course of density of snow cover in the winters of 1909/10 - 1917/18., Gåsbornshyttan.
 ————— curve showing national means;
 - - - - - curve showing zone means;
 ————— mean for station
 (Nord and Taesler 1973).

Recently done measurements in Sweden (Nilsson 1971) and Czeckoslovakia (Martinec 1965) show the same results as above. Williams and Gold (1958) report 10 years of observations on snow covers and the mean and standard deviation of their density at different places in Canada. The conductivity is also calculated and the density as a function of meteorological variables is discussed.

Reasonable bulk densities for dry snow covers are 200 to 300 kg/m³. The porosity of snow can, of course, be calculated by equation 3.2, but the dependence on temperature can be neglected. Thus:

$$\rho_s \approx \rho_o (1 - v) \quad \dots (3.3)$$

where

- v is the porosity of snow by volume
- ρ_o the compact density of ice at 0°C
- ρ_s the bulk density of snow

3.3 Density of Sea Ice

From the phase relations of saline ice the density of columnar sea ice without air inclusions can be calculated. This has been done by for example Riemer (see Kalle 1943), Anderson (1960) and Schwerdtfeger (1963). The two former scientists' results are approximately the same. Schwerdtfeger has deduced a simple analytical expression, but, unfortunately, working with an erroneous expression for the brine density, his sea-ice density values are 2 % too small.

The theoretical values calculated from the phase relations show general agreement with the experimental data given by Petterson (in Malmgren, 1927). It should be stressed that the densities are assumed to follow the volume variations of the components calculating with the formation of neither voids nor internal pressures.

3.31 Sea-Ice Density calculated from Phase Relations

For temperatures above -7.6 °C the following expression holds for the density of columnar sea ice without air inclusions.

$$\rho(\theta, S) = (m_b / \rho_b + m_i / \rho_i)^{-1} \quad \dots (3.4)$$

$$-7.6^\circ\text{C} \leq \theta \leq \theta_f$$

where the weight ratios m_b and m_i are given by the equations 2.9a and b respectively, and the density of ice $\rho_i = \rho(\theta)$ by equation 3.1.

The expression 3.4 was set up by Schwerdtfeger (1963) who, however, used an uncorrect expression for the density of the brine namely $\rho_b = (1 + s_b) \rho_w$ where ρ_w is the density of pure water. An approximate expression for the density at low salinities is $\rho_b = (1 + 0.7 S_b) \rho_w$ and as $s > S$ Schwerdtfeger's expression for the brine density is around 10 % wrong at -20°C , which is reflected as 2 % in the bulk density of the ice.

A better fit to real values is given by the polynomial

$$\begin{aligned} \rho_b(\theta) = & 999.9 - 16.04 \theta - 0.520 \theta^2 - 0.00800 \theta^3 \\ & - 30^\circ\text{C} \leq \theta \leq 0^\circ\text{C} \end{aligned} \quad \dots (3.5)$$

which gives the density of the brine correctly to within 4 % in the interval $-30^\circ\text{C} \leq \theta \leq 0^\circ\text{C}$. The polynomial is constructed from the density values at 0, -8, -16 and -30°C , and is consequently correct at these temperatures. The value at 0°C is taken from "Kalle's tables", the others from Anderson (1960).

Observe that the density of the brine is a function of temperature θ only. This is due to the fact that it is the density at the equilibrium salinity for each temperature in the closed voids. The salinity of the brine is thus implicitly given by the temperature and can be evaluated by, for example, the curve of figure 2.18.

For temperatures below -7.6°C the density is given by the following expression

$$\begin{aligned} \rho(\theta, S) = & (m_b/\rho_b + m_p/\rho_p + m_i/\rho_i)^{-1} \\ \theta < & -7.6^\circ\text{C} \end{aligned} \quad \dots (3.6)$$

where the mass ratios of brine m_b , precipitated salts m_p , and ice m_i are given by the equations 2.11, and the density ρ_p of the precipitated salt $\text{Na}_2\text{SO}_4 \cdot 10 \text{H}_2\text{O}$ is set to 1500 kg/m^3 according to Anderson (1960).

Strictly the mass ratios of the equations 2.11 do not hold below -23°C , but still the function 3.6 for the bulk density gives reasonably accurate results, for the purpose of calculating thermal pressures, that is.

In figure 3.4 below the density of sea ice according to the approximate relations derived in this chapter is compared to values given by Anderson (1960) and Schwerdtfeger (1963) for $S = 20 \text{ ‰}$. It is seen how Schwerdtfeger's calculations deviate 2% from the others. A comparison at $S = 15 \text{ ‰}$ with a diagram given by Kalle (1943) also gives a good fit to equation 3.6 or Anderson's values. The latter's figures are supposed to be most correct. In figure 3.5 the density is drawn for different ice salinities according to the derived expressions.

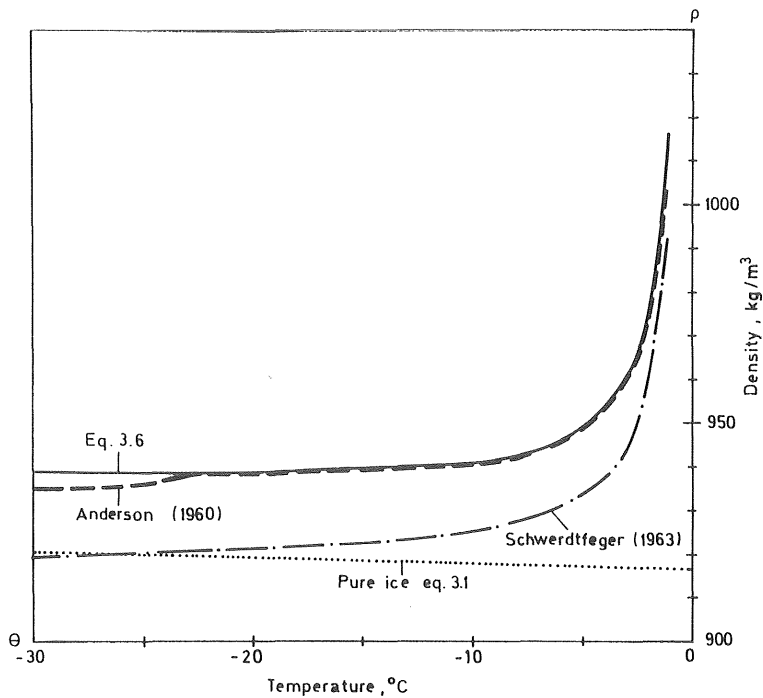


Figure 3.4 A comparison of the density of columnar sea ice with the salinity 20 ‰ as a function of temperature according to the relations in this chapter, and according to Anderson (1960) and Schwerdtfeger (1963).

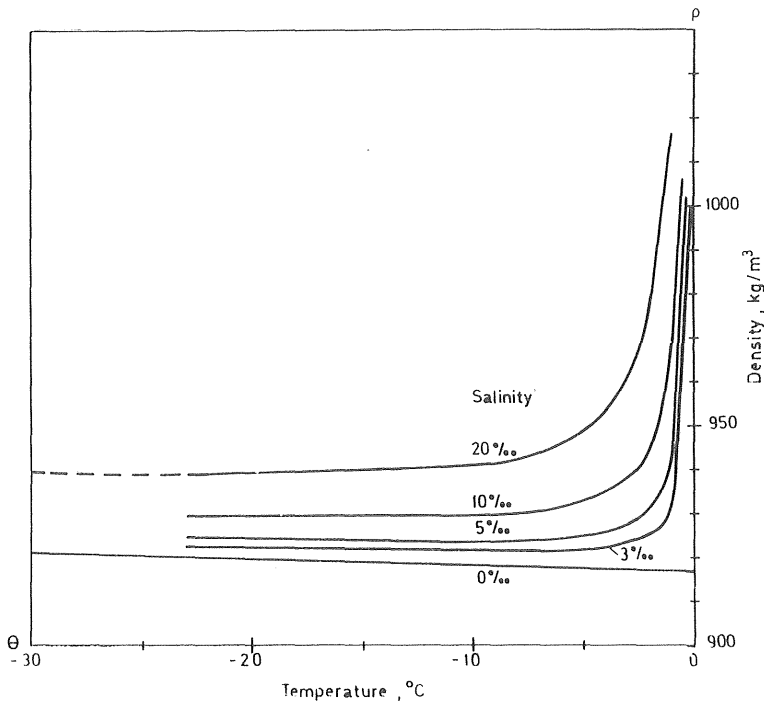


Figure 3.5 The density of columnar sea ice without air inclusions as a function of temperature for different salinities.

3.32 Density of Natural Sea Ice

Natural ice always contains air, and if this air and the brine were in the same voids, it would make density calculations from phase relations misleading. However, experiments largely confirm the assumption that air bubbles and brine voids are separated. It is thus justified to neglect the effect of the included air on the thermal expansion.

For heat conduction and capacity or mechanical properties, however, it is important to know the total void content of the ice. If temperature θ , density $\rho(\theta, S, \nu)$, and salinity S is measured the air content ν can be decided by comparing the actual density $\rho(\theta, S, \nu)$ with the density $\rho(\theta, S)$ according to the theoretical estimations above. The obvious relation is

$$\rho(\theta, S, \nu) = (1 - \nu) \rho(\theta, S) \quad \dots (3.7)$$

The actual density of natural sea ice varies within wide limits. For example Malmgren (1927) reported numerous measurements of arctic sea ice which gave the extremes of 857 through 924 kg/m^3 . As concerns a thickening ice sheet the two main mechanisms influencing the density are the trapping of sea water and the formation of air bubbles. When the ice grows fast a lot of air and salt water is trapped. The air inclusions tend to lessen the density while the salt inclusions have the opposite effect. If the ice grows slowly less air and less salt is confined thus giving more compact but less salty ice. By these mechanisms winter ice gets an astonishingly constant density. Nice examples are the vertical density and salinity profiles taken by Schwerdtfeger (1963), see figure 3.6. For older sea ice gravitational drainage, the temperature gradient effect described above, and the seasonal variations throughout the years have a greater influence, see for example Cox and Weeks (1973) or Malmgren (1927).

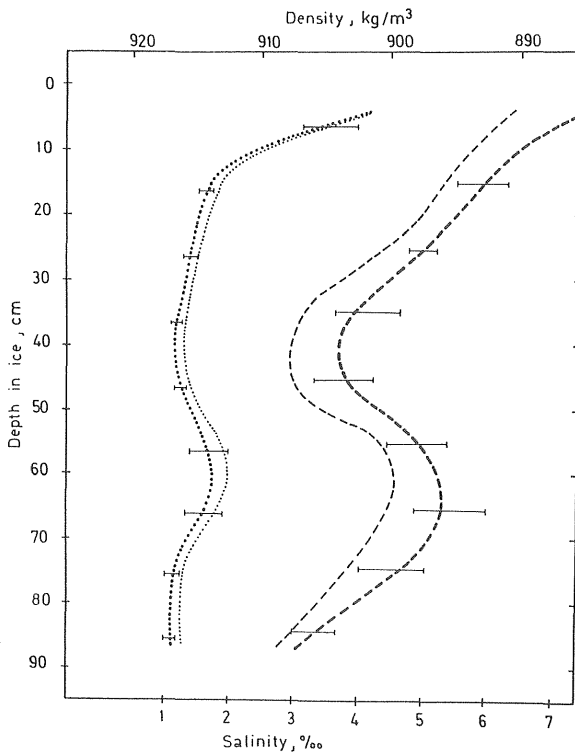


Figure 3.6 Plots of density and of salinity as a function of depth. Curves from left to right are for density on 22 February, density on 3 April, salinity on 3 April and salinity on 22 February. Annual sea ice in Hudson Bay near Churchill, Manitoba. From Schwerdtfeger (1963).

3.4 Thermal Expansion of Ice

While fresh-water ice expands almost linearly, as do most substances the calculations of the density of saline ice show the anomalous behaviour of such ice. For example ice with the salinity 20 ‰ expands with decreasing temperature down to approximately -29°C .

If the curves on densities as functions of temperatures were translated into coefficients of volume expansion γ , these coefficients would be seemingly erratic. An expression for the translation is

$$\gamma = \rho_0 \frac{\partial}{\partial \theta} (\rho^{-1}(\theta, S)) \quad \dots (3.8)$$

Again, the volume of the ice is considered to follow faithfully the volume variations of the components ruling out formation of either voids or internal pressures. The resulting coefficients varies over several orders of magnitude and can be negative (expansion) or positive (contraction). Calculations done by Anderson (1960) are shown in figure 3.7 together with data by Pettersson (Malmgren, 1927) on real ice which show general agreement.

To avoid the discontinuities of equation 3.8 at -7.6°C and -23°C it is more convenient to use the volume as a function of temperature directly when calculating the thermal expansion of sea ice.

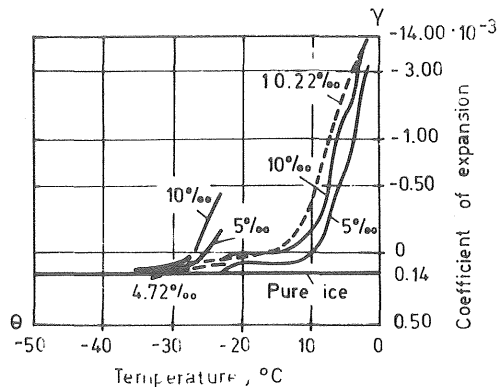


Figure 3.7 Coefficient of volume expansion versus temperature for three salinities for void free sea ice. $S = 0, 5, 10$ ‰. The continuous curves were calculated by Anderson (1960) the dash curves are drawn between points of Pettersson's data.

4. THERMAL CONDUCTIVITY

The thermal conductivity of a homogeneous and isotropic solid is readily defined by the equation

$$q = -\lambda \frac{\partial \theta}{\partial x} \quad \dots (4.1)$$

where

λ is the thermal conductivity

$\partial \theta / \partial x$ the temperature gradient in x-direction

and q the heat flux

For a fluid the conductivity is unimportant in many situations as the main part of the heat is transferred by the motion of the fluid itself. The conductivity of water is for example 0.53 W/(m K) which makes it a good heat insulator in situations where it is kept immobile like in a frog-man's wet suit. Ice conducts heat four times better, but, still the same, ice-covers effectively insulates lakes and rivers in winter, because the turbulent and advective heat transfer are non-existent in the solid ice. In many situations water is used as a coolant because of its high heat capacity and abundance. In the cooling situation the heat is advected or convected away.

Due to the absence or presence of mass transfer the heat flow can be equal to the expression 4.1 or magnitudes higher. Below we will disregard the existence of convection in the brine voids in the ice as well as in the pores of the snow.

Also the distribution and shape of the voids in the ice have important effects on the conductivity. Special simplified assumptions must be made to reach a quantitative result.

4.1 Thermal Conductivity of Fresh-Water Ice

The disparity in values of the coefficient of thermal conductivity of pure ice is rather great, approximately 10 % at -20°C , see figure 4.1. All curves shown in the figure are the results of thorough experiments, and therefore it is difficult to prefer one result to another. Drouin and Michel (1971), for example, used Veinberg's

values, while Pounder (1965) and Hobbs (1974) judged Jacob and Erk's function as being most accurate. Their function for the conductivity $\lambda(\theta)$ as a function of temperature θ can be written

$$\lambda(\theta) = \lambda_0 (1 - a\theta) \quad \dots (4.2)$$

where

$\lambda_0 = 2.24 \text{ W/(mK)}$ is the conductivity at 0°C
and $a = 4.8 \cdot 10^{-3} \text{ }^\circ\text{C}^{-1}$.

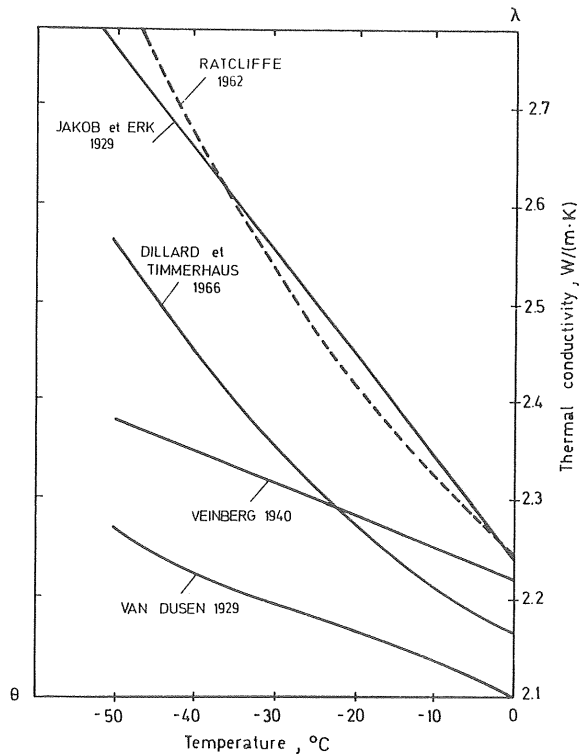


Figure 4.1 Thermal conductivity of ice as a function of temperature according to different authors. (Drouin and Michel 1971, Hobbs 1974).

Equation 4.1 is only valid for pure polycrystalline ice without air inclusions. The thermal conductivity of a single crystal is 5 % greater in directions parallel to the optical axis than perpendicular

to it. The conductivity of polycrystalline ice and single crystals is, however, not significantly different in the light of the variation of absolute values. (See Hobbs, 1974).

For porous ice a technique to evaluate the influence of the voids on the thermal conductivity has been developed by Schwerdtfeger (1963). Considering the air voids uniformly distributed as small spheres in the ice, he utilized a model of the electrical resistivity by Maxwell. The thermal conductivity, $\lambda(\theta, v)$ as a function of temperature θ , and air content v is given as

$$\lambda(\theta, v) = \frac{2\lambda(\theta) + \lambda_a - 2v(\lambda(\theta) - \lambda_a)}{2\lambda(\theta) + \lambda_a + v(\lambda(\theta) - \lambda_a)} \lambda(\theta) \quad \dots (4.3)$$

Here λ_a is the conductivity of air, which is approximately $0.03 \text{ W}/(\text{mK})$ at temperatures between -30°C and 0°C , and thus can be set to nil compared to the conductivity of the compound medium. Then the equation 4.3 reduces to

$$\lambda(\theta, v) = \frac{2(1-v)}{2+v} \lambda(\theta) \approx (1 - 1.43v) \lambda(\theta)$$

$$0 \leq v \leq 0.1 \quad \dots (4.4)$$

As can be seen from figure 4.2 below the reduced equation is a nearly linear function within the interval $0 \leq v \leq 0.1$. It is well approximated by the right hand side of equation 4.4.

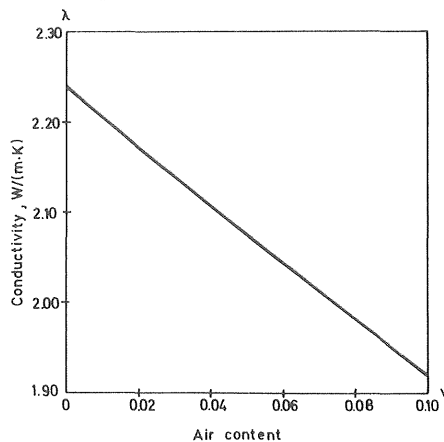


Figure 4.2 The conductivity of porous fresh-water ice as a function of air content at 0°C . The air is supposed to be uniformly distributed as minute spheres.

Because of the assumptions that there is no convection in the air voids, and that they are spherical and evenly distributed, the equation 4.4 is not valid for snow. Most natural ice has an air content of less than 10 % and therefore the equation 4.4 should be reasonably correct for columnar ice (S1, S2, S3), frazil ice (S4) and snow ice (T1). The conductivity of drained snow ice (T2) and frazil ice (S5) with densities as low as 600 kg/m^3 are probably not well described by equation 4.4. In paragraph 4.3 there will be a discussion over the validity of different functions of conductivity in snow. For saline ice the brine voids must also be considered, see the next paragraph.

4.2 Thermal Conductivity of Columnar Sea Ice

Columnar sea ice contains vertical strings of oblong brine voids (see figure 2.17, page 34) as well as more uniformly distributed air bubbles. Schwerdtfeger (1963) computed the vertical conductivity of heat in sea ice considering the ice as consisting of uniformly bubbly ice enclosing vertical brine cylinders. In the vertical direction the ice and brine cylinders then act as parallel thermal resistances.

Anderson (1960) also calculated the thermal conductivity perpendicular to the brine cylinders, and for cases with the brine distributed as spheres and plates as well as according to observations of real ice. He did not include the effect of air bubbles.

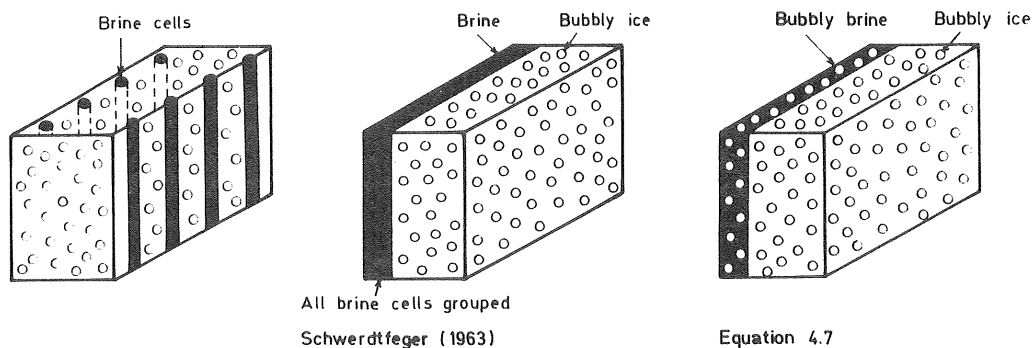


Figure 4.3 Models of columnar sea ice to be used for calculating thermal conductivity in the vertical direction. Compare figure 2.21 page 41.

In connection with thermal ice pressure and the study of heat transfer between the atmosphere and an ice-covered ocean only the vertical conductivity of the columnar sea ice will play a role. Schwerdtfeger modified the diagram of columnar sea ice according to figure 4.3. If the relative cross-sectional areas of brine and ice are denoted A_b and A_i respectively and the thermal conductivities λ_b and $\lambda(\theta, v)$, the conductivity of sea ice in the vertical direction $\lambda(\theta, v, S)$ as a function of temperature θ , air content v , and salinity S becomes

$$\lambda(\theta, v, S) = \lambda_b A_b + \lambda(\theta, v) A_i \quad \dots (4.5)$$

Here $\lambda(\theta, v)$ is in principle decided by equation 4.4 and 4.2 although it may be argued that the air content by volume should be calculated on the bubbly-ice part only and not on the ice as a whole. Thus the relative areas of brine and ice should be corrected for the air, and the volume fractions cannot be used directly. On the other hand, it is not likely that all air bubbles escape the brine voids when these are growing or shrinking. Therefore I think it is equally justified to calculate the vertical conductivity by a simpler set of equations according to the diagram to the right in figure 4.3. This diagram is of course not a sketch of the real physical situation which is better described by the diagram to the extreme left in the figure. The simpler set is

$$\lambda(\theta, S) = \lambda_b \cdot V_b + \lambda(\theta) \cdot V_i \quad \dots (4.6)$$

$$\lambda(\theta, S, v) = \frac{2(1-v)}{2+v} \lambda(\theta, S) \quad \dots (4.7)$$

where $\lambda(\theta)$ as before is calculated by equation 4.2, and the volume fraction of brine is given by equation 2.10, or 2.12 for temperatures below -7.6°C . $V_i = 1 - V_b$ by definition. Equation 4.7 corresponds to equation 4.4.

The conductivity of the brine at equilibrium with ice is by Schwerdtfeger set to

$$\lambda_b = 0.53 (1 + 0.024 \theta + 0.00011 \theta^2) \text{ W/(mK)} \quad \dots (4.8)$$

The conductivity of the precipitated solid hydrates below -7.6°C is not well known, but it has a small influence on the bulk conductivity, why it will be neglected here. For low temperatures when $V_i \rightarrow 1$ the bulk conductivity of columnar sea ice will asymptotically tend to the value of fresh-water ice.

For temperatures close to the melting point, where the ice is more than half liquid by volume, it is felt that the relations above give a bad description of the heat flow. Probably convection will play a great role, and may be the downward resistance to heat transfer will be greater than the upward resistance.

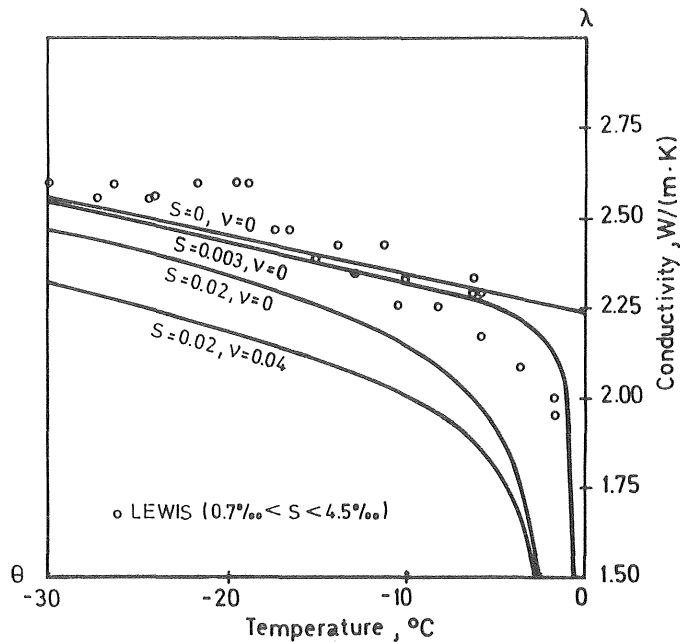


Figure 4.4. The bulk conductivity of columnar sea ice as a function of temperature for different salinities S and air contents v according to the equations 4.6 and 4.7. The plotted values \circ are estimated by Lewis (1966) from temperature profile data $0.7\text{‰} < S < 4.5\text{‰}$.

In figure 4.4 the hypothetical conductivity of sea ice according to the equation 4.7 and 4.6 above is drawn for some combinations of air content and salinities. Values from an arctic-sea ice cover calculated from measured temperature and salinity profiles by

Lewis (1966) are also plotted in the figure for comparison. His values roughly confirm the ideas in this paragraph.

4.3 Thermal Conductivity of snow

The thermal conductivity of snow is much lower than that of ice, because of the great contents of air. Therefore, a snow cover effectively insulates an ice sheet from the temperature variations in the air. Quite a few scientists have put up relations between snow density and thermal conductivity. The results are rather scattered, see below.

The scatter of conductivity coefficients might be due to the fact that in snow the heat is only partly conducted. Other processes in dry snow are radiant energy transfer between grains, mass transfer and sublimation of water vapour along vapour-pressure gradients, and mass transfer of air and vapour in convective flow. The radiant energy transfer between grains is unimportant. Solar radiation must be considered, however, see chapter 7. The convection could be important for the upward flow of energy in loose snow in the ordinary case with cold air and "warm" ice, as this implies an unstable density profile of the included air. In the warming-up case the profile is however different, why the process does not matter.

In wet snow, on the other hand, the only important heat transfer process is the percolation of meltwater. All other processes give no contribution as the gradients of temperature, vapour pressure and air density are all nil. Solar radiation can still penetrate, of course.

In the discussion below it is assumed that the snow is considered completely dry with neither vapour nor melt water in its pores. The effect of the diffusion of water vapour and, especially, its condensation and sublimation will be discussed in paragraph 6.3. The oversimplification may be responsible for some of the disparity between the results on thermal conductivity of snow (Bader and Kuroiwa 1962).

Some results on snow conductivity was quoted by Mellor (1964), table 4.5, and an attempt to evaluate the proposed functions was made by Anisimov (1961). The functions of table 4.5 are drawn in figure 4.6.

Table 4.5 The thermal conductivity of snow as functions of its bulk density. After Mellor (1964) with changes.

Scholar	Year	No. in figures	Conductivity (W/(mK))	Density range ρ_s (kg/m ³)
Abel	1984	1	$2.84 \cdot 10^{-6} \rho_s^2$	140 - 340
Bracht	1949	2	$2.05 \cdot 10^{-6} \rho_s^2$	190 - 350
Deveaux	1933	3	$2.9 \cdot 10^{-2} + 2.93 \cdot 10^{-6} \rho_s^2$	100 - 600
van Dusen	1929	4	$2.1 \cdot 10^{-2} + 4.2 \cdot 10^{-4} \rho_s + 2.2 \cdot 10^{-9} \rho_s^3$	> 50
Jansson	1901	5	$2.1 \cdot 10^{-2} + 8 \cdot 10^{-4} \rho_s + 2.5 \cdot 10^{-12} \rho_s^4$	80-500
Kondrat'eva	1945	6	$3.56 \cdot 10^{-6} \rho_s^2$	350
Proskur'akov	?	7	$2.1 \cdot 10^{-3} + 1.01 \cdot 10^{-3} \rho_s$?
Sulakvelidze	1958	8	$5.1 \cdot 10^{-4} \rho_s$	350
Yosida	1955	9	$419 \exp(0.004606 \rho_s)$	70 - 400
Equation 4.4, ice		10	$4.48 \rho / (2750 - \rho_s)$	825 - 917

Anisimov (1961) explained that in snow the heat is conducted mainly through the ice grains because their conductivity is, by far, greater than the conductivity of air, if convection and vapour diffusion are neglected. Compare paragraph 4.1. Therefore there ought to exist a relationship between the density and the thermal conductivity, but they should not be linearly related, because an increase in density brings about not only a greater ice volume per unit volume of snow, but also a proportionally faster increase of the area of contact points, the grain size being the same.

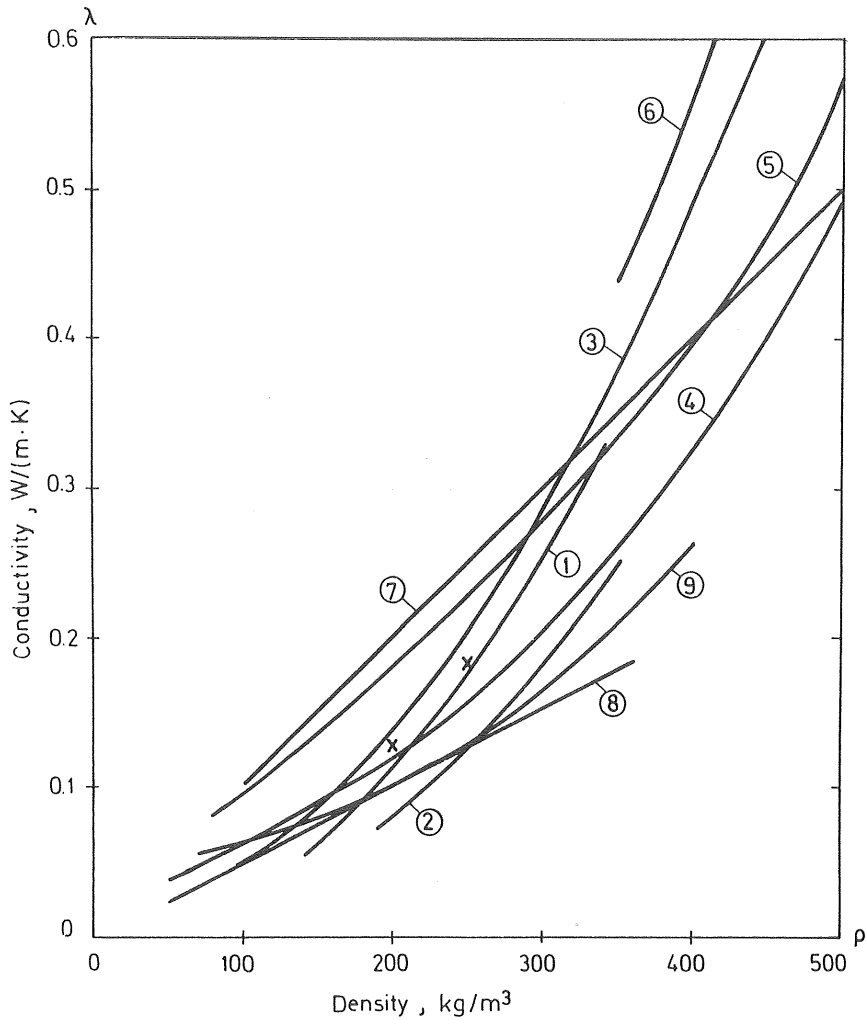


Figure 4.6 The thermal conductivity of snow as functions of its bulk density. The numbers of the curves correspond to those of table 4.5.

x Values given by Gold (1958).

He then divided the proposed expression for the specific conductivity as a function of snow density by the thermal conductivity of an ice monolith of the same height and mass as a unit volume of snow but with a smaller cross section. In this way he formed an expression for the relative heat conductivity of snow, and from the reasoning

above this relative conductivity should increase with increasing density, and formulas giving constant or even decreasing values were dismissed. See figure 4.7. The functions disqualified are numbers 4, 5, 7, 8 and 9

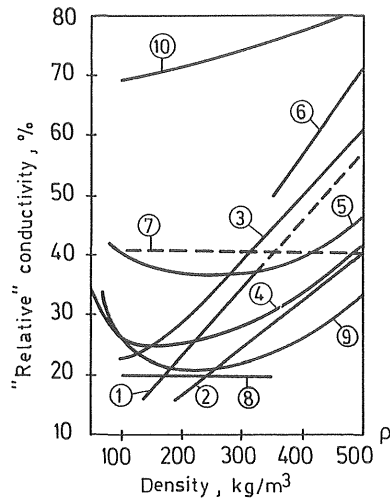


Figure 4.7 The "relative" conductivity of Anisimov (1961) in per cent. For an explanation see the text. The numbers of the curves are listed in table 4.5 and correspond to those in figure 4.6.

Kondrat'eva's function, 6, on the other hand, that should be valid when the density is greater than 350 kg/m^3 , is disregarded because it gives too high a specific conductivity. At 700 kg/m^3 , for example, it gives the same conductivity as that of pure ice, which obviously must be wrong.

Equation 4.4, that is included in the list for reference only, gives a "relative" conductivity of around 70 % within the range of snow densities of interest. This is far better than what is reasonable for snow, and, of course, that is because the snow structure and ice structure is very different. The equation passes Anisimov's test in the respect that the conductivity grows slightly faster than the content of solid ice.

Of the remaining functions, numbers 1, 2 and 3, it is difficult to prefer one to the other, because the conductivity of the snow is likely to depend on the structure of the snow as well as on density. The effect of grain size and shape have not been evaluated, to my knowledge. In paragraph 3.2 we concluded that reasonable bulk density values of dry snow covers are 200 to 300 kg/m³. A conservative value at 300 kg/m³, giving an overestimation of the heat flow through the snow cover, could be picked as 0.3 W/(mK) according to figure 4.6.

5. SPECIFIC AND LATENT HEATS

To estimate the heat exchange through an ice surface the condensation or sublimation on the ice surface can be important. The heat capacity of a piece of sea ice depends on the latent heat of melting of the ice in it and the heat capacity of the contained brine and ice. Therefore some information on the specific and latent heats of the substance of water is given below. Most of the information is taken from Pounder (1965) or Dorsey (1940).

5.1 Specific and Latent Heats of Water

The specific heat capacity of water is $4.23 \cdot 10^3$ J/(kgK) at 0°C , $4.27 \cdot 10^3$ at -10°C , and $4.35 \cdot 10^3$ at -20°C .

To be able to calculate the heat capacity of a piece of sea ice, we have to know the specific latent heat of fusion of water at different temperatures. A rise of the temperature of sea ice involves, as pointed out before, a gradual melting of ice. The specific latent heat of fusion can be described by the following equation

$$L_i = 3.34 \cdot 10^5 (1 + 6.77 \cdot 10^{-3} \theta) \text{ J/kg} \quad \dots (5.1)$$

The latent heat of sublimation is mostly supposed to be the sum of the latent heat of fusion and the latent heat of vapourization. Since the latter two change in opposite directions with temperature the specific heat of sublimation decreases but slowly from $2.84 \cdot 10^6$ J/kg at -40°C to $2.83 \cdot 10^6$ J/kg at 0°C .

5.2 Heat Capacity of Fresh-Water Ice

The determination of the specific heat capacity of fresh-water ice presently considered most accurate was done by Dickinson and Osborne in 1915, see for example Pounder (1965). For their measurements they used four very pure samples of ice between -40°C and 0°C . Their result could be fitted by equations of the form

$$C_i = a + b \theta + c/\theta^2 \quad \dots (5.2)$$

where θ is the temperature in $^\circ\text{C}$ and a, b and c constants. a and b were the same for all specimens while c varied, $c < 0$.

The absolute value of c decreased with increasing purity of the specimens, and c/L_i , where L_i is the specific latent heat of fusion of ice, was interpreted as the actual freezing point of the solution. This will be shown to be true in paragraph 5.3 below. The first two terms of equation 5.1 would thus represent the true specific heat of pure ice at constant pressure.

$$C_i = C_o (1 + d \theta) \quad \dots (5.3)$$

where

$$C_o = 2.12 \cdot 10^3 \text{ J/(kg K)}$$

$$\text{and } d = 3.68 \cdot 10^{-3} / ^\circ\text{C}$$

5.3 Heat Capacity of Sea Ice

Essentially the heat capacity of a piece of sea ice depends on the mass of water changing state during the change of temperature, and on the specific heat capacity of brine and pure ice. The heat capacity of dissolved salts is neglected. Denoting the specific heat capacities of pure water and ice by C_w and C_i respectively, the mass ratios by m_w and m_i , and the specific latent heat of melting of ice by L_i , the following relation holds for the change of heat content, dQ , at an increase in temperature $d\theta$, between -7.6°C and 0°C .

$$dQ = -L_i dm_i + C_w m_w d\theta + C_i m_i d\theta \quad \dots (5.4)$$

The ratio of the mass of pure water to the whole mass is

$$m_w = 1 - m_i - S = m_b - S \quad \dots (5.5)$$

and introducing m_b and m_i from equations 2.9a and b yields

$$dQ = -L_i \frac{S ds_b}{s_b} + \left[\frac{S}{s_b} (C_w - C_i) + C_i (1 - S) \right] d\theta \quad \dots (5.6)$$

From equation 2.5 $s_b = \alpha_1 \theta$ and $ds_b = \alpha_1 d\theta$, and thus the specific heat capacity of sea ice between the melting point θ_m and -7.6°C is

$$C(\theta, S) = \frac{dQ}{d\theta} = -\frac{L_i}{\alpha_1} \frac{S}{\theta^2} + \frac{S}{\alpha_1 \theta} (C_w - C_i) + (1 - S) C_i \quad \dots (5.7)$$

Inspecting this equation it can be seen that for $\theta \approx -1^\circ\text{C}$ the first term on the right hand side is two order of magnitudes greater than the second term and that the first term corresponds to c/θ^2 in equation 5.2. Setting them equal gives

$$-c/L_i = S/\alpha_1 \quad \dots (5.8)$$

which according to equation 2.5 is a good approximation of the melting point $\theta_m = s/\alpha_1$ for low salinities.

Schwerdtfeger (1963) has shown that a calculation in the interval $-23^\circ\text{C} \leq \theta < -7.6^\circ\text{C}$ within 2 % gives the same result as equation 5.7, in this way justifying its extension down to -23°C . Since it

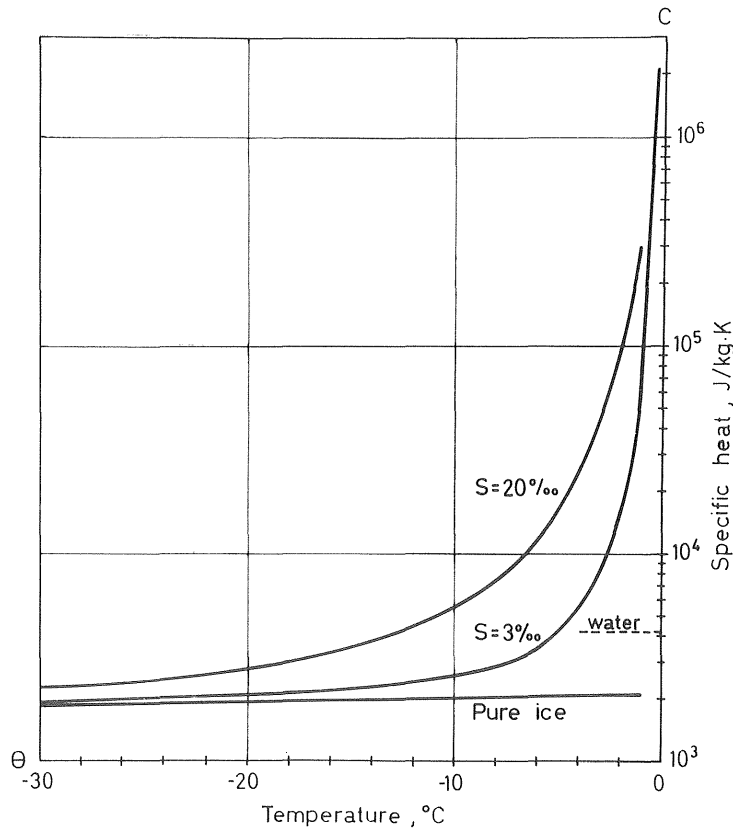


Figure 5.1 The specific heat capacity of sea ice as a function of salinity and temperature.

approaches the specific heat of pure ice asymptotically for decreasing temperatures, it can be used for practical purposes at even lower temperatures. The specific heat capacity of the ice is drawn in figure 5.1 according to equation 5.7 for some salinities.

From the discussion above it is evident, that there is no true latent heat of melting or melting temperature of sea ice, since the phase change is continuous from sea ice to sea water. At the temperature, θ the heat deficit per unit mass (enthalpy) relative to the melting point θ_m is by integration of equation 5.7.

$$Q = \int_{\theta}^{\theta_m} C(\xi, S) d\xi =$$

$$= \int_{\theta}^{\theta_m} \left\{ -\frac{L_i S}{\alpha_1 \xi^2} + \frac{S}{\alpha_1 \xi} (C_w - C_i) + (1-S) C_i \right\} d\xi \quad \dots (5.9)$$

Assuming L_i , C_w , C_i as constants the following relation appears

$$Q = \frac{L_i S}{\alpha_1} \left(\frac{1}{\theta_m} - \frac{1}{\theta} \right) + (1-S) C_i (\theta_m - \theta) + \frac{S}{\alpha_1} (C_w - C_i) \ln \theta_m / \theta \quad (5.10)$$

The melting temperature is calculated by equation 2.5. The result of the integration is shown in figure 5.2. As a comparison the curve for pure ice with constant heat capacity is also plotted.

Strictly equation 5.10 is valid only for $\theta \geq -7.6^\circ\text{C}$ but, in the light of other uncertainties and that the deviation is only 2% to the correct value, it can be used for calculating the temperature change of a sea-ice cover down to -30°C .

It should again be observed that equation 5.10 only holds for a closed system of sea ice and brine. That is, the equation can be used for daily temperature changes. For periods like months or years, gravitational drainage and the movements of brine voids along temperature gradients will change the salinity and thus the heat capacity of the layers in an ice sheet. For fast temperature changes Ono (1966) observed a temperature lag of 0.5°C for 20 minutes and 0.25°C for 1 h in the voids of sea ice, so that the rate of change of tem-

perature must not be too fast either. At temperatures close to the melting point it is also doubtful whether equations 5.7 or 5.10 give a good description as the ice is fairly permeable to sea water.

Sometimes the concept latent heat is used about sea ice. It is then meant the latent heat of the pure ice in an ice cover with a certain salinity, S . If the salinity of the originally trapped brine was equal to that of the ambient sea, S_a , it was shown in paragraph 2.53 that the brine ratio at trapping was $m_{bo} = S/S_a$ (equation 2.13). Thus the corresponding ice ratio is $m_{io} = (1 - S/S_a)$ and consequently the released latent heat is

$$L_S = (1 - S/S_a) L_i \quad \dots (5.11)$$

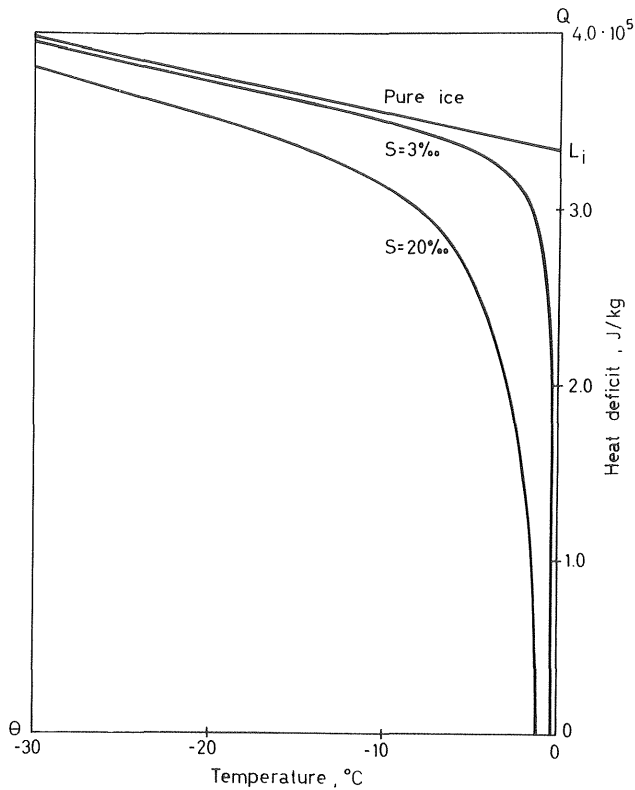


Figure 5.2 The deficit of heat (negative enthalpy) of sea ice relative to its freezing point as a function of temperature for the salinities 3 and 20 ‰, according to equation 5.10.

5.4 Heat Capacity of Snow and Porous Ice.

The heat capacity of the ice phase of snow and porous ice is by definition the product of its density and specific heat capacity. This is, however, only true for snow or ice whose pores do not contain melt water or vapour. In a similar way to what was done with sea ice, the very correct heat capacity should be corrected for the freezing, condensation or sublimation in the pores. For snow, the migration or diffusion of water vapour should also be taken into account. The melt water leaking down through a snow cover may also cause a considerable redistribution of energy.

For snow an attempt to evaluate the influence of water vapour is done in paragraph 6.3. Cold fresh-water ice could, however, be considered completely dry. The small amount of water vapour that is included has little influence on the thermal diffusion. In a candled ice cover, whose structure is very loose and filled with water, the thermal diffusion will, of course, be greatly influenced.

6. TEMPERATURE DIFFUSIVITY

The diffusion equation 1.1 is the basic tool for describing the rate of change of temperature in a solid in terms of the boundary conditions. The properties of the solid appear in this equation in terms of a single parameter, a , called the temperature diffusivity or the coefficient of thermal diffusion. It is defined as

$$a = \frac{\lambda}{\rho C} \quad \dots (6.1)$$

where

- λ is the thermal conductivity
- ρ is the density
- C is the specific heat capacity

The factor λ is the quantity known with least accuracy. This is, because it is difficult to evaluate it by the comparatively direct way of equation 4.1, that is, by measuring a temperature gradient and the corresponding heat flux, for the heat flux is extremely difficult to measure. In fact most of the values in the literature on the thermal conductivity of ice were obtained from studies on the rate of change of temperature distributions, so that actually the diffusivity was the constant measured. This was for example the case with Lewis's values on thermal conductivity in figure 4.4.

The quality of the values on thermal conductivity must, of course, be judged with these problems in mind. For saline ice the difficulties are still more pronounced, because the temperature diffusivity is strongly dependent on the temperature and consequently the solution of the equation of diffusion is extremely difficult. It is felt that, may be, the diffusivity of saline ice is better calculated indirectly from known properties of its constituents.

6.1 Temperature Diffusivity of Fresh-Water Ice

The coefficient of thermal diffusion of fresh-water ice can be calculated according to the functions for density, thermal conductivity and capacity chosen in the earlier chapters. Experiments give however the coefficient directly, see above.

$$a(\theta) = \frac{(1 + \gamma \theta)(1 - a_0)}{(1 + d\theta)} \cdot \frac{\lambda_0}{\rho_0 C_0} \approx (1 + b\theta) a_0 \quad \dots (6.2)$$

The functions used for ρ , λ and C are 3.1, 4.2 and 5.3.
The constants used are given again as follows

$$\begin{aligned} \rho &= 916.82 \text{ kg/m}^3 \\ \gamma &= 1.445 \cdot 10^{-4} / ^\circ\text{C} \\ \lambda_0 &= 2.24 \text{ W/(mK)} \\ a &= 4.8 \cdot 10^{-3} / ^\circ\text{C} \\ C_0 &= 2.12 \cdot 10^3 \text{ J/(kg K)} \\ d &= 3.68 \cdot 10^{-3} / ^\circ\text{C} \end{aligned}$$

The function 6.2 is drawn in figure 6.1 below and it is seen that it is decreasing with temperature. It can be well approximated by a linear function, $b = -9.28 \cdot 10^{-3} / ^\circ\text{C}$

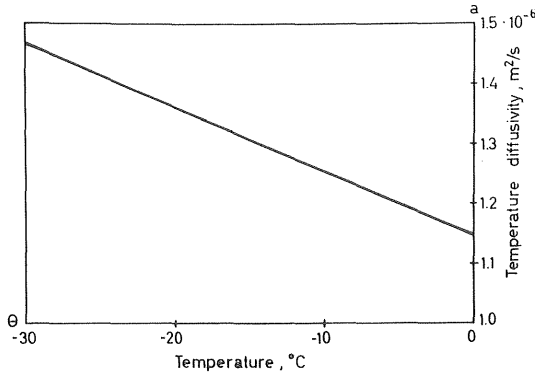


Figure 6.1 The temperature diffusivity of fresh-water ice as a function of temperature.

For many practical purposes the dependence on temperature can be neglected, although the temperature diffusivity is more strongly dependent on temperatures than its constituent parameters.

The diffusivity of ice as a function of its air content v is likewise had from equations 3.2 and 4.4

$$a(\theta, v) = \frac{2}{2+v} a(\theta) \approx (1 - 0.5v) a(\theta) \quad \dots (6.3)$$

At 10 % air content this gives a 5 % decrease of the diffusivity. The diffusivity is thus less sensitive to air content variations than its factors, and actually it can be treated as independent of the air content. For very accurate calculations it can be noted that equation 6.3 is an almost linear function.

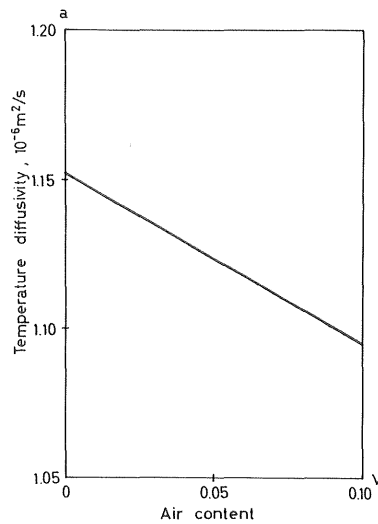


Figure 6.2 The temperature diffusivity of porous fresh-water ice as a function of its air content at 0°C .

6.2 Temperature Diffusivity of Sea Ice

As opposed to fresh-water ice the temperature diffusivity of saline ice is extremely dependent of temperature. The diffusivity varies over several orders of magnitude. This is due to the fact that all the factors of equation 6.1 contribute to the decrease with temperature. The diffusivity is shown for some salinities in figure 6.4 below. It is calculated according to the tedious system of equations that are necessary, namely equation 2.9 through 2.12,

3.4 through 3.6, 4.6, 4.8 and 5.7

$$a(\theta, S) = \frac{\lambda(\theta, S)}{\rho(\theta, S) C(\theta, S)} \quad \dots (6.4)$$

As is the case with fresh-water ice the temperature diffusivity is practically independent of the air content, and the uncertainty of equation 6.4 is so great that it is not meaningful to regard the air content in any context.

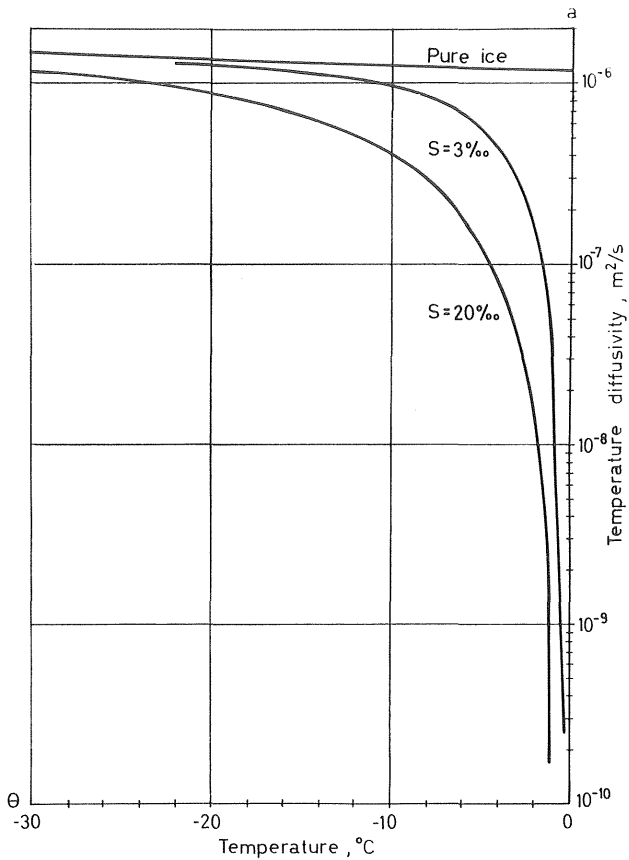


Figure 6.3 The temperature diffusivity of columnar sea ice in the vertical direction as functions of temperature for the salinities 0, 3 and 20 ‰.

6.3 Temperature Diffusivity of Snow

The main factor for the conductivity and diffusivity of dry snow is its bulk density. Equation 6.1 gives with the conductivity function of Deveaux, table 4.5,

$$a_s = \frac{\lambda_s}{\rho_s C} = \frac{a + b \rho_s^2}{\rho_s C_o} \quad \dots (6.5)$$

where

$$\begin{aligned} a &= 2.9 \cdot 10^{-2} \text{ W/(mK)} \\ b &= 2.93 \cdot 10^{-6} \text{ Wm}^2 / (\text{kg K}) \\ C_o &= 2.12 \cdot 10^3 \text{ J/ (kg K)} \\ \rho_s &= \text{the bulk density of snow} \end{aligned}$$

The function 6.5 is drawn in figure 6.4 below. At the bulk density value 300 kg/m^3 it gives a reasonable value of $4.6 \cdot 10^{-7} \text{ m}^2/\text{s}$ which is approximately 40 % of the value for solid fresh-water ice.

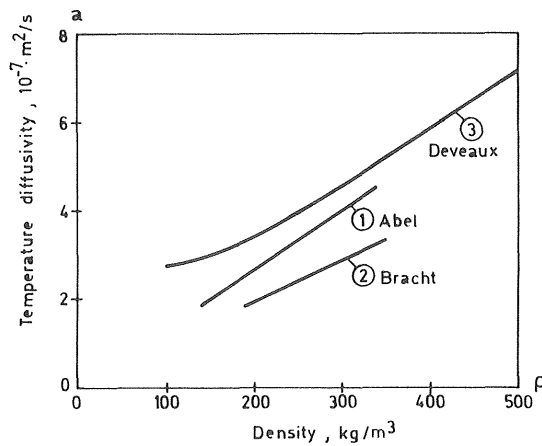


Figure 6.4 The temperature diffusivity of snow as a function of its bulk density according to the relations for thermal conductivity of Abel, Bracht and Deveaux. See table 4.5.

Now, it has been pointed out that the diffusion, sublimation, and condensation of water vapour may add to the heat diffusion in snow, to such extent that the equation of thermal diffusion in its ordinary

form is no longer valid, and consequently values are not reliable if they are founded on 6.5 or on experiments presupposing equation 1.1.

$$\frac{\partial \theta}{\partial t} = a_s \frac{\partial^2 \theta}{\partial x^2} \quad \dots (6.6)$$

Assume that the water vapour is saturated in the pores of the ice. The mass of water vapour per unit volume, a_w , can then be considered a function of only temperature.

In the equation of thermal diffusion the rate of sublimation of water vapour per unit volume is included, that gives

$$\frac{\partial \theta}{\partial t} = a \frac{\partial^2 \theta}{\partial x^2} - \frac{L}{\rho C_i} q \quad \dots (6.7)$$

where

- a is the bulk thermal diffusivity due to conduction
- θ temperature
- t time
- x space coordinate
- L the specific heat of sublimation
- ρ the bulk density
- C_i the specific heat capacity of ice
- q the mass rate of sublimation per unit volume

The equation of gas diffusion has a form equal to that of equation 6.7 and if the source of water vapour is included the following relation appears

$$\frac{\partial a_w}{\partial t} = D \frac{\partial^2 a_w}{\partial x^2} + q \quad \dots (6.8)$$

where a_w is the mass content of water vapour per unit volume, and D is the coefficient of gas diffusion in the porous medium considered. D is of course a function of the structure of the snow. In snow avalanches the vapour transport itself is of great importance, because the migration of the ice is responsible for the development of an avalanche structure of the snow.

A combination of 6.7 and 6.8 gives

$$\begin{aligned} \frac{\partial \theta}{\partial t} \left(1 + \frac{L}{C_i \rho} \frac{\partial a_w}{\partial \theta} \right) = \\ = a \left(1 + \frac{D}{a} \frac{L}{C_i \rho} \frac{\partial a_w}{\partial \theta} \right) \frac{\partial^2 \theta}{\partial x^2} + \frac{L D}{C_i \rho} \frac{\partial^2 a_w}{\partial \theta^2} \left(\frac{\partial \theta}{\partial x} \right)^2 \end{aligned} \quad \dots (6.9)$$

This equation was formulated by Sulakvelidzw (1959). If we study processes where $\partial^2 \theta / \partial x^2$ is of the same order of magnitude as $(\partial \theta / \partial x)^2$, the last term on the right hand side can be neglected. A comparison with equation 6.6 then gives the temperature diffusivity as

$$a_s = \frac{1 + \frac{D L}{a C_i \rho} \frac{\partial a_w}{\partial \theta}}{1 + \frac{L}{C_i \rho} \frac{\partial a_w}{\partial \theta}} a \quad \dots (6.10)$$

From equation 6.10 it can be seen that if a and D are of the same order of magnitude the equation 6.6 is essentially correct. If $D \ll a$ there will be a small reduction of the rate of change of temperature due to local sublimation or condensation of water vapour. On the other hand, if $D \gg a$ the temperature diffusivity will be greater than the diffusivity due to conduction.

The molecular diffusion of equation 6.10 can be set to the free diffusion of air $D = 3.13 \cdot 10^{-4} \text{ m}^2/\text{s}$ and the thermal diffusion can be set to that of the ice phase $a = 1.15 \cdot 10^{-6} \text{ m}^2/\text{s}$. Both constants are overestimations because the molecular diffusion is restricted by the snow flakes and the conduction is restricted by the bad contact between grains. Inserted in 6.10 they give the quotient a_s/a to 1.45 at 0°C and 1.10 at -20°C for $\rho = 300 \text{ kg/m}^3$. At -30°C the difference between a and a_s can be neglected. For very loose snow the quotient a_s/a grows to over 2 at 0°C . ($\rho = 150 \text{ kg/m}^3$, $\theta = 0^\circ\text{C} \rightarrow a_s/a = 1.9$). It is thus obvious that the heat transport by mass diffusion along the gradient of vapour pressure should not be disregarded.

As the temperature of the snow is not given in context with recommended formulas on heat conduction, the mass diffusion is one reason to blame the discrepancies between the formulas as well as the structure of the snow. It would be interesting to evaluate the formulas by means of equation 6.10. In lack of this evaluation the function of Deveaux will be used.

7. OPTICAL PROPERTIES

In this chapter some optical concepts and definitions will be given that are necessary for the understanding and calculation of the energy balance of ice or snow fields. This involves some fundamentals of solar radiation as well.

7.1 Radiation from Black Bodies

An ideal black body emits radiation at a rate that is proportional to the fourth power of its absolute temperature according to the Stefan-Boltzmann law:

$$J = \sigma T^4 \quad \dots (7.1)$$

where

J is emitted effect per unit area
 T the absolute temperature of the body
 σ the Stefan-Boltzmann constant = $5.76 \cdot 10^{-8} \text{ W/K}^4 \text{ m}^2$

The emitted radiation is distributed over the wave-lengths according to the Planck law

$$J_\lambda = c_1 \lambda^{-5} (\exp(c_2 / \lambda T) - 1)^{-1} \quad \dots (7.2)$$

where

λ is the wave-length
 J_λ the emitted effect per unit area and unit band width
 c_1 and c_2 constants

and the maximum intensity of the spectrum J_λ can be calculated by the Wien law

$$\lambda_{\max} = a / T \quad \dots (7.3)$$

where a is a constant = $2.898 \cdot 10^{-3} \text{ mK}$.

The integral over all wave-lengths of the spectrum ordinate gives, by definition, the total emitted radiation that is

$$J = \int_{\lambda} J_{\lambda} d\lambda \quad \dots (7.4)$$

In a first approximation the sun and the surface of the earth, or a snow field, can be considered as black bodies. The temperature of the sun is often given as 6000 K which gives the maximum of solar radiation at the wave-length 0.5 μm . The ideal spectrum is given by equation 7.2, and it is shown in figure 7.1 below where it is adjusted for the distance to the sun. More than 99 % of the energy is emitted at wave-lengths less than 4 μm .

The temperature of an ice cover or snow field is approximately 270 K which gives its black radiation maximum at 11 μm and most of the energy is emitted at wave-lengths greater than 4 μm . The solar irradiation and the thermal radiation from an ice field are thus of very different wave-lengths and they consequently have very different properties.

- a) Radiation distribution from a body with the temperature 6000 K 1.6 kW/m²
- b) Solar radiation outside the atmosphere 1.4 kW/m²
- c) Direct solar radiation at the surface of the earth perpendicular to the direction of radiation 0.9 kW/m²
- d) Diffuse solar irradiation at the surface of the earth 0.1 kW/m²
- e) Band of absorption for water vapour and carbon-dioxide
- f) Absorption for oxygen and ozone
- g) Radiation from a black body with the temperature 270 K (0°C) 0.3 kW/m²

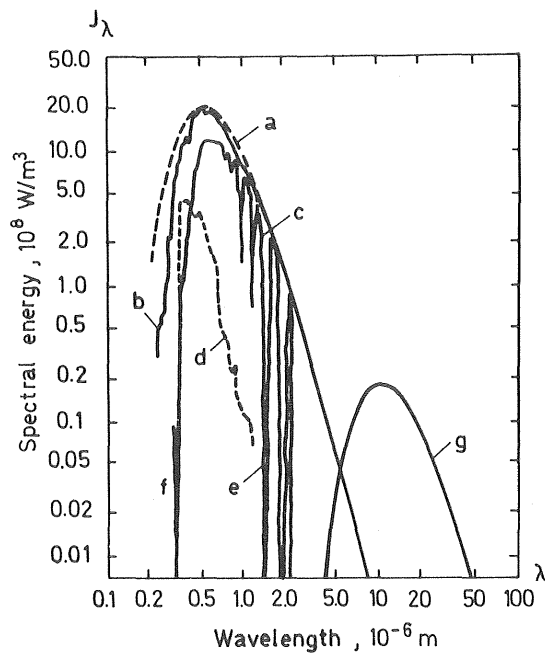


Figure 7.1 Spectra for solar and sky radiation at clear sky. After Sellers (1965) with changes.

7.11 Solar Radiation

At the outer boundary of the atmosphere the distribution of solar radiation is very accurately given by equation 7.2 for the visible and infrared part of the spectrum ($\lambda > 0.4 \mu\text{m}$). See figure 7.1. The radiation flux is approximately 1.4 kW/m^2 , and although this figure depends on the distance to the sun, $\pm 3.4 \%$, it is sometimes referred to as the solar constant.

When the solar radiation enters and penetrates the atmosphere of the earth it is effected in several ways by the gases, clouds and particles in the atmosphere. It is out of scope of this book to give detailed information on this matter. A few facts will, however, be given. For further details it is referred to standard literature like the textbooks by Sellers (1965), Liljequist (1962) or Brunt (1944).

Radiation of wave lengths shorter than $0.2 \mu\text{m}$ is completely absorbed by ozone and oxygen, and therefore this radiation never reaches the surface of the earth. Furthermore water-vapour and carbon dioxide absorb radiation within several wave-length bands. The absorbed radiation is of course transformed into heat.

The direct solar radiation is also reduced by scattering. The scattering caused by the molecules of the air is most intensive for short wave-lengths, and this makes the sky blue. Bigger particles as water drops, ice crystals and dust, on the other hand, scatter light equally over the spectrum. Hazy or dusty air therefore gives the sky a whitish complexion, and the clouds look white. When the altitude of the sun is lowered, the rays of the sun have to pass a longer way through the atmosphere, and a greater part of the short waves is scattered causing the sun to appear red.

The irradiation at the ground level is composed of direct solar radiation and scattered so called sky radiation. On a clear day the direct radiation is approximately 0.9 kW/m^2 and the sky radiation 0.1 kW/m^2 . On an overcast day the global irradiation is largely diffuse and only a fourth of that of a clear day.

The spectral distribution of the irradiation depends on the shifting atmospheric conditions particularly the water vapour content and

cloudiness. Generally, however, 50 % of the incident energy lies between 350-700 μm , 25 % between 700-1200 μm and 25 % between 1200-4000 μm . The reflectivity and absorptivity of ice will be given below in these three wave-length bands. (Lyons and Stoiber, 1959b).

7.12 Emissivity

The ratio of the emissive power of a surface to the emissive power of a black body is called the emissivity of the surface. At thermal equilibrium the emissivity is equal to the absorptivity. Water, snow and ice are, for example, nearly perfect black bodies to radiation with approximately the same "temperature" ($\lambda \approx 10 \mu\text{m}$). To solar radiation, which has another "temperature" ($\lambda \approx 0.5 \mu\text{m}$), their behaviour is quite different. Their properties with respect to solar radiation is treated in subsequent paragraphs.

The emissivity of water and ice is accurately measured to 0.97 (Hobbs 1974, Paily et al 1974). For snow the information given by Sellers (1965) range from 0.82 - 0.995 but for a sufficiently thick layer it should be taken the same as for ice.

7.2 Refraction

The refraction of a beam of light passing from one material into another depends on the difference of the speed of light in the two materials. This gives the Snell law

$$\frac{\sin \alpha}{\sin \beta} = \frac{c_1}{c_2} \quad \dots (7.5)$$

where α and β are the angles of incidence and refraction respectively and c_1 and c_2 the speed of light in the two materials, see figure 7.2

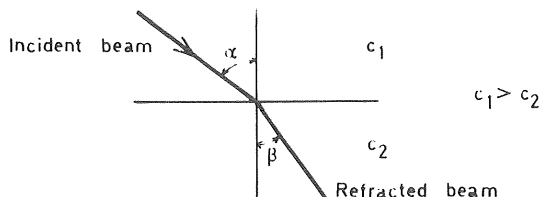


Figure 7.2 Refraction of light.

The refractive index of a material is defined as the speed of light in empty space c_0 to the speed of light in the material. If the refractive indices are denoted $n_1 = c_0/c_1$ and $n_2 = c_0/c_2$, equation 7.5 can be written

$$n_1 \sin \alpha = n_2 \sin \beta \quad \dots (7.6)$$

7.21 The Optic Axis

In a beam of unpolarized light the electric vector oscillates in any direction normal to the beam. If such a beam is passed through a polaroid filter the electric vector in the emergent beam vibrates in one direction only and the light is said to be plane-polarized.

In an isotropic material the speed of light is the same in all directions. Like many other crystalline materials, however, ice is optically anisotropic. A beam of light is generally broken up into two waves which travel at different velocities. The crystal is said to be doubly refracting. One wave travels with the same velocity in all directions and is called the ordinary wave. Its vector surface of velocity is a sphere, see figure 7.3.

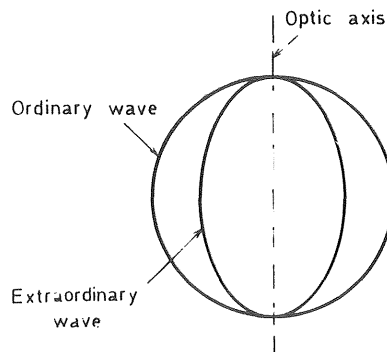


Figure 7.3 The spherical and ellipsoidal vector surfaces for an optically uniaxial and positive crystal. The difference between the surfaces is exaggerated.

The velocity of the other wave varies with the direction of propagation, and it is called the extraordinary wave. Its vector surface

wave is an ellipsoid of revolution, and in the case of optically uniaxial crystals, like ice, the spherical vector surface coincides with the ellipsoidal surface at two points only, and these are the ends of the axis of revolution of the ellipsoid. If the extraordinary wave is slow relative to the ordinary wave the crystal is said to be optically positive, otherwise optically negative.

The electric vector of the ordinary wave always oscillates perpendicular to the optic axis, that is, perpendicular to a plane defined by the direction of propagation and the axis. The electric vector of the extraordinary wave oscillates in the plane. The ordinary wave and extraordinary wave are thus polarized at right angles to each other.

Ice is a doubly refracting, uniaxial, and optically positive crystal. The optic axis coincides with the crystallographic c-axis.

7.22 Refractive Indices

Two principal indices are defined for uniaxial crystals, one based on the velocity of the ordinary wave c the other on the velocity of the extraordinary wave perpendicular to the c-axis. For ice this is the minimum velocity c_e . Thus

$$\begin{aligned} n_o &= c_o / c \\ n_e &= c_o / c_e \end{aligned} \quad \dots (7.7)$$

The quantity $n_e - n_o$ is called the birefringence of the crystal.

Measurements of n_e and n_o are accounted for by Hobbs (1974). They vary both with wave-length and temperature. Here, we shall only notice that ice has the lowest refractive indices of all the known minerals. At -3°C and $0.4916 \mu\text{m}$ $n_o = 1.3126$ and $n_e = 1.3140$. The birefringence is thus also small: 0.0014.

7.23 Polarization Effects

Plane-polarized light that is transmitted through an ice crystal at some angle of incidence to the optic axis will generally not be polarized in the original plane when leaving the crystal, due to the re-

sulting phase difference of the ordinary and extraordinary wave. Placing an ice crystal between two polaroid filters, polarizer and analyser, it is then possible to decide the direction of the optic axis or c-axis. This is done using a universal stage, see for example Michel and Ramseier (1971).

Another effect of polarization is, that when white light is used for the illumination, a crystal may appear coloured between crossed polaroids. If the crystal is just thick enough the shortest waves in the visible spectrum will be out of phase when leaving the crystal. These waves, violet, is then subtracted from the light and the complementary colour of green-yellow appears. For successively thicker crystals other wave-lengths are subtracted and other colours emerge.

7.3 Reflection

The solar radiation incident on a cover of snow or ice is partly reflected, partly absorbed, and the remainder is transmitted to the ground and water underneath. Estimations of the absorption of solar radiation have been of interest to scientists studying the heat budget of arctic areas, for the prediction of snow melting, and for forecasting snow avalanches. Recently some attention has also been given to the biological productivity in ice-covered seas. The rather extensive literature contains numerous contradictory data caused by the variation of ice properties and the difficulty of measuring transmission of light.

The reflection against ice and snow varies within wide, limits due to the nature of the surface and the altitude of the sun. For solar radiation the reflection coefficient, r , for polished surfaces is given by

$$r = \frac{1}{2} \left[\frac{\sin^2(\alpha - \beta)}{\sin^2(\alpha + \beta)} + \frac{\tan^2(\alpha - \beta)}{\tan^2(\alpha + \beta)} \right]; \lambda < 4 \mu\text{m} \quad \dots (7.8)$$

For notations see figure 7.2. Equation 7.8 is drawn in figure 7.4 for $0 \leq \alpha \leq \pi/2$ rad.

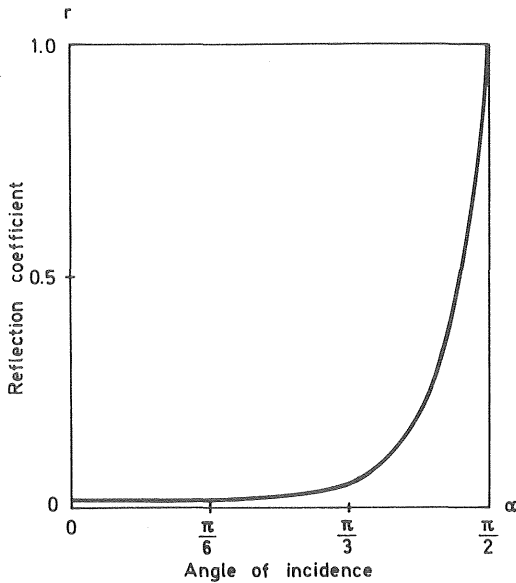


Figure 7.4 The reflection coefficient of a polished flawless ice surface at -3°C and $\lambda = 0.5 \mu\text{m}$.

In equation 7.8 the first term is for light polarized perpendicular to the plane of incidence and the second term for light polarized in the plane of incidence. For normal incidence ($\alpha = 0$) in the visible range equation 7.8 reduces to approximately

$$r = \left[\frac{n - 1}{n + 1} \right]^2 \quad \dots (7.9)$$

where n is the refractive index between the adjoining materials. For air-ice equation 7.9 gives the reflection coefficient 1.8 % and for ice-water 1.6 %.

7.31 Reflection Coefficients of Ice and Snow

For a polished surface of clear ice the reflection coefficient is given by equation 7.8 in the visible range. At normal incidence this means that approximately 2 % is reflected. However, hoar-frost markedly increases the reflection. Lyons and Stoiber (1959 b), for example, tell that a breath of air on a sample made the transmissivity drop from 90 to 3 %.

Light may also be reflected from particles, bubbles or brine voids enclosed in the ice and not only from the very surface. Thomas (1964) measured reflection coefficients of 65 and 66 % at solar altitudes of $24^{\circ}09'$ and $9^{\circ}27'$ respectively for sea ice under natural conditions. For the corresponding angles of incidence figure 7.4 gives 9 and 68 %. In both cases the reflection must have been largely diffuse. Gaitskhoki (1970a) measured coefficients of reflection for normal incidence on sea ice in the laboratory in the wave-length band $0.35 \mu\text{m} - 1.0 \mu\text{m}$. They are given for different types of ice in figure 7.8. For ice, bubbly ice, snow ice, and sea ice the results range from 4% to 15%. For snow he got 65 to 80 %.

Mellor (1965) measured reflection against natural snow fields. His results showed a reflection coefficient ranging between 77 and 98 %, see figure 7.5. By comparing extinction data, paragraph 7.4, with the measured surface reflection he could show that only 40-80 % of the reflected energy was reflected from the very surface of the snow field. The remainder must therefore be reflected from grains at some depth in the snow. Bergen (1975) tried to relate the albedo to the grain size and density of the snow cover. The deduced expression looks promising, but the only available test values were reflection coefficients between 85 and 78 %. See also Bader and Kuroiwa (1962).

The crystal orientation in an ice cover is observed to influence the reflection coefficient of ice. Lyons and Stoiber (1963) state that microscopic vapour bubbles form within the ice crystals when an ice cover is warmed. The phenomenon is called Tyndall figures. The vapour leaves the crystal along the basal planes, and therefore ice with vertical basal planes (horizontal c-axes, ice S2) soon get rid of the vapour bubbles, but if the basal planes are horizontal (vertical c-axes, ice S1) the figures stay in the ice. The latter ice gets a grayish appearance and reflects light better. Because of this the crystal orientation of an ice field can some times be seen with the bare eye in spring, when the ice cover has been exposed to the sun. The vertically oriented crystals are grayish and a little elevated above the surrounding crystals.

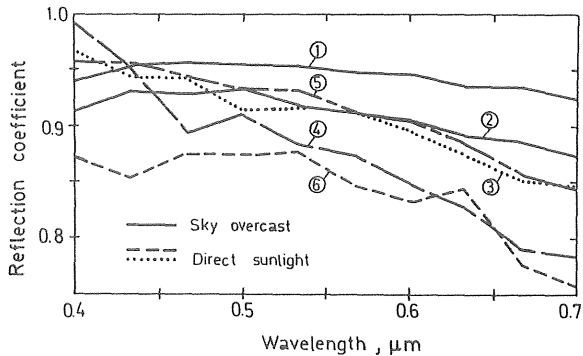


Figure 7.5 Field measurements of reflection coefficient

1. Fresh dry snow, 280 kg/m^3 , 0°C
2. 1-2 cm fresh snow, 100 kg/m^3 , on older snow, 400 kg/m^3 , 0°C
3. Metamorphosed snow, 430 kg/m^3 , 0°C
4. Slightly metamorphosed new snow, 200 kg/m^3 , 0°C
5. Wet snow, two days old, 400 kg/m^3 , melting during test
6. Same as 5. after 5 hours more melting

After Mellor (1965).

The reflection of ice for the infrared parts of the solar spectrum is not much discussed in ice-engineering literature although 50 % of the incident energy lies at wave-lengths between 0.7 and $4 \mu\text{m}$. Bergen (1975) includes the infrared waves when integrating over the spectrum. Hobbs (1975) cites a lot of information. In the range $0.7 - 4 \mu\text{m}$ the reflection coefficient varies between 5.1 and 0.7 %, if the angle of incidence is smaller than $\pi/3$ rad. At $\lambda = 10 \mu\text{m}$ the same source gives the reflexion coefficient to 0.4 % which is a proof of the statement that ice is a nearly perfect black body for radiation characteristic of its own temperature.

A simplified summary of coefficients of reflexion found in the literature or guessed is given below in table 7.6 for normal incidence.

Table 7.6 Reflection coefficient for different types of ice at normal incidence. Generalized values found in literature and guessed values. The latter are within parentheses.

Type of Ice	Wave-length μm	Coefficient %	Reference
Clear mono- or polycrystalline ice, wet or smooth surface	0.35 - 0.7	2 - 4 [*]	Equation 7.9
	0.7 - 1.2	2 - 4 [*]	Gaitskhoki (1970 a)
	1.2 - 4.0	2 - 5 [*]	Bode 1909 (in Hobbs 1974) Gaitskhoki 1970 a Bode 1909 (in Hobbs 1974)
Columnar sea ice, snow ice, hummocked ice, wet or smooth surface	0.35 - 0.7	5 - 15 ^{**}	Gaitskhoki (1970 a)
	0.7 - 1.2	5 - 12 [*]	"-
	1.2 - 4.0	(2 - 10) ^{**}	Guess
Bubbly columnar ice, old wet snow, snow ice and sea ice common rough surface or hoar-frosted	0.35 - 0.7	40 - 80	Thomas (1963) Mellor (1965)
	0.7 - 1.2	(60)	Lyons and Stoiber (1959 b)
	1.2 - 4.0	(30)	Guess "-"
Dry snow	0.35 - 0.7	80 - 96	Gaitskhoki (1970 a)
	0.7 - 1.2	60 - 70	Thomas (1963) Mellor (1959 b)
	1.2 - 4.0	(60)	Gaitskhoki Guess

* These values should be adjusted upwards according to figure 7.4 for angles of incidence greater than 60°. (Solar altitudes less than 30°)

7.4 Absorption of Solar Radiation

Of the sun radiation incident on a snow or ice field some is reflected, some absorbed and some transmitted, see figure 7.7. The attenuation with depth of the refracted fraction of the light is due to the absorption of the radiation in the ice but is also caused by the scattering of air bubbles, brine voids, snow grains, or dust. Some of the light is even scattered back out of the ice or snow cover and is actually measured as a part of the reflected light.

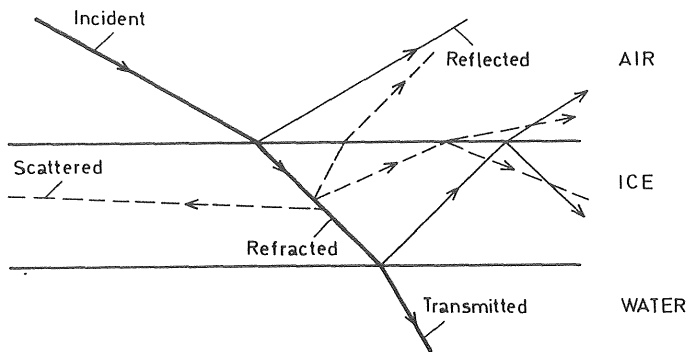


Figure 7.7 Reflexion, refraction, scattering, and transmission of a beam of light in an ice cover.

Although Gaitskhoki (1970b) has set up a sophisticated model taking into account the internal scattering, the ordinary exponential law of attenuation will be used here, because of its simplicity and the lack of detailed data for the other

$$J_z = J_o e^{-kz} \quad \dots (7.10)$$

Here J_z is the intensity of radiation at the distance z from the upper surface and J_o is the intensity of refracted radiation. If the incident radiation is J then by definition

$$J_o = (1 - r) J \quad \dots (7.11)$$

where r is the reflection coefficient.

For flawless fresh-water ice k equals the absorption coefficient. For natural ice, snow, or turbid water, where the equation is only approximately valid, k is often called the coefficient of extinction. In such cases it takes into account both absorption and scattering. It should be pointed out that in optics another quantity is meant by the extinction coefficient μ which is the imaginary part of the complex refractive index and related to k (for flawless ice) by

$$k = 4 \pi \mu / \lambda \quad \dots (7.12)$$

where λ is the wave-length.

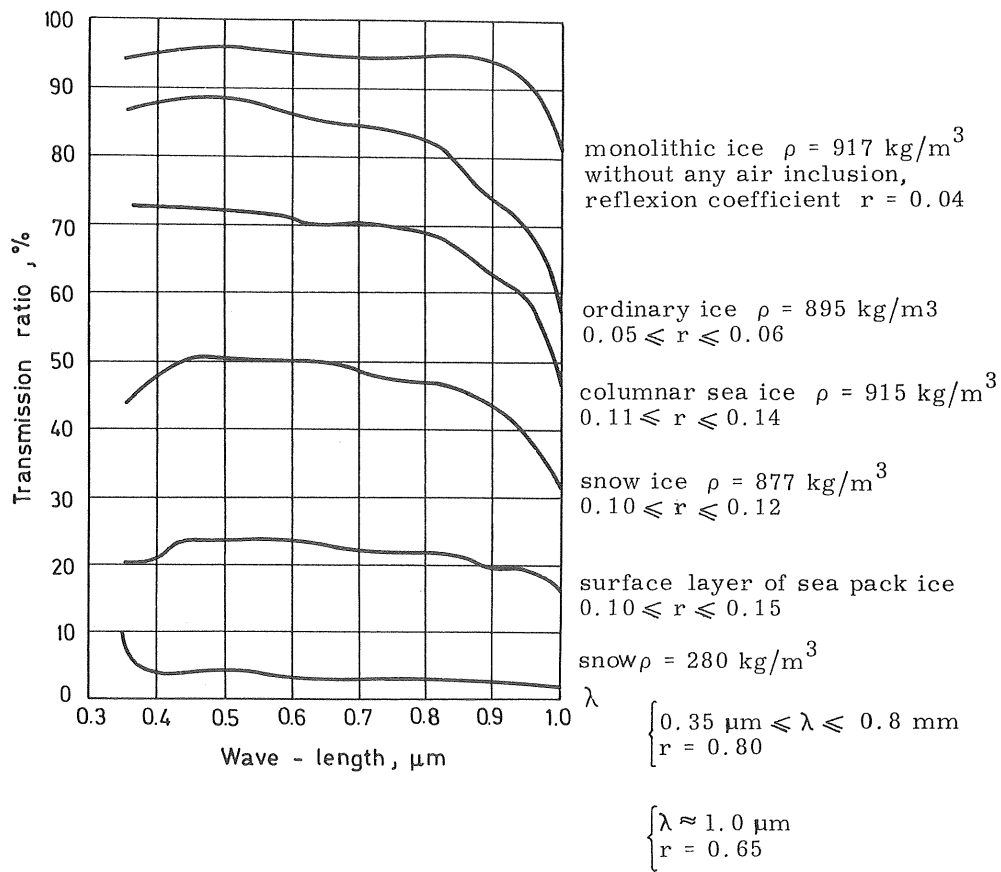


Figure 7.8. Spectral curves of the ratio of transmitted light for sample of ice 2 cm thick. Gaitskhoki (1970 a).

7.41 Absorptivity of Ice

Lyons and Stoiber (1959b) have written a critical review of older investigations on the absorptivity of ice and have also performed a lot of measurements themselves. They measured the transmission through samples and corrected for reflection at the upper and lower surfaces using equation (7.9). Another method is to embed photocells at different depths in an ice cover, that is, to measure J_z at several different depths. This latter method was used by Thomas (1964). Gaitskhoki (1970 a) used samples but measured both reflected and transmitted light. Older investigations cited by Lyons and Stoiber (1959 b) were made with samples of different thicknesses. This method is, however, less accurate according to them.

In order to show how greatly the absorption can differ, the transmission ratio through 2 cm thick samples of ice and snow as measured by Gaitskhoki (1970 a) is given in figure 7.8.

The order of magnitude of the extinction coefficient in the visible region is 1 m^{-1} , but passing into the infrared region the absorptivity of ice increases sharply. For example a plate of ice 1 mm thick absorbs practically all radiation for which the wavelength is greater than $3 \mu\text{m}$ and a frozen soap-film cuts off nearly all radiation with wave-lengths greater than $6 \mu\text{m}$. A part of the infrared absorption spectrum is given in figure 7.9 below. The absorption for long wavelengths ($\lambda > 1.2 \mu\text{m}$) is less dependent on the air content and purity of the ice, because the absorption is due to molecular and intermolecular vibrations in the lattice. For further details see Hobbs (1974).

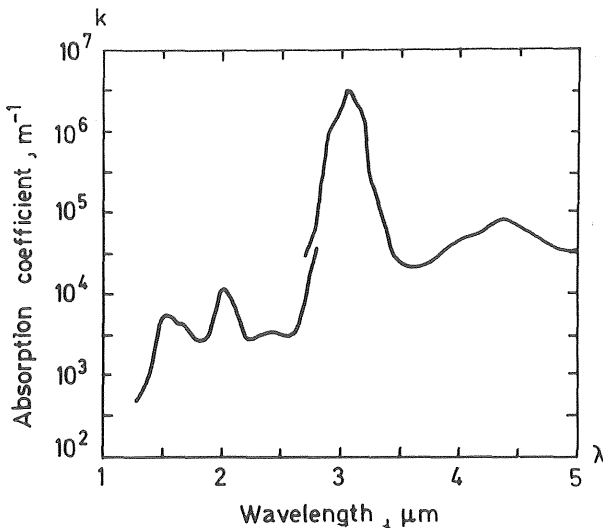


Figure 7.9 Infrared absorption spectrum of ice in the range $1.4 \mu\text{m} \leq \lambda \leq 4 \mu\text{m}$. After Hobbs (1974) with changes.

7.42 Absorptivity of snow.

Mellor (1965) has measured the extinction coefficient of snow with various properties, see figure 7.10. Unfortunately he only conducted experiments within the visible range $0.4 - 0.7 \mu\text{m}$. This is very unsatisfactory as 50% of the energy of the direct sunlight lies over $0.7 \mu\text{m}$. The extinction coefficient was found to depend on both grain size and snow density.

Mellor's conclusions run as follows. "Extinction in snow depends on scattering and absorption. In fine-grained snow (diameter $\approx 0.2 \text{ mm}$), such as cold wind-packed snow, scattering is dominant and k is inversely proportional to λ . k is inversely related to grain size; it increases sharply as grain size decreases below 0.3 mm , the rate of increase being directly related to λ . In low density snow k increases with increasing density, eventually reaching a maximum and thereafter declining as density tends to the ice limit". "In coarse-grained snow typical of a melting snow cover absorption becomes important. As grain size increases and angularities are subdued, spectral selection in extinction tends to reverse so that k gradually becomes directly related to λ ".

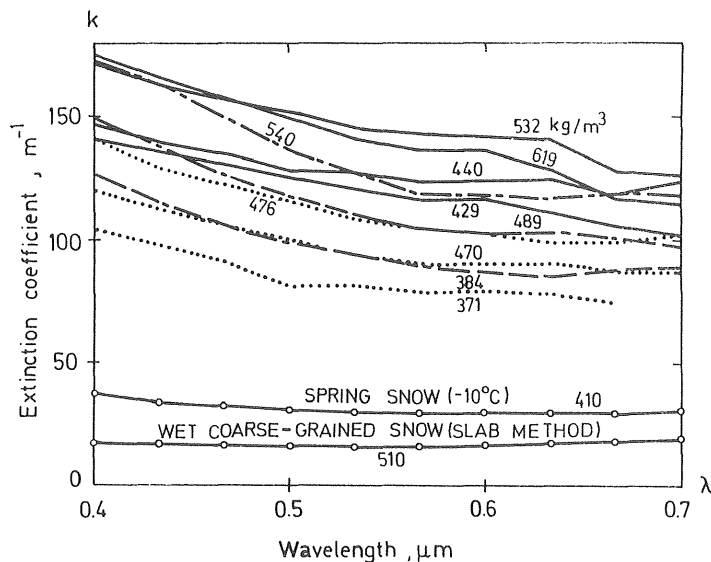


Figure 7.10 Summary of results from Mellor's (1965) attenuation experiments. The figures on the curves are snow densities (kg/m^3). The dry snow was of the mean grain size 0.2 mm (very uniform) —, 0.3 mm (range $0.2 - 0.7 \text{ mm}$) — — — —, and 0.6 mm (range $0.2 - 1.1 \text{ mm}$) — — — —. The spring snow had the mean grain size 2 mm (range 0.5 to 5 mm) and the wet coarse-grained snow 1 mm .

7.43 Generalized Values on the Extinction Coefficient.

Table 7.11 below is a summing-up of available information on the extinction coefficient. The values for clear ice and bubbly ice are those recommended by Lyons and Stoiber (1959 b). The basis for the other figures are given in the table. The given values are supposed to be accurate within one order of magnitude if taken as mean values over respective range of wave-length. For reference some values for water are also listed.

Table 7.11. Coefficient of extinction for different types of ice. Generalized values found in literature and guessed values. The latter are within parentheses.

Type of ice	Wave-length μm	Coefficient m^{-1}	Reference
Clear fresh-water ice	0.35 - 0.7	0.2	Lyons and Stoiber (1959 b)
	0.7 - 1.2	2	"-
	1.2 - 4	(5000)	"-
Bubbly fresh-water ice	0.35 - 0.7	3	Lyons and Stoiber (1959 b)
	0.7 - 1.2	(10)	"-
	1.2 - 4	(10000)	"-
Columnar sea ice	0.35 - 0.7	2	Thomas (1964)
	0.7 - 1.2	10	Gaitskhoki (1970)
	1.2 - 4	(10000)	Guess
"Bubbly" sea ice	0.35 - 0.7	40	Gaitskhoki (1970)
	0.7 - 1.2	70	"-
	1.2 - 4	(10000)	Guess
Snow ice	0.35 - 0.7	30	Gaitskhoki (1970)
	0.7 - 1.2	50	"-
	1.2 - 4	(10000)	Guess
Fine-grained snow mean diameter 0.2 - 0.6 mm	0.35 - 0.7	120	Mellor (1965)
	0.7 - 1.2	200	Gaitskhoki (1970)
	1.2 - 4	(10000)	Guess
Course-grained snow, mean dia- meter 1-2 mm	0.35 - 0.7	30	Mellor (1965)
	0.7 - 1.2	(200)	Guess
	1.2 - 4	(10000)	Guess
Pure water	0.35 - 0.7	0.05	Harvey (1966)
Ocean water	0.35 - 0.7	0.20	"-
Coastal water	0.35 - 0.7	0.45	"-

8. ENERGY BALANCE OF AN ICE OR SNOW COVER

The energy balance of ice or snow covers have mostly been studied in order to evaluate their growth or decay. Although such studies have often been performed with sophisticated methods, they work with daily, weekly, or monthly mean values, why they can seldom be used directly for the calculation of the fast temperature fluctuations that are responsible for thermal ice pressure.

On the other hand, studies aiming at thermal ice pressures tend to oversimplify the energy balance of the surface by simply setting the surface temperature equal to the air temperature, or only calculating advective heat transfer. The short and long wave radiation play, however, very important roles. The short wave radiation increases the rate of change of temperature, especially, at clear weather. The long wave back radiation can cause a considerable depletion of the ice surface temperature, which is very pronounced by clear and calm weather. Omitting radiation therefore results in an underestimation of the daily temperature variations in an ice cover.

Below follows some fundamentals of the heat balance just in order to place the thermal and optical properties of ice and snow in a wider context. For evaluations of heat balance functions it is referred to Paily et al (1974) or Sweers (1976) and for a discussion of the balance of ice or snow fields to Pounder (1965), Liljequist (1962), or Bengtsson (1976).

The energy flux of an ice cover can be written

$$q_t + q_e + q_m = q_c - q_b + q_l + q_s \quad \dots\dots(8.1)$$

where

q_t is the rate of change of stored heat per unit area due to change of temperature of the ice or snow

q_e the rate of heat per unit area used for evaporation

q_m the rate of heat used to melting per unit area

q_c convective (sensible) heat flux

q_b intensity of long-wave back radiation

q_l intensity of incoming long-wave radiation

q_s net incoming short-wave radiation flux

The only term of equation (8.1) above that has not been accounted for at all in this text is the convective heat transfer q_c which is a complicated function of wind speed, the stability of the air near the ground, and the difference between air and surface temperature. The evaporation term depends also on these conditions as the rate of evaporation must be identical to the transport of vapour away from the surface. The term q_e can therefore be moved to the right hand side of the expression (8.1).

8.1 Radiation Balance

The radiation fluxes of the ice cover consists of the absorbed solar radiation, q_s , the incoming long-wave radiation, q_l , and the long-wave back radiation, q_b .

Net flux of solar radiation

$$q_s = (1 - r) \cdot J \quad \dots\dots(8.2)$$

where r is the reflexion coefficient or albedo of the surface and J the solar irradiation calculated on a unit horizontal area. See paragraph 7.11. J is a function of solar altitude, cloudiness and the transmissivity of the air but can be reasonably well calculated or measured.

Flux of back radiation

$$-q_b = -\epsilon \sigma T^4 \quad \dots\dots(8.3)$$

where ϵ is the emissivity of the surface. For ice or snow $\epsilon = 0.97$. See paragraph 7.12. σ is Stefan-Boltzmann's constant and T is the absolute temperature of the surface.

Flux of incoming long-wave radiation.

$$q_l = \epsilon \epsilon_a \sigma T_a^4 \quad \dots\dots(8.4)$$

where ϵ and ϵ_a are the emissivities of the surface and the atmosphere respectively and T_a the absolute temperature of the air.

The long-wave term (8.3) is easily estimated but the term (8.4) can cause problems. Air temperature, T_a , and humidity, e_a , are mostly measured 2 m above the ground, but the incoming radiation originates from higher altitudes since the long-wave radiation easily penetrates the atmosphere at least at clear weather. By clean, calm and cold weather the difference in air temperature between the ground level and 5 or 10 m

level can be 10 to 20 K or more. At Maudheim (71°S) (midnight, July 2, 1950) the temperature at 10 m was measured to -30°C but at ground level to -44°C. This was not unusual. If this strong inversion was broken up by a strong wind the temperature often rose 10 K and sometimes 20 K (Liljequist, 1962). Another problem is to estimate the emissivity of the air, ϵ_a , which is mainly a function of its content of water vapour. An Ångström type formula is

$$\epsilon_a = a + b \exp(-ce_a) \quad \dots (8.5)$$

where e_a is the water vapour pressure of the air measured at 2 m level. $a = 0.802$, $b = 0.236$ and $c = 1.15 \cdot 10^{-3} \text{ Pa}^{-1}$. The cloudiness also influences the emissivity of the atmosphere, which can be roughly estimated by multiplying q_l in equation (8.4) by $(1 + 0.027 C_s)$ where C_s is the cloud cover in eighths (octas) of the sky.

The total radiation balance, that is the sum of equations (8.2), (8.3) and (8.4), is often negative for winter conditions. Below in figure 8.1 radiation fluxes, measured by Schwerdtfeger and Ponder (1963) on the ice of Hudson Bay (58°49'N, 94°14'W), are shown as an example.

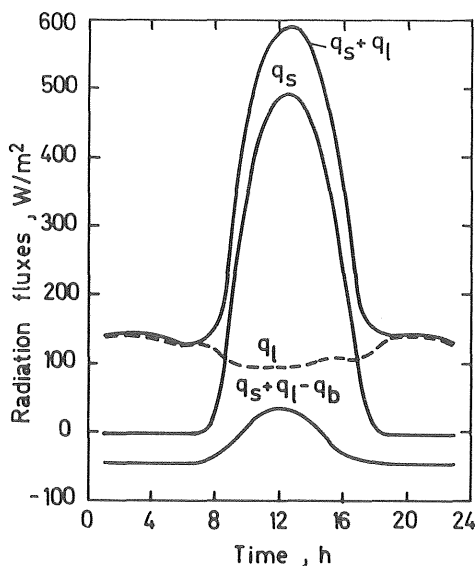


Figure 8.1 Radiation fluxes on Feb. 28, 1962? clear day. Measured by Schwerdtfeger and Ponder (1963) on the ice of Hudson Bay (58°49'N, 94°14'W). For notations see under equation (8.1).

8.2 Heat transfer

The convective heat transfer from the air to the surface consists of "sensible" heat, because of the temperature difference between air and surface, and latent heat, because of the vapour transport to the surface and condensation on it. The latent heat transfer is often written

$$- q_e = f(u)(e_a - e) \quad \dots\dots(8.6)$$

where e_a is the vapour pressure of the air and e the saturation vapour pressure at the ice or snow surface, and $f(u)$ is the wind-speed function. The wind-speed function have been extensively measured and Paily et al (1974) refer to over 50 very different formulae, but recommend one by Rymsha - Donchenko for winter conditions over a water surface.

$$f(u) = \rho L a (1 + bu + c(T - T_a)) \quad \dots\dots(8.7)$$

where ρ is the density of water
 L the specific heat of sublimation
 u the wind speed at 2 m
 T the surface temperature
 T_a the air temperature at 2 m
 $a = 2.42 \cdot 10^{-11}$ m/sPa
 $b = 0.49$ s/m
 $c = 4.36 \cdot 10^{-2}$ K⁻¹

The water vapour (latent heat) as well as the temperature (sensible heat) of the air are transported away in the same mass of air. The transport of the two properties then ought to be governed by the same wind-speed function. The sensible heat transfer is usually written

$$q_c = f(u) \gamma (T_a - T) \quad \dots\dots(8.8)$$

where $\gamma \approx 61$ Pa/K is called pycrometric constant. The total convective heat transfer is consequently

$$q_c - q_e = f(u) (\gamma (T_a - T) + (e_a - e)) \quad \dots\dots(8.9)$$

8.3 Examples on the Energy Balance

It might be of interest to show some examples on the heat balance of an ice cover. If the energy-flux equation (8.1) is rewritten for stationary conditions, for which the rate of change of stored heat $q_t = 0$, it runs

$$q_m = q_c - q_b + q_l + q_s - q_e \quad \dots\dots(8.10)$$

For notations see under equation (8.1). Where the surface temperature of the ice is below freezing the melting term q_m only consists of the freezing at the lower boundary of the ice, where the temperature is 0°C . Thus the melting term can be written

$$q_m = -\lambda \theta / h \quad \dots\dots(8.11)$$

where

- λ is the conductivity of the ice
- θ is the surface temperature ($^\circ\text{C}$)
- h is the depth of the ice cover

The assumptions are approximately true if the growth of the thickness of the ice cover is not too fast.

Equation (8.10) can now be solved for the surface temperature, θ , of the ice cover. The absolute temperatures T and T_a must, of course, be exchanged for $\theta + 273.15^\circ$ and $\theta_a + 273.15^\circ$ respectively. Below some examples are shown for the weather and ice conditions given in the figures.

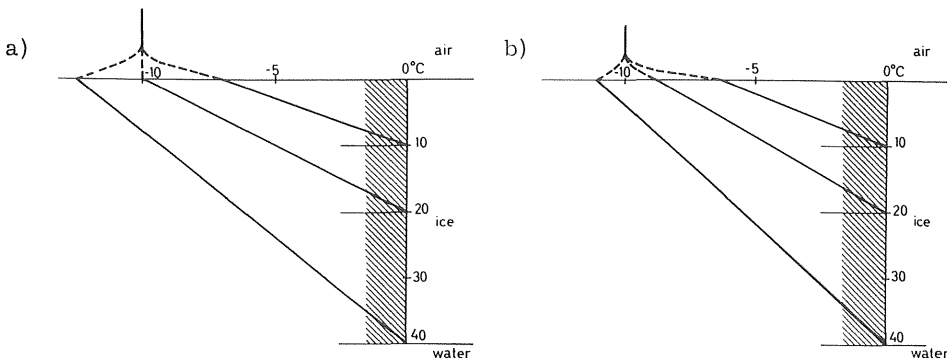


Figure 8.2 Temperatures in ice covers free from snow:

air temperature	a)	-10°C	b)	-10°C
wind speed		2 m/s		2 m/s
vapour pressure		0.03 Pa		0.03 Pa
cloudiness in octas		0/8		8/8
short-wave radiation (night conditions)		0		0

Depth of the ice covers 0.10, 0.20 and 0.40 m.

Computed according to Bergdahl and Wernersson (1977).

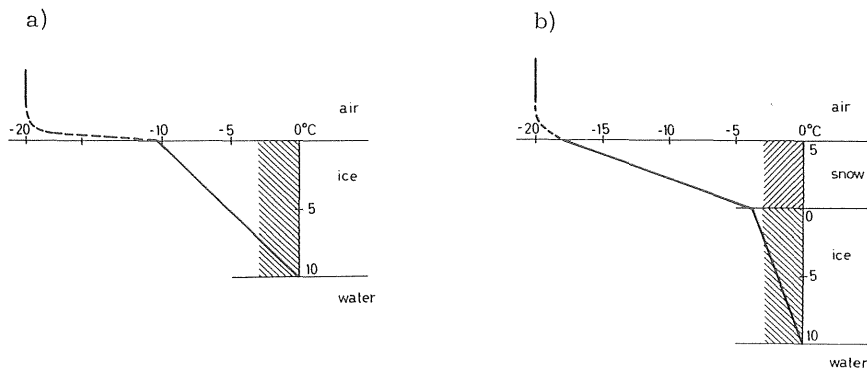


Figure 8.3 The temperature in a 0.10 m thick ice cover
 a) without snow and b) with 5 cm of snow
 ($\lambda = 0.3 \text{ W/mK}$), wind speed 2 m/s,
 air temperature -20°C , vapour pressure 0.03 Pa,
 cloudiness 4/8 and no short-wave radiation (night
 conditions).
 Computed according to Bergdahl and Wernersson (1977).

9 MECHANICAL PROPERTIES

Natural ice shows many peculiar properties, distinguishing it from other materials, and it is most important to bear this in mind when studying the mechanics of ice or when using values of ice strength for design purposes.

9.1 Structural Considerations

Ice is a crystalline material with very coarse crystals compared to for example steel. The ice crystals also vary widely in size. The diameter is of the order of 10^{-3} m in snow ice and can be of the order of 10^{-1} m in columnar fresh-water ice. See chapter 2.

Furthermore, the ice crystals have an anisotropic structure, and the orientation of the c-axis varies from one crystal to another. In columnar sea-ice the crystals have a preferred orientation (horizontal c-axes), in columnar fresh-water ice the preference is weaker, and in snow ice there is a completely random orientation of the axes.

Polycrystalline ice usually contains impurities e.g. air bubbles, salts, organic or inorganic matter. In fresh-water ice most of the impurities are concentrated to the crystal boundaries. In a saline sea, on the other hand, the brine is mostly contained within the ice crystals between the platelets. See paragraph 2.52.

The coarse texture of ice is the reason why samples of ice, of the same size, contain parts of one, two, three or several crystals with different orientations and, of course, this fact influences the values of measured quantities. See figure 9.1.

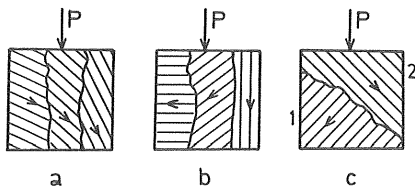


Figure 9.1 Dependence of properties of ice on its structure.

Another consequence of the coarse texture of ice is that ice strength values are strongly dependent on the size of the samples, as the number of contained crystal boundaries and crystal defects increases with size. For fine-grain materials, like steel, this effect becomes apparent only for samples with very small dimensions such as strings and slender axes. This so called scale effect is treated in paragraph 9.6.

Because of all these factors the observed mechanical properties of ice show a large scatter in values even if samples are taken from nearby parts of a large ice field.

9.2 The Role of Temperature

Being a crystalline solid, ice should tentatively show similar mechanical properties as for example steel, if one takes into due account the difference in crystal size. However, ice is generally confronted at temperatures very close to its melting point.

At such elevated temperatures the mechanics of a crystalline solid is controlled by thermally activated processes. At temperatures between 50-100% of the absolute melting temperature, T_m , the mechanical properties are strongly dependent on strain rate and temperature. For ice $T_m = 273$ K and as it usually occurs at temperatures above $0.8 T_m$ ($220 \text{ K} \approx -50^\circ\text{C}$) it is understood that temperature plays an important role.

Evidence of the thermal activity of ice is the self diffusion of whole water molecules in the solid, and the strong dependence of the rate of diffusion on temperature. The diffusion coefficient D can be written

$$D = D_0 \exp(-Q_s/RT) \quad \dots\dots(9.1)$$

where

$$\begin{aligned} D_0 &= (9.13 \pm 0.57) 10^{-4} \text{ m}^2/\text{s} \\ Q_s &= 59.8 \text{ kJ/mol}; \text{ the activation energy for self diffusion} \\ R &= 8.31 \text{ J}/(\text{mol} \cdot \text{K}) = \text{the universal gas constant} \\ T &= \text{the absolute temperature.} \end{aligned}$$

The diffusion coefficient D is used as a parameter in the creep models presented in paragraph 9.32. (Ramseier, 1967a, b).

Furthermore, it has been observed that ice recrystallizes when deformed, and that on reloading it behaves in a harder and stronger manner. The results from first loadings show considerable scatter, but good reproducibility has been observed for repeated loading tests. A conclusion from this is that the deformation history of an ice-cover significantly affects its response to a load (Gold 1965). Compare the elastic lag described in paragraph 9.43.

The recrystallization activity in the ice and the slippage between the basal planes (paragraph 2.2), add up to an appreciable viscous deformation or creep of ice already at low stresses. In older investigations, when trying to establish a modulus of elasticity for ice, this fact caused a lot of contradictory data, as there was no general agreement as to loading rates or other test arrangements.

9.3 Deformation of Ice

The deformation of a loaded ice specimen can be divided into three separate parts, namely elastic deformation, elastic lag, and viscous deformation or creep. In figure 9.2 is shown an idealized graph over the deformation following instantaneous loading and unloading of a sample.

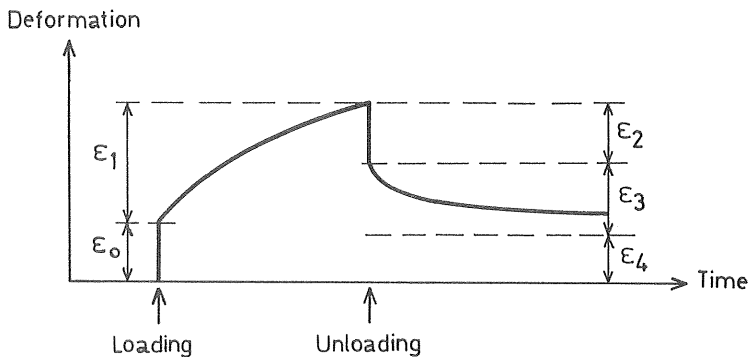


Figure 9.2 An idealized deformation-time curve for instantaneous loading and unloading of an ice sample.

When loaded there at first appears an instantaneous elastic deformation, ϵ_0 . This deformation is supposed to be completely recovered when the sample is unloaded, $\epsilon_2 \cdot \epsilon_2 = \epsilon_0$. Then there is transient creep, A, part of which constitutes the elastic lag, ϵ_3 , and the rest of which is perma-

nent viscous deformation, ϵ_4 . $\epsilon_3 + \epsilon_4 = \epsilon_1$. The elastic lag is supposed to be recovered after some time.

A rheological model describing such a behaviour could be constituted of a spring, representing the elastic deformation, in series with a dashpot, representing the permanent viscous deformation, and a Voight- (or Kelvin-) unit, representing the elastic lag. The Voight-unit is a dashpot in parallel with a spring. See figure 9.3

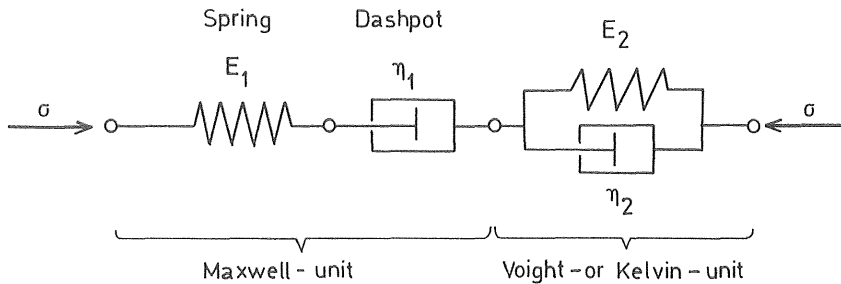


Figure 9.3 A composite rheological model of ice. σ is the load stress, E_1 and E_2 are elastic moduli, and η_1 and η_2 are viscosity moduli.

9.31 Linear Rheological Models

If a rheological model is constituted by springs and dashpots with constant moduli of elasticity and viscosity, the mathematical formulation of its deformation will give rise to ordinary partial differential equations with constant coefficients. The model shown in figure 9.3 will, for example, yield

$$\ddot{\epsilon} + \frac{E_2}{\eta_2} \dot{\epsilon} = \frac{1}{E_1} \ddot{\sigma} + \left(\frac{1}{\eta_1} + \frac{1}{\eta_2} + \frac{E_2}{E_1 \eta_2} \right) \dot{\sigma} + \frac{E_2}{\eta_1 \eta_2} \sigma \quad \dots (9.2)$$

where ϵ is the strain and σ the stress $\dot{}$ and $\ddot{}$ denote the first and second time derivatives respectively.

The solution of such a differential equation is easily performed with the help of hereditary integrals for any time history of load or deformation. The technique is founded on the fact that the solution of the linear equation for a varying stress can be had by superposing sol-

utions where the stress is considered constant for infinitely short time intervals.

The deformation ϵ under a constant stress σ_0 applied for $t > 0$ is given by

$$\epsilon(t) = \sigma_0 J(t) \quad \dots\dots(9.3)$$

where $J(t)$ is characteristic for each linear model. It is a monotonously increasing function for $t > 0$, for $t < 0$ $J(t) \equiv 0$. It is called the creep compliance.

In the same manner a constant deformation ϵ_0 applied for $t > 0$ will yield the force

$$\sigma(t) = \epsilon_0 Y(t) \quad \dots\dots(9.4)$$

where $Y(t)$ is called the relaxation modulus and is, at least, a non-increasing function of time.

The superposing of load increments $d\sigma$ at their corresponding times and integrating equation (9.3) gives the hereditary integral

$$\epsilon(t) = \int_{\tau=0}^{t=\tau} J(t-\tau) d\sigma(\tau) \quad \dots\dots(9.5)$$

The technique is described in for example Flügge: Viscoelasticity (1975), where also the creep compliance and relaxation modulus are given for some rheological models.

The linear model of equation (9.2) has been used for sea ice by Tabata (cited by Weeks and Assur 1967) and by Lindgren (1968) for columnar fresh-water ice. Both scientists tried to evaluate their experiments in terms of moduli independent of strain rate and stress. It was, however, found that especially the viscosity modulus η_1 is strongly dependent on stress and strain.

Jumppanen (1973) calculated the pressure against the walls of water reservoirs by evaluating the creep compliance, $J(t)$, directly from experiments. In his experiments he found that for 0.7 MPa the ice showed weak nonlinearity and for 1.2 MPa strong nonlinearity. For a stress greater than 1 MPa the linear rheological model will thus give an inadequate description of deformation or stress.

9.32 A Nonlinear Rheological Model

Because of the limitations of the linear rheological model above other approaches have been made by for example Glen(1958), Ramseier (1971) and Drouin et Michel (1971), making use of the similarities between the deformation of ice and other crystalline solids.

These authors disregard the elastic lag and use models with a linear spring in series with a nonlinear dashpot. See figure 9.4.

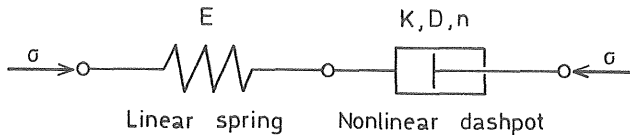


Figure 9.4 A nonlinear rheological model of ice. E is an elasticity modulus. K, D and n is defined by equation 9.5

For constant temperature the equation of the proposed model can be written

$$\dot{\epsilon} = \frac{1}{E} \dot{\sigma} + KD (\sigma / E)^n \quad \dots\dots(9.6)$$

where K and n are functions of strain, strain rate, and stress. D is the self-diffusion coefficient for the water molecules in ice.

Neither the linear nor the proposed nonlinear model can give a complete picture of the deformation of ice because of the complexity of its structure and deformation. The linear model has four parameters who actually cannot be considered constant for but narrow intervals of stress and strain. The described nonlinear model has three parameters. The product KD can be considered as one. Experimental curves are easier to fit but still the parameter constants must be changed for one mode of deformation to another, see paragraph 9.44.

It should be stressed that all constants in this chapter are functions of temperature, type of ice, the angle between load and crystal axes and type of load (tension, bending, compression). The separate parts of the models are treated in the following paragraphs.

9.4 Rheology of Fresh-Water Ice

If one looks at the rheological models for ice described in the previous paragraphs it is understood that the values on the different model parameters are very sensitive to test arrangements. The elastic modulus, for example, is often calculated on deformation that includes some creep. For great stresses the creep can constitute a considerable part of the deformation, and it must be measured extremely quickly after the application of the stress. If the time between load and measurement varies, the value on the elasticity will, of course, also vary although the "true" property does not.

9.41 Elasticity

As discussed above the values on the modulus of elasticity varies due to the used test method. But the desired magnitude of the modulus also depends on how it is to be used. If, for example, a pure elastic model shall be applied on the deflexion of an ice cover under a concentrated load, it is advisable to use rather low values that include reasonable viscous deformation. Otherwise, the deflexions will be grossly underestimated.

Dynamic elasticity

The most reliable results on the dynamic modulus of elasticity (E_1 of figure 9.3 or E of figure 9.4) are received from seismic methods measuring the speed of the propagation of sound. The phase speed of the compression wave is $\sqrt{E_1/\rho}$, where ρ is the density of the ice. The load rate is fast enough that the creep can be disregarded, and the true elasticity or the tangent modulus at the origin is actually measured.

By separating compression and shear waves, which have different phase velocities it is also possible to get the elastic shear modulus or the Poisson modulus.

For natural lake ice Boyle et Sproule and Northwood, cited by Pounder (1965), found that the elastic modulus was independent of crystal orientation. Their values also agree well with results by Frolov et Slesarenko (1972), Ewing, Berdennikov, Serikov, Bogorodskii and Lavrov all cited by Lavrov (1969). Taking Bogorodskii's results for ice with almost no bubbles the elastic modulus as a function of

temperature θ could be written:

$$E_1 = (1 - c\theta) \cdot 8.4 \text{ GPa} \quad \dots\dots (9.7)$$

where $c = 0.011 \text{ } ^\circ\text{C}^{-1}$. All results reported by the cited scientists lie within $\pm 10\%$ of this expression in the interval $-30^\circ\text{C} \leq \theta \leq 0^\circ\text{C}$.

It should be pointed out that the elasticity of turbid ice or deteriorating spring ice may be only 30% of that given by equation 9.7.

Static elasticity

In compression tests, when applying either one of the models, there is inevitably a lot more scattered results. One reason for this is the inclusion of a part of the viscous deformation. Another reason is that each specimen contains only a few crystals whose orientation can vary widely, see figure 9.1 page 101. A third reason is the difficulty to get flawless specimens and the fact that the more crystal boundaries per specimen the lower elasticity. See the scale effect paragraph 9.6. In the seismic tests, local irregularities or faults play little role as they occupy only a small fraction of the tested volume. Often the measurements are made on ice-fields in situ.

Experiments by Lindgren (1968) and Gold (1968), performed on columnar fresh-water ice (S1) with the stress applied perpendicular to the growth direction, are in good agreement with each other, and the expression (9.8) is a reasonable approximation of their results holding in mind that the standard deviation of, for example, Lindgren's values are 0.8 GPa.

$$E = (1 - c\theta) \cdot 6.1 \text{ GPa} \quad \dots\dots(9.8)$$

where $c = 0.012 \text{ } ^\circ\text{C}^{-1}$.

For snow ice (T1) and granular shelf ice Ramseier (1971) proposed

$$E = (1 - c\theta) \cdot 5.1 \text{ GPa} \quad \dots\dots(9.9)$$

where $c = 0.012 \text{ } ^\circ\text{C}^{-1}$

For ice monocrystals Gold (1958) found that the modulus of elasticity was not a function of temperature, and the elasticity parallel to or perpendicular to the c-axis was found to be 8.3 GPa. It appears

therefore, that the fairly large variation with temperature of the static elastic modulus of polycrystalline ice is due to the temperature dependence of grain boundary slip.

The elastic modulus of ice shows different values for compression and tension. For "structurally simulated" ice Lavrov (1969) received a secant modulus of elasticity of 1.3 GPa in compression and 0.12 GPa in tension. (Structurally simulated ice is ice seeded with hoar-frost crystals in the moment of formation. In this way an ice cover is made with columnar structure and with extremely small diameters of the columns). The duration of load action was 13 s and thus the modulus included some viscous deformation. Johnson (1972), who reexamined sea ice data by Peyton (1966), concluded that the secant modulus in tension was five to ten times that in compression. The modulus varied with crystal orientation and compressive strength of the samples. The modulus in tension was approximately 7 GPa and in compression 1.4 GPa (sic). The relations are thus quite contradictory.

Generally, the secant modulus in tension is 5 ± 4 GPa for columnar ice (S1). 5 GPa is assigned by Lavrov (1969) for moderate load duration (4 s) but, of course, higher values are received for shorter duration and lower for longer duration of load action.

The elastic modulus for bending is the most investigated property of ice. According to the theory of strength of materials the modulus received in bending tests, assuming the beams to have a constant elasticity, is a reduced modulus, E_b , which combines the moduli in compression, E_c , and tension, E_t :

$$E_b = \frac{4 E_c E_t}{(\sqrt{E_c} + \sqrt{E_t})^2} \quad \dots \quad (9.10)$$

Published bending test values show great differences, but it has recently been shown by Lavrov (1969) that the values received in bending tests are due not only to ice structure, temperature and load duration but also to sample dimensions. This is an example of the scale effect which is discussed in paragraph 9.6.

9.42 The Poisson Modulus

For dynamic tests Lavrov (1969) reported the Poisson modulus ν to

0.35 ± 0.04 . In compression tests measured values of the Poisson modulus vary widely due to the complicated pattern of crystals in the samples. See figure 9.1. Lavrov reported values varying between 0.0014 and 2.66.

Note that for pure viscous deformation the modulus is 0.5, and for creep tests with isotropic and homogeneous samples the Poisson modulus should approach this value. Drouin et Michel (1971) verified this in experiments with snow ice.

9.43 Creep

Studying the creep of ice by means of a constant load test it is possible to distinguish three stages of creep. Typical creep curves in tension at different temperatures are depicted in figure 9.5, where the initial increase of the true creep strain to ϵ_0 can be considered as the elastic deformation. The part between ϵ_0 and ϵ_1 is called primary or transient creep. In this stage the substructure changes and the creep rate is strongly dependent on the creep stress but in a minor way on temperature. From ϵ_1 to ϵ_2 secondary or steady state creep develops, where the rate of deformation is constant and the substructure remains practically unchanged. Finally, in the last stage the creep accelerates, the specimen necks, voids are formed near the grain boundaries, and cracks develop leading to a tensile creep failure.

For secondary creep there is a relation between strain rate and stress but for tertiary or primary creep no such relation has been proposed.

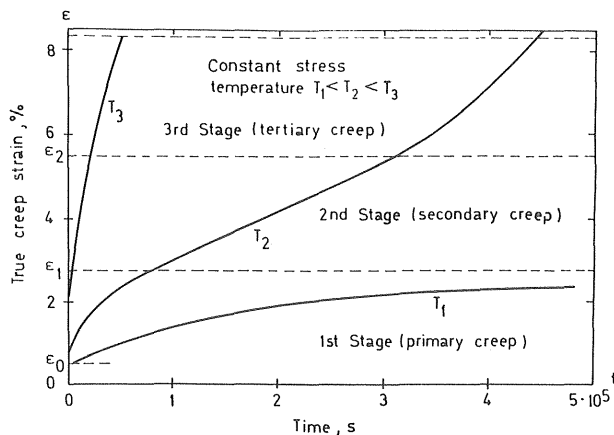


Figure 9.5 Typical creep curve in tension depicting three stages of creep using a constant load but at different temperatures. After Ramseier (1971).

On the other hand, if ice specimens are exposed to a constant strain rate, curves like those in figure 9.6 are obtained, and a relation between the strain rate and maximum stress is found for both primary and secondary creep. The maximum stress for secondary creep in these tests is equal to that found in the constant load tests. If the strain rate is too high, however, the specimen will show brittle behaviour. Such tests are rather to be referred to as strength tests than as creep tests. The strength of ice is discussed briefly in paragraph 9.5.

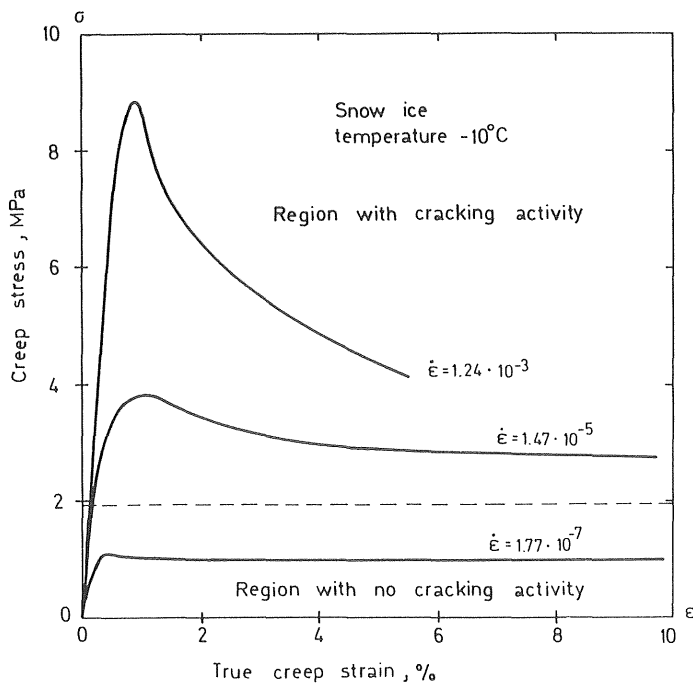


Figure 9.6 Compression creep curves conditions obtained under constant strain rate. After Ramseier (1971).

9.44 Creep of Single Crystals

Single crystals of ice undergo plastic deformation easily if there is a component of shear along the basal planes. Actually, an ice crystal can be likened to a bundle of cards, in which the faces of the cards represent the basal planes. The pack is readily deformed if the cards are able to glide over one another. The reason for the preference of basal glide is briefly explained in paragraph 2.2.

The glide along other planes than the basal planes can be induced under special conditions, but such so called hard glide require ten times greater stresses.

In figure 9.7 below the consequences of the basal glide for the deformation of beams of single crystals are illustrated. When the bending takes place in the direction of the c-axis and the deformation is small, the crystal assumes a V-shape. (Figure 9.7a). Grain boundaries develop over the supports and under the load. That is, for loads of the order of 0.1 MPa. If the deformation proceeds further several new boundaries develop from each of the three lines of loading. When the c-axis is in 45° to the applied load the deformation is more nearly circular (Figure 9.7b). When the c-axis is horizontal, and coincides with the length of the crystal gliding on the basal planes is concentrated adjacent to the three load lines. (Figure 9.7c). No glide takes place in the free ends. Finally, when the c-axis is horizontal and perpendicular to the length of the crystal, there is no shear stress to produce glide on the basal planes and the deformation is negligible. (Hobbs, 1974).

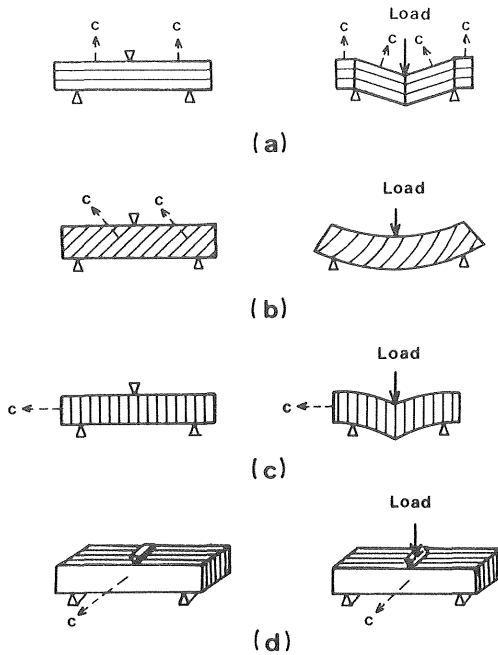


Figure 9.7 Schematic diagrams representing types of bending of single crystals of ice under stress. The parallel lines within the crystals represent the basal planes. (Hobbs 1974).

For monocrystals the creep rate $\dot{\epsilon}$ can be written

$$\dot{\epsilon} = KD\sigma^n \quad \dots \dots (9.11)$$

where K and n are quasi-constants depending on the creep behaviour, σ is the creep stress, and D the coefficient of selfdiffusion of the molecules in ice. See equation (9.1).

Ramseier (1972) did creep tests on ice monocrystals with the force acting at 45° to the basal planes, and Drouin et Michel (1971) with the force parallel. See figure 9.8 below. The former crystals deformed by basal glide, but the latter must yield to hard glide, and thus the force to induce the same rate of deformation in the latter crystals as in the former ones was much greater. The evaluations of equation (9.11) are given in table 9.9 below.

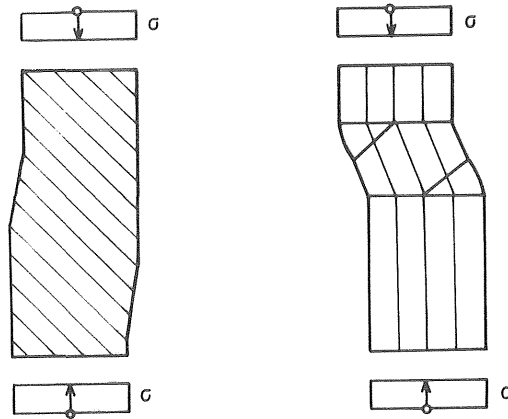


Figure 9.8 The deformation of two monocrystals with different orientation of crystal axes. The left crystal exhibit basal glide and the right one hard glide along the marked planes. The parallel lines within the crystals represent the basal planes.

Table 9.9 Ice monocrystals the stress at 45° to the basal planes. Values of the constants K and n in equation 9.11 for two ranges of temperature compensated creep rate, $\dot{\epsilon}/D$. Ramseier (1972).

$\dot{\epsilon}/D$ (m^{-2})	$K(m^{-2}Pa^{-n})$	n
$10^9 - 6.21 \cdot 10^{10}$	$1.560 \cdot 10^{-2}$	1.712
$6.21 \cdot 10^{10} - 4.9 \cdot 10^{12}$	$4.49 \cdot 10^{-7}$	2.329

Table 9.10 Ice monocrystals the stress parallel to the basal planes. Values of the constants K and n in equation 9.11. Calculated on data from Drouin et Michel (1971).

$\dot{\epsilon}/D$ (m^{-2})	$K(m^{-2}Pa^{-n})$	n
$2 \cdot 10^7 - 8 \cdot 10^9$	$4.40 \cdot 10^{-16}$	3.651

The function (9.11) is illustrated in figure 9.12 in the next paragraph with the constants from table 9.9 and 9.10. It is clearly seen that in the common interval of $\dot{\epsilon}/D$ the deformation due to easy glide is ten-fold faster than the deformation due to hard glide.

9.45 Creep of Polycrystalline Ice

The deformation of polycrystalline ice is composed of the basal glide within the crystals, of grain-boundary sliding and of liquid water at triple junctions caused by stress concentrations at these points. Below -10°C the basal glide is dominating. Because of the varying orientation of the grains in polycrystalline ice, the rate of flow is much smaller than for basal glide of ice monocrystals. Some grains are forced to deform by hard glide because of their orientation. Above -10°C the creep of polycrystalline ice is dominated by the grain boundary sliding and the melting at triple joints due to the stress concentrations caused by the sliding.

Most experiments on the creep of polycrystalline ice have been made with snow ice or nucleated columnar ice with small diameter of the grains. Experiments with such ice give good reproducibility, because there are enough grains in a specimen to give reliable bulk properties. If, however, a specimen contains only a few grains, as would be the case with an ordinarily sized specimen from a lake ice cover, the shifting orientation from specimen to specimen would give experimental results that showed vast scatter. See figure 9.1.

Ramseier (1971) and Drouin et Michel (1971) gave the creep rate of polycrystalline ice in secondary creep (see figure 9.5) as

$$\dot{\epsilon} = KD \left(\frac{\sigma}{E} \right)^n \quad \dots \dots (9.12)$$

where K and n are quasi-constants and functions of the creep behaviour, σ the maximum stress, E the elastic modulus and D the coefficient of selfdiffusion of the molecules in ice. D and E are both functions of temperature. $x/$

Equation (9.12) combined in series with an appropriate elastic member to a nonlinear rheological model (see figure 9.4) will give good fit to curves within the no-cracking region in figure 9.6. Within the region with cracking activity, however, the maximum stress will be somewhat delayed and furthermore the stress will not decrease with time as it should.

$x/$ Later Ramseier and Dickins (1972) have modified the equation (9.12) for polycrystalline ice to

$$\dot{\epsilon} = DA(\sinh(\alpha\sigma/E))^n$$

where α , n and A are constants throughout the whole range of deformation: $2 \cdot 10^2 < \dot{\epsilon}/D < 2 \cdot 10^{13} \text{ m}^{-2}$, on the other hand it will give a four-parameter model. For small values on $\alpha\sigma/E$ it approaches (9.12).

Drouin et Michel (1971) have succeeded in making a better fit to constant strain rate curves by using dislocation theory. Taking into account the number of edge dislocations (see figure 2.9b) and their increase in number with the deformation, ϵ , they end up with the expression

$$\dot{\epsilon} = 2 b (n_0 + \beta \epsilon) \left(\frac{\sigma}{2p}\right)^n \quad \dots \dots (9.13)$$

where b is Burgers vector (see paragraph 2.2), n_0 is the original number of dislocations per unit area, and β the rate of increase of dislocations. b and n_0 are constants for all types of hexagonal ice. β varies with the type of ice and p is both a function of temperature and the type of ice. The equation is dimensionally incorrect. Combined with an elastic member to a rheological model it will give a four-parameter model (β , p , n , E), while the use of equation (9.12) will result in a three-parameter model (K , E , n).

If one applies equation (9.13) to the case with the constant load, σ , it is evident that it will yield an accelerated creep also for primary and secondary creep, which is not the case. See figure 9.5, which agree with experiments by e. g Lindgren (1968) and Lavrov (1969). One can therefore not state that equation (9.13) is superior to the more common and more easily used creep rate function (9.12).

The constants K and n of equation (9.12) is given for snow ice in table 9.11 below. For columnar ice covers there are some experiments that justify the use of the constants for uniaxially loaded monocrystals, table 9.10, also for biaxially restricted plates containing several crystals. This may be explained by the fact that it is not possible that all crystals have a vertical orientation in a natural ice cover. For seeded ice covers or columnar ice covers with horizontal optical axes (S2) the pressure in expansion tests was found not to exceed the pressure in ordinary (S1) ice covers. (See Bergdahl 1978).

Table 9.11 Snow ice (T1). Values of the constants K and n of equation (9.12) for different ranges of temperature-compensated creep rate $\dot{\epsilon}/D$

- 1) calculated from figure of Ramseier (1971) founded on data from Butkovich and Landauer
- 2) Ramseier's (1971) own results

$\dot{\epsilon}/D$ (m^{-2})	K (m^{-2})	n
$< 0.7 \cdot 10^6$	$8.47 \cdot 10^{10}$	1.148 1)
$0.7 \cdot 10^6 - 10^9$	$4.712 \cdot 10^{19}$	3.118 2)
$10^9 - 10^{13}$	$1.297 \cdot 10^{27}$	5.27 2)

Drouin et Michel (1971) have also made two experiments with nucleated columnar ice. The columnar crystals had a diameter of approximately 2 mm and horizontal c-axes were dominating (S2). The specimens were found to be stiffer than the monocrystals loaded at 45° to the basal planes but weaker than the snow ice.

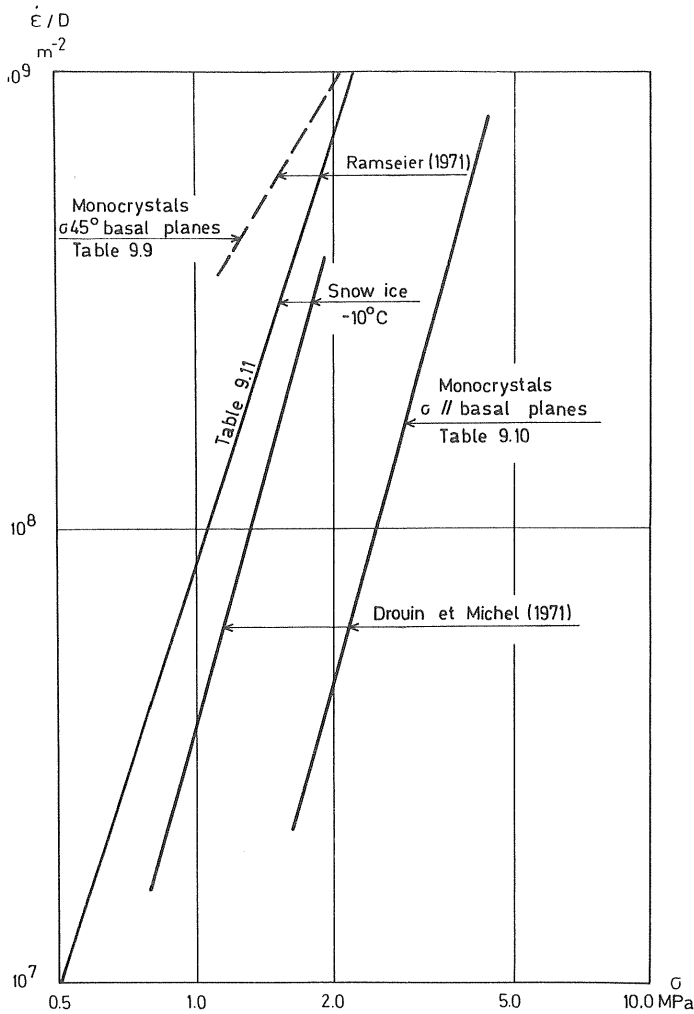


Figure 9.12 Temperature compensated creep rate $\dot{\epsilon}/D$ as a function of the applied stress σ . The monocrystals obey equation (9.11) and the snow ice equation (9.12). $D = D_0 \exp(-Q_s/RT)$, equation (9.1).

9.46 Activation Energies for Creep and Self Diffusion

Experimental results on the creep rate of ice can be brought into coincidence by using the function

$$\dot{\epsilon} = f(\sigma) \exp(-Q_c/RT) \quad \dots\dots (9.14)$$

where Q_c is the activation energy for creep
 σ the applied stress
 R the universal gas constant
 T the absolute temperature

For a large number of metals and components it has been shown that Q_c and the activation energy for self diffusion Q_s should be approximately equal. Q_s is a constant in the equation for self-diffusion (9.1):

$$D = D_0 \exp(-Q_s/RT)$$

The activation energy of creep Q_c can be calculated from 9.14, if the creep rate is known at two different temperatures for the same load.

$$Q_c = R \frac{\ln \dot{\epsilon}_1 / \dot{\epsilon}_2}{1/T_2 - 1/T_1} = -R \frac{d(\ln \dot{\epsilon})}{d(1/T)} \quad \dots\dots (9.15)$$

Now, if one takes the logarithm of and differentiates equation (9.12), which is the experimentally established function for (9.14), the following result of the differentiation with respect to $(1/T)$ is had

$$\frac{d(\ln \dot{\epsilon})}{d(1/T)} = \frac{d(\ln D)}{d(1/T)} + n \frac{d(\ln E)}{d(1/T)}$$

Inserting this result into (9.15) the first term can be identified as the activation energy for self-diffusion. Q_s according to equation (9.1), and thus

$$Q_c = Q_s - n R \frac{T^2}{E} \frac{dE}{dT} \quad \dots\dots (9.16)$$

This result is interesting in two ways. First, for monocrystalline ice the elasticity E is not a function of temperature so that the activation energies for creep and self-diffusion ought to be equal. Secondly, for polycrystalline ice the elasticity decreases with

temperature, that is $dE/dT < 0$, and consequently the activation energy for creep is greater than the activation energy for self diffusion.

The result mirrors the different deformation behaviour of polycrystalline and monocrystalline ice. In the former ice the creep and slip at the grain boundaries play a considerable role but in monocrystals there is, of course, only creep within the crystal structure.

Drouin and Michel (1971) found in their experiments with monocrystals, that in tests with the stress applied parallel to the basal planes $Q_c = 60.7$ kJ/mol which is nearly equal to $Q_s = 59.8$ kJ/mol.

For snow ice below -4°C they received $Q_c \approx 83$ kJ/mol and $n = 4$. With the values listed below equation (9.16) yields 84.5 kJ/mol.

$$\begin{aligned} R &= 8.31 \text{ J}/(\text{mol K}) \\ T &= 263.15 \text{ K } (-10^\circ\text{C}) \\ E &= 5.71 \text{ GPa (eq. 9.9)} \\ dE/dT &= -0.0612 \text{ (eq. 9.9)}. \end{aligned}$$

9.47 Elastic Lag

Structurally inhomogeneous materials show so called elastic lag or delayed elasticity, that is, when a specimen of such a material is unloaded some of the deformation is recovered after some time, see figure 9.2, paragraph 9.3.

For an ice specimen, that contains grains of different orientation, the phenomenon can be explained as follows. Some grains, like grains 1 and 3 in figure 9.13, creep by easy glide and after a comparatively short duration of load a great part of their deformation is permanent viscous deformation. Other grains, like grain 2 in figure 9.13, respond to the load by almost only elastic deformation, while the creep by hard glide is rather slow. The compressive stress in the specimen could be distributed like the hypothetical distribution of figure 9.13b. When unloaded the stress cannot disappear immediately but will be balanced internally, so that the expansion of the stiff grain (2) is restricted by the more deformed weak grains (1, 3). The resulting stress

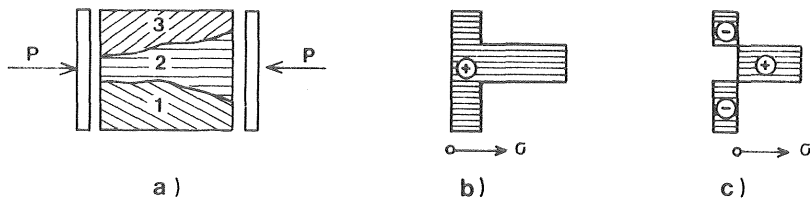


Figure 9.13 Hypothetical stress distributions in an ice specimen: b) during loading and c) shortly after unloading. The parallel lines within the crystals represent the basal planes.

distribution could be something like that shown in figure 9.13 c. The internal stresses will be gradually relaxed by creep and the specimen will then regain some of its deformation.

From laboratory experiments Lavrov (1969) drew the following conclusions, which agree with the description above:

- 1) The elastic lag is a maximum in macrocrystalline ice.
- 2) The elastic lag is less pronounced near the melting point than at lower temperatures.
- 3) The elastic lag is a maximum at loads amounting to between 11-20 % of the breaking load irrespective of the type of ice.
- 4) The elastic lag decreases under repeated load applications whatever the structure of the ice.

Lavrov also found that the elastic lag was noticeably reduced, when the salinity of the ice exceeded 1 ‰.

Furthermore, Gold (1965) among others has observed that the reproductability of loading tests increases at repeated loading. This is due to viscous flow and consequent homogenizing of the sample. In creep tests this stage of deformation is called primary creep. A stable substructure develops which is strongly dependent on the creep stress.

Using the linear rheological model of figure 9.3 (page 104) where the Voight-unit represents the elastic lag Tabata (1958) studied beams of sea ice and Lindgren (1968) columns of fresh-water ice. Because the columns contain only a few crystals each and because of the inhomogeneity of the sea ice beams there was bound to be a vast scatter of the elastic-lag constants E_2 and η_2 . Lindgren found for fresh-water ice

$$\left. \begin{array}{l} 3.4 \text{ GPa} < E_2 < 14 \text{ GPa} \\ \eta_2 \approx 10^{13} \text{ Ns/m}^2 \end{array} \right\} \theta = -10^\circ\text{C} \quad \dots\dots (9.17)$$

and Tabata found for sea ice

$$\left. \begin{array}{l} 0.18 \text{ GPa} < E_2 < 0.73 \text{ GPa} \\ 6 \cdot 10^{10} \text{ Ns/m}^2 < \eta_2 < 43 \cdot 10^{10} \text{ Ns/m}^2 \end{array} \right\} -5.0^\circ\text{C} < \theta < -2.3^\circ\text{C} \\ \dots\dots (9.18)$$

The latter also found that in situ beams of sea ice showed less elastic lag when deflected horizontally than vertically.

9.48 Relaxation Times

Time Scale of Elastic Lag

The behaviour of an ice specimen after an instantaneous unloading can be described by, for example, the linear model equation (9.2) which with $\ddot{\epsilon} = \dot{\epsilon} = \sigma = 0$ and integrated twice gives

$$\epsilon = \epsilon_3 \exp(-E_2 t / \eta_2) + \epsilon_4 \quad \dots\dots (9.19)$$

where ϵ is the deformation for $t > 0$

t the time

E_2, η_2 the constants of delayed elasticity

ϵ_3 the elastic lag

ϵ_4 the permanent viscous deformation

$\epsilon_3 + \epsilon_4$ the initial deformation at $t = 0^+$

see figure 9.2 page 103.

The time when the exponent of e in equation (9.19) equals -1 is called the relaxation time and it can be used as a measure of the time scale of the elastic lag. The relaxation time thus equals the quotient η_2/E_2 . Using Lindgren's values (9.17) it is found to be of the order of 10^3 s for fresh-water ice and Tabata's values (9.18) give the same order of magnitude for sea ice.

In load cases where the duration of load or deformation is much longer than the relaxation time the elastic lag can be disregarded. Such cases are then treated as visco-elastic using linear or non-linear Maxwell-units. A Maxwell-unit is a spring in series with a dash-pot.

For loads of very short duration, that is, only a fraction of the relaxation time, the elastic lag can again be disregarded, and the case treated as an elastic one. In this case even the viscous part of the model can be dropped which can be seen from the time scale of the creep.

Time Scale of Creep

If an ice specimen is instantaneously loaded by a deformation ϵ_0 it will respond with a stress, σ , that will gradually decrease as time lapses. A linear Maxwell-unit can be used as a model for the behaviour. Its equation is

$$\ddot{\epsilon} = \dot{\sigma} / E + \sigma / \eta \quad \dots\dots(9.20)$$

where $\dot{\epsilon}$ is the rate of deformation

σ the stress

E the modulus of elasticity

η the modulus of viscosity

As $\epsilon = \epsilon_0$ is constant, $\dot{\epsilon} = 0$ equation (9.20) gives for $t > 0$

$$\sigma = \epsilon_0 E \exp(-Et/\eta) = \sigma_0 \exp(-Et/\eta) \quad \dots\dots(9.21)$$

That is, the stress will relax exponentially with time, and here the quotient η/E is a measure of the time scale. The time when the exponent of e equals -1 is called the relaxation time.

For a nonlinear model (see figure 9.4) the relaxation time is not so easily defined, but bearing in mind that at the relaxation time the stress is $e^{-1} = 0.37$ of the original value, ϵ_0 , it is possible to make a numerical calculation. A consequence of the nonlinearity is also, that the time scale is not independent of the forced deformation ϵ_0 nor the stress σ_0 , as the creep rate is not a linear function of the stress. For -10°C and ice monocrystals loaded parallel to the basal planes the relaxation time is calculated to 50 h for $\sigma_0 = 1 \text{ MPa}$ and $1\frac{1}{2}$ h for $\sigma_0 = 10 \text{ MPa}$.

A conclusion is that you have to consider the creep of ice for load cases where the stress is considerable or of long duration.

9.5 Strength of Ice

The strength of ice is not a simple property to define. For some situations it may designate the stress at which fracture occurs, for others, the stress when the ice no longer can sustain the applied load, but is in a state of yield. Actually, the compression strength of ice cannot be stated as a certain value since it does not only depend on the type of ice, crystal-axis orientation, temperature etc. but also on the stress rate, strain rate and size of specimen.

This chapter will only give an introduction to the understanding of the problems to be met when trying to establish the strength of ice. For the purpose of calculating thermal ice pressure the strength is of minor importance.

We have already seen in paragraph 9.43, that for moderate strain rates there exists a fairly well defined relation between the strain rate, $\dot{\epsilon}$, and stress, σ . See for instance equation (9.12). If solved for the creep stress σ , the equation gives

$$\sigma = (\dot{\epsilon} / DK)^{1/n} E \quad \dots (9.22)$$

where D, K, n and E are quasi-constants defined in paragraph 9.43.

If the strain rate exceeds a certain limit, however, the deformation of a sample will no longer be viscous but brittle, and the sample will fail at a stress lower than the creep stress according to equation (9.22).

At the transition from viscous to brittle behaviour thus a maximum stress, σ_{\max} , occurs, and this is the maximum strength of ice that can be observed experimentally.

9.51 Crack Initiation and Propagation

Plastic deformation of the ice crystals occurs primarily by the movement of dislocations along the basal planes. In a polycrystalline material the sudden change in crystallographic orientation at the crystal boundaries can create barriers to the movement of the dislocations. The dislocations will then queue up in the basal plane

against the boundary, and a concentrated stress is created at the end of the plane.

This stress may be strong enough to initiate a crack. For moderate stresses it creates melting at these triple junctions. Compare paragraph 9.45. Complete fracture of the specimen does not necessarily follow immediately on this crack formation, since the formation will relax the concentrated stress and the crack will stop growing unless it becomes self propagating.

Carter (1970) has shown that under a uniaxial tensile load the crack will spread catastrophically throughout the ice, but under a compressive stress the first formed cracks will come to a rest after a finite length.

9.52 Tensile strength

In his work Carter (1972) gives a theoretical value for the tensile strength by

$$\sigma_t = \frac{3 \pi \gamma E}{2 (1 - \nu^2) d_{cr}}^{1/2} + 2 \tau_o \quad \dots (9.23)$$

where $\tau_o = 0.3 \text{ MPa}$ for snow ice and independent of temperature

$\gamma = 10.9 \text{ J/m}^2$ the surface energy

$E =$ the elastic modulus

$\nu =$ Poisson's coefficient

and $d_{cr} =$ the grain diameter

Equation (9.23) agrees well with Carter's (1970) own experimental data, and also with results by for instance Jellinek (cited by Gold 1968), who for granular ice at 0°C received the ultimate tensile strength to 1.6 MPa . Equation (9.23) gives $\sigma_t = 2.1 \text{ MPa}$ for this case.

The tensile strength of ice at different temperatures and strain rates would then ideally be given by the lowest of the two values received from equations (9.22) and (9.23) for polycrystalline ice and from (9.11) and (9.23) for ice monocrystals, if the appropriate constants are applied.

Equation (9.23) is, however, of limited practical interest as it gives the highest possible tensile strength for a given type of ice. Other factors as the contents of voids or impurities in a cross section tend to decrease the tensile strength drastically. This is illustrated in

figure 9.14. For sea ice, see paragraph 9.7 and for deteriorating spring ice this effect is very pronounced.

It should also be observed that the number of limiting defects in a sample is proportional to its volume, why the sample dimensions influence the values of ice strength. This problem is treated in paragraph 9.6.

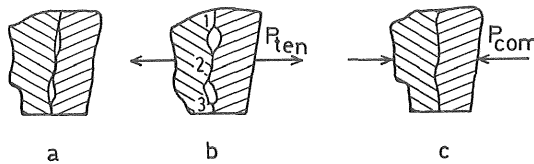


Figure 9.14 Causes of differences in compressive and tensile strength of ice. After Lavrov (1969).

9.53 Compressive Strength

From theories on the propagation of elastic-plastic cracks Carter (1970, 1972) has deduced that beyond the transition from ductile to brittle behaviour the compressive strength σ_c is not a function of the strain rate but is given by

$$\sigma_c = 0.6 \sigma_{max} \dots (9.24)$$

where σ_{max} is the maximum yield strength of ice that can be observed experimentally.

He also verified this in a series of compression tests for frazil ice (S4, angular grains diameter 1 mm), snow ice (T1 diameter 1 mm) and columnar ice (S2? diameter of columns 4 mm). One example is given in figure 9.15.

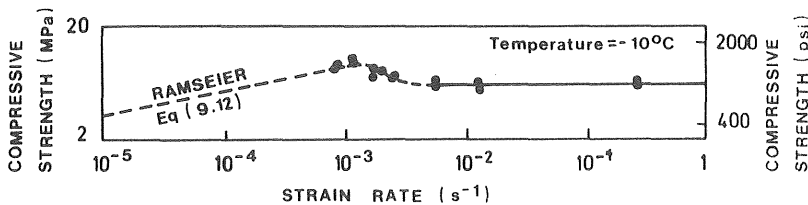


Figure 9.15 Compressive strength of snow ice under increasing strain rates at -10°C. Carter (1972)

Yet, there is the problem of choosing σ_{\max} . The theory gives no lead to this value, but looking at the curves in figure 9.15 it would, for snow ice, be reasonable to insert the value $\dot{\epsilon} = 10^{-3} \text{ s}^{-1}$ into the equation (9.22) with the appropriate constants given in table 9.11 in order to calculate σ_{\max} . Equation 9.11 would then give a value for the crushing strength of snow ice. The same can of course be done for other types of ice as for example the investigated frazil ice and columnar ice. For the frazil ice the maximum stress was reached for $\dot{\epsilon} = 10^{-3} \text{ s}^{-1}$ approximately and for the columnar ice (specified above) for 10^{-4} s^{-1} .

Returning to figure 9.15 it can be seen that there is not an abrupt decrease of the compressive strength from σ_{\max} to $0.6\sigma_{\max}$ when the strain rate is increased, but the strength gradually diminishes within a transition zone. A consequence of this is, for example, that for snow ice the strength of ice is proportional to the strain rate $\dot{\epsilon}$ when $\dot{\epsilon} < 10^{-3} \text{ s}^{-1}$ but for columnar ice it is inversely proportional when $\dot{\epsilon} > 10^{-4} \text{ s}^{-1}$, that is, within the same range of strain rate.

From the discussion above it should be clear that it is a very difficult task to state a value on the compressive strength of ice even when discussing ideal ice, and reality makes things worse since ordinary ice contains voids, old unhealed cracks etc., which means that the "scale effect" will also influence the received or chosen values. See paragraph 9.6. This influence is maybe somewhat counteracted in compression by the fact that small voids and discontinuities will be pressed together and partly healed if the strain rate is not too fast, see figure 9.14.

9.54 Design Strength

It is usually recommended that the strength of ice, used for design at a site, be founded on laboratory and field tests on the ice from that specific area. It is, however, extremely important that these tests are performed under well controlled conditions as to the rate of loading, temperature, sample dimensions etc, and that the tests are thoroughly related to the design problem to be solved.

Paragraph 9.5 can be seen as an introduction to the understanding of the problems encountered when choosing a strength value for ice

but if specific values are needed, I recommend for instance Gold's (1968) comprehensive paper on the "Elastic and Strength Properties of Fresh-Water Ice". or Butiagin's (1966) or Lavrov's (1969) books.

9.6 The Scale Effect

Many scientists have found that the measured strength values of ice are dependent on the size of ice specimens. The reason for this is as yet not fully understood.

The most wide-spread explanation is that, given a certain density of different defects in ice, the probability to include some of these into a specimen increases with the size of the specimen. The fact that when cutting a big ice block into smaller pieces you are apt to and sometimes forced to discard defective pieces will, of course, enhance the strength values of small specimens.

The described theory is mostly referred to as the statistical theory and it is founded on a general theory of brittle strength developed by Weibull (1939 a, b) and applied to ice strength by Russian scientists, see for example Butiagin (1966) or Lavrov (1969, 1971).

Recently, Hirayama et al (1974) pointed to the fact that the ice strength should rather be related to the ratio of sample diameter, d , to crystal size, d_{cr} . He also found in his experiments that if this ratio was greater than 25 the ice strength was practically independent of the sample size. According to him this is consistent with Butkovich's (1954) and Butiagin's tests. Lavrov, on the other hand, found a relationship between cross sectional area, S , and compressive strength that holds for $d/d_{cr} < 32$ or $S < 90 \text{ cm}^2$,
 $d_{cr} = 3 \text{ mm}$

$$\sigma_c = 1.9 \cdot 10^6 \cdot S^{-0.20}$$

This function shows a slight decrease in σ_c even when $d/d_{cr} > 25$, and Lavrov's conclusion was that an extrapolation should be made for larger pieces of ice.

For compressive strength it can thus be concluded that the scale effect can be neglected provided the ice crystals are small compared to the tested ice specimens. This is rather easily achieved

for snow ice. For columnar sea ice, where $d_{cr} \approx 5$ mm, the diameter of the specimen must be at least 125 mm. For columnar fresh-water ice with $d_{cr} \approx 50$ mm one must use field experiments or resort to some relation like the above equation.

For bending strength, however, the dependence on specimen volume is not merely caused by the random distribution of defects but also by the low resistance to shear. For further information see Lavrov (1969).

9.7 Mechanics of Columnar Sea Ice

In paragraph 2.52 was described how an ice cover developed on a sea surface. The resulting sea-ice cover consists of columnar crystals with horizontal c-axes and diameters of approximately 5 mm. It was also stated that the formed ice lattice was pure, and that brine was trapped in narrow voids within the ice crystals parallel to their basal planes.

These brine-voids can be shown to be responsible for many characteristic features of the mechanics of sea ice as well as they play a great role for the temperature variation of density, conductivity and heat capacity, which has been derived earlier. A crack in a failed specimen of sea ice, for instance, consists to a considerable part of brine voids.

The brine voids are rather regularly shaped and orderly spaced in the ice. However, the ice also contains trapped air bubbles which are less orderly arranged and of variable size. Discussing the thermal expansion of sea ice it was concluded that these air-bubbles were completely separated from the brine voids, which seemed to be justified in the light of experimental values on the density of sea ice. As a consequence we disregarded the air-bubbles when calculating the sea ice density as a function of salinity and temperature. We will not consider them, when discussing strength or elasticity either, although it has no other justification than the air-bubble content being rather small compared to the brine content.

On the other hand, taking samples in a sea-ice cover and storing them, makes some of the brine drain off, especially, if the storing

temperature is too high. The total void volume of the ice will, of course, be related to the original ice salinity. As pointed out by Weeks and Assur (1967) this drained brine volume should be considered as it sometimes constitutes an appreciable part of the voids. The brine content by volume of the ice can be calculated with the phase relations given in paragraph 2.53.

9.71 Strength

A potential failure plane in sea ice only partly consists of ice. A simple model of sea ice strength would then be to consider the brine uniformly distributed in the ice and reducing the failure area by the plane porosity, which in this case equals the volume porosity or brine content by volume, V_b . Letting σ_f be the strength of sea ice and σ_o the strength of some fictitious brine-free sea ice the following simple relation holds

$$\sigma_f = \sigma_o (1 - V_b) \quad \dots\dots(9.25)$$

Observe, that the strength, σ_o , is not the strength of fresh water ice. The substructure and failure mechanism are too different for this to hold.

From the strength of materials it is known that near spherical holes in uniaxially loaded elastic bodies there are stress concentrations two times the mean stress, and it has been suggested that the fictitious strength, σ_o , because of this should be a half of the strength of fresh water ice of the same temperature, but fresh-water ice also contains stress risers such as air bubbles and vapour voids. Furthermore, the failure does not necessarily start at the voids in fresh-water ice while it mostly does so in sea ice. (Assur 1958).

As the brine voids are not uniformly distributed in the ice but concentrated to certain basal planes, potential failure planes can be situated to cut only a few ice-ice bonds in warm ice, although the sea ice still is solid to a considerable part. In cold ice, however, such a plane is ice to a great extent. The warmer ice would be expected to have a tensile strength close to zero even though it contains an appreciable amount of ice. This is also observed in strength tests, see figure 9.16, where the ring tensile strength of NaCl ice is drawn as a function of tem-

perature. The extrapolated function gives zero strength for a brine volume of 70%. For sea ice with the salinity 3 ‰ this corresponds to the temperature -2°C .

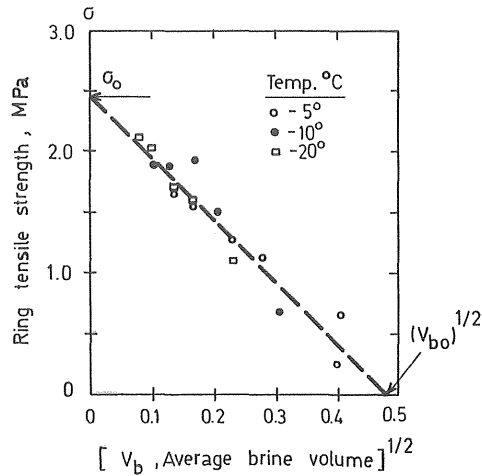


Figure 9.16 Average ring tensile stress versus square root of the average brine volume, NaCl-ice. (Weeks 1963).

The failure strength, σ_f , decreases from a maximum, σ_0 , at zero brine volume, $V_b = 0$, to a strength of zero at a brine volume V_{b0} . Therefore, it should be possible to express sea-ice strength in the general form

$$\sigma_f = \sigma_0 (1 - \psi) \quad \dots (9.26)$$

where ψ is the "plane porosity" or relative reduction of area of the failure plane because of the presence of brine and, possibly, air inclusions. ψ is a function of V_b for $V_b \leq V_{b0}$, and should satisfy the conditions: $\psi = 0$ for $V_b = 0$ and $\psi = 1$ for $V_b = V_{b0}$.

Bearing in mind the characteristic features of the brine inclusions in sea ice described in paragraph 2.52. Assur (1958) made an idealized diagram over the distribution and shape of the inclusions in order to calculate ψ as a function of the brine volume V_b . The diagram is shown in figure 9.17 again. In the diagram the c-axis is

the optical axis of the crystal. The C-axis is horizontal and the G-axis vertical. Now, the next step is to assume how the brine voids varies with the void volume V_b . The most simple assumption is that only the cross-sectional area in the basal plane BG varies, the width $2r_a$ being constant. In this case the potential failure area must change proportionally to V_b , for stresses in the horizontal direction.

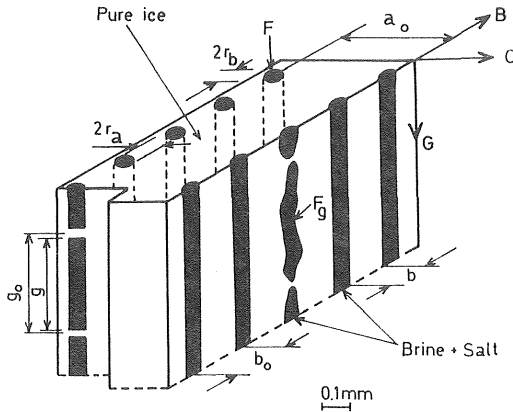


Figure 9.17 An idealized diagram of the shape of the brine inclusions in columnar sea ice and NaCl-ice. (After Assur 1958).

$$\sigma_f = \sigma_o (1 - cV_b) \dots\dots(9.27)$$

If, on the other hand, the average length and spacing of the brine cylinders remain constant, the volume change will be reflected as a change in the area $\pi r_a r_b$ only, and thus our equation, for horizontal loads, will be of the form

$$\sigma_f = \sigma_o (1 - cV_b^{1/2}) \dots\dots(9.28)$$

If all brine pockets remain of a similar shape during the changes in V_b all linear dimensions will change proportionally to $V_b^{1/3}$. This results in an equation of the form

$$\sigma_f = \sigma_o (1 - cV_b^{2/3}) \dots\dots(9.29)$$

In "The Mechanical Properties of Sea Ice" Weeks and Assur (1967) brought together a considerable amount of data on sea-ice strength and evaluated them by means of equations (9.27) through (9.29).

The best fit was mostly obtained with equation (9.28). See for example figure 9.16 for NaCl-ice.

The most extensive research have been done with ring tensile tests. Experiments by Graystone, Langleben, Dykins, Pounder and Frankenstein (cited by Weeks and Assur 1967) give values on σ_o ranging between 2.65 MPa and 2.96 MPa and on c of equation (9.28) between 1.31 and 2.07 for $V_b < 0.63$. For $0.63 < V_b < 0.8$ the failure strength is approximately constant $\sigma_f = 0.67$ MPa (Frankenstein), which might be explained by the hypothesis that there still must exist some skeleton of ice even at this high content of brine.

In connection with thermal ice pressure we are mostly concerned with stress in horizontal directions, that is parallel to the plane BC of figure 9.17. Unfortunately, published results from such compression tests have not been evaluated in terms of the sea-ice model described in this paragraph. However, Butkovich (Weeks and Assur 1967) found median strength values ranging from 7.8 MPa at -5°C to 12 MPa at -16°C for stress applied vertically, that is along the G-axis. Average values for horizontal stress in the same temperature interval vary from 2.1 to 4.3 MPa. Unfortunately, the salinity or void volume of the cores is unknown. The ring tensile tests seem to be insensitive to the orientation of the specimens, while tensile and compressive tests show that horizontal loads give strength values approximately $1/3$ of those received from tests with vertical loads. (Johnson 1972).

9.72 Elasticity

It should be possible to extend the use of the structural model of sea-ice described in the previous paragraph to calculating elasticity.

For stress in the vertical direction (G-axis) the following relations will approximately hold for the deformation, again assuming the voids to be full of brine and neglecting the interruptions of the vertical oblong voids. See figures 9.17 and 9.18.

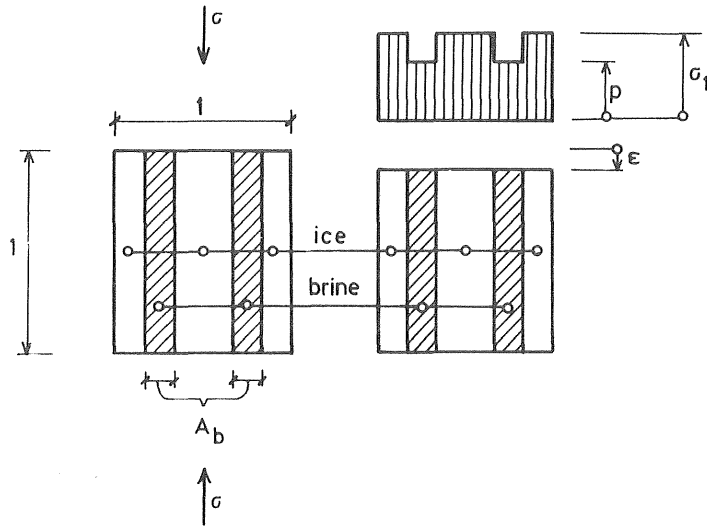


Figure 9.18 The compression of an ice specimen in G-axis direction. Vertical section through a unit piece of the specimen.

The deformation can be set equal for the brine voids and the ice if lateral expansion is neglected ($\nu = 0$), and the load is considered as dynamic.

$$\epsilon = pK = \sigma_1/E_1 = \sigma/E \quad \dots\dots(9.30)$$

- where ϵ is the strain
- p is the pressure in the voids
- σ_1 is the stress in the ice
- σ is the stress averaged over the cross section A , $\sigma = P/A$
- K is the compressibility of the brine
- E_1 is the elasticity of pure ice
- E is the bulk elasticity of the sea ice.

Equation (9.30) gives directly

$$\sigma = E \cdot \epsilon \quad p = \epsilon/K \quad \sigma_1 = \epsilon E_1 \quad \dots\dots(9.31)$$

and the average stress is

$$\sigma = \sigma_1(1 - A_b) + p A_b \quad \dots\dots(9.32)$$

where A_b is the relative cross sectional area of brine.

The combination of equations (9.30) to (9.32) yields the bulk elasticity modulus

$$E = E_1 + (1/K - E_1) A_b \quad \dots (9.33)$$

or if $V_b = A_b$ is inserted

$$E = E_1 + (1/K - E_1) V_b \quad \dots (9.34)$$

The modulus of elasticity in the vertical direction is thus hypothetically a linear function of the brine volume. By equation (9.34) the elasticity modulus as a function of temperature and ice salinity can be obtained, calculating the brine volume from equation (2.10) or (2.12), the ice elasticity from equation (9.7) or (9.8), and assuming a value on the compressibility of the brine.

$$K = (57 \cdot 10^{-11} \text{ Pa}^{-1}) \quad \dots (9.35)$$

K is a value for air free water at 5°C and normal pressure. Of course, it had been desirable to have a value for brine in the relevant temperature range.

Equation (9.34) should also hold for a random distribution of brine voids since the relative brine area A_b in any cross section equals the brine volume V_b .

If one considers the horizontal deformation in a sea-ice cover, however, a more complicated model should be built. For this purpose the diagram of figure 9.17 is simplified further by substituting the brine voids by rectangular tubes with the horizontal cross-sectional area $l_a \cdot l_b$. See figure 9.19.

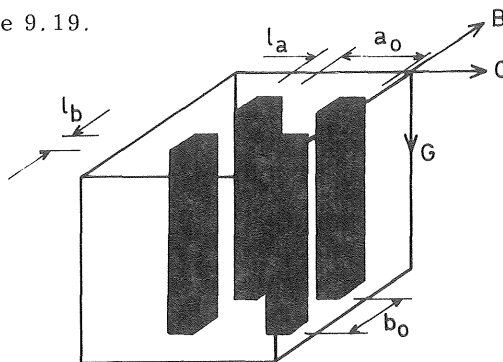


Figure 9.19 A further simplification of the diagram of sea ice for the purpose of calculating its modulus of elasticity.

The deformation along the c-axis will then give the following equation

$$a_o \epsilon = a_o \sigma / E_h = l_a \sigma / E_b + (a_o - l_a) \sigma / E_1 \quad \dots\dots(9.36)$$

- where ϵ is the average strain along the c-axis
- a_o is the spacing of the platelets, figure 9.19
- σ is the average stress over the cross section
- E_h is the bulk modulus of elasticity
- E_b is the bulk modulus of the brine layer eq. (9.33)
- E_1 is the elasticity of pure ice

Solving equation (9.36) for E_h gives

$$E_h = E_b E_1 / ((E_1 - E_b) l_a / a_o + E_b) \quad \dots\dots(9.37)$$

Equation (9.34) applied on the brine layer gives

$$E_b = E_1 + (1/K - E_1) l_b / b_o \quad \dots\dots(9.38)$$

If this is inserted in equation (9.37) the bulk elasticity can finally be simplified to

$$E_h = E_1 / (1 - (1/K - E_1) V_b / E_b) \quad \dots\dots(9.39)$$

As a consequence of the hypothetical expression (9.39) the elastic modulus in the horizontal direction is expected to be a function of both brine volume and the shape of the brine voids. For a sample crystal the modulus should even vary with the deviation from the c-axis direction. In a piece of ice, however, the c-axis is randomly oriented in the horizontal plane, why a specimen containing enough crystals will not show this anisotropy.

To evaluate equation (9.39) we must state a relation between the ratio l_b/b_o and the brine volume V_b . If the brine voids are assumed to be square tubes i. e. $l_a = l_b$ the following relation holds

$$\frac{l_b}{b_o} = \sqrt{\frac{a_o}{b_o} V_b} \quad \dots\dots(9.40)$$

Assume further that the distance between the brine layers is 0.5 mm and that their thickness is 0.05 mm when ice bridges start to form across them. Compare paragraph 2.52. Square tubes will then imply

that $a_o/b_o = 10$ and for brine volumes V_b less than 0.10 then

$$\frac{l_b}{b_o} = \sqrt{10 V_b} \quad \dots\dots(9.41)$$

For brine volumes greater than 10% the ice structure consists of unconnected ice plates, if the assumptions in this paragraph is faithfully followed. The ice structure is however irregular so that the ice will still show some elasticity. Recall that experiments on ice strength still shows the strength $\sigma_f \approx 0.2 \sigma_o$ for $V_b \approx 60\%$. For enduring loads the brine would be squeezed out of the ice structure till the ice platelets got into contact again.

It is, of course, theoretically possible to extend the elasticity modulus to brine volumes greater than 0.10 for which equation (9.41) yields $l_b/b_o = 1$, (9.38) reduces to $E_b = 1/K$, and the bulk modulus becomes

$$E_h = E_1 / (1 - (1 - E_1 K) V_b) \quad \dots\dots(9.42)$$

This expression might have some meaning for acoustic waves in very warm sea ice.

Weeks and Assur (1967) reproduce a diagram by Langleben and Pounder showing the elastic modulus as a function of brine content, figure 9.20. Unfortunately the ice temperature is not accounted for. The slope of the continuous line must be a combined effect of the change in the pure ice elasticity because of increasing temperature, the change of brine volume, and may be the loss of brine at high temperatures.

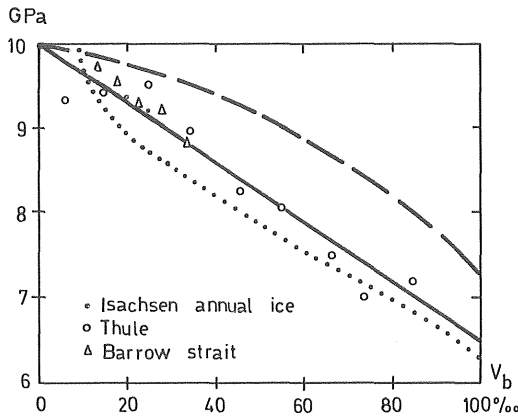


Figure 9.20 Dynamic modulus of sea ice versus brine volume.

Continuous line: Cold ice, small specimen tests by Langleben and Pounder (Weeks and Assur 1967).
 Dashed line: According to equations (9.37-41) and constant temperature, $\theta = -15.3^{\circ}\text{C}$, $0 \leq S \leq 25$ ‰
 Dotted line: According to equations (9.37-41) and constant salinity, $S = 3$ ‰, $-15.9^{\circ}\text{C} \leq \theta \leq -1.6^{\circ}\text{C}$

The dashed and dotted lines in figure 9.20 represent the dynamic modulus of sea ice according to the equations (9.37-41) using equation (9.7) for the pure-ice dynamic elasticity and (9.35) for the brine compressibility. The dashed line is for ice at constant temperature -15.3°C ($E_1 = 9.8$ GPa). The dotted line is for ice with the constant salinity 3 ‰ and the brine volume calculated according to equations (2.10) or (2.12). This curve is thus a function of temperature too. At $V_b = 0.01$ the temperature is -15.9°C while at $V_b = 0.10$, $\theta = -1.6^{\circ}\text{C}$.

From the figure it is seen that the assumption of constant salinity gives a very good fit to the test values.

For static loads there are very few determinations of the tangent modulus. Values given in the literature (Weeks and Assur, 1967) are 10 to 20 % lower than the dynamic ones. A fair appreciation of the elastic modulus of sea ice could be had using equation (9.8) for pure-ice elasticity together with the technique described above.

9.73 Creep

An evaluation of the creep of sea ice by means of the structural model and the power law equation (9.12) $\dot{\epsilon} = KD (\sigma/E)^n$ is difficult as the creep rate is not a linear function of stress. Adding the strain in the stress direction as in equation (9.36) it is not possible to eliminate the stress. Furthermore, I have found no tests on sea ice evaluated in terms of the power law (9.12). Resorting to linear models, values from Tabata and Ono are found (Weeks and Assur 1967).

If one uses a simple Maxwell model

$$\dot{\epsilon} = \dot{\sigma} / E + \sigma / \eta \quad \dots (9.43)$$

it is possible to calculate the viscosity modulus in the same manner as the elastic modulus above. Then for $V_b < 0.1$

$$\eta = \eta_1 / (1 + V_b / (1 - \sqrt{10 V_b})) \quad \dots (9.44)$$

where η_1 is the viscosity modulus of pure ice
 V_b is the brine volume
 η is the viscosity modulus of sea ice

In equation (9.44) we have put the viscosity modulus of brine to zero, and subsequently it gives $\eta = 0$ in the limit for $V_b = 0.1$. Equation (9.44) is thus only working for a very limited range of void volumes. Furthermore after a finite deformation the brine will be squeezed out and the value of η should thus increase with increasing compressive strain.

The available information on viscosity moduli is too small to test equation (8.44). It might also be that the substructure of sea ice is so different from that in fresh-water ice that the value on η_1 should be completely different.

Lindgren (1968) gives a viscosity modulus of approximately $3 \cdot 10^{13}$ Ns/m² for columnar fresh-water ice at the compression stress 0.6 MPa and the temperature - 3.5°C. An evaluation of the results by Drouin and Michel (1971) referred in table 9.11 in terms of a viscosity modulus gives between $0.8 \cdot 10^{13}$ Ns/m² and $4.6 \cdot 10^{13}$ Ns/m². A value of $\eta_1 = 5 \cdot 10^{13}$ Ns/m² should then result in conservative values on thermal ice pressure. However, experiments by Tabata (Weeks and Assur

1967) show that sea ice with the salinity 4.9 ‰ and temperature - 1.9°C has a horizontal modulus of viscosity of $\eta \approx 7 \cdot 10^{12} \text{Ns/m}^2$. For this combination of salinity and temperature equation (9.44) gives $\eta = 0$ since $V_b > 0.10$ according to figure 2.20.

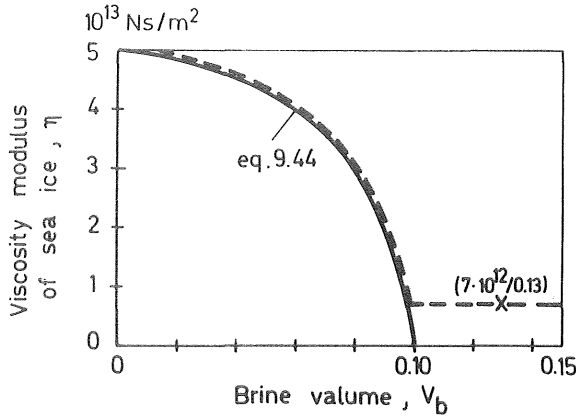


Figure 9.21 The viscosity modulus of sea ice as a function of brine volume V_b according to equation (9.44) and with $\eta_1 = 5 \cdot 10^{13} \text{Ns/m}^2$. For $V_b > 10\%$ the constant value $\eta = 7 \cdot 10^{12} \text{Ns/m}^2$ is recommended.

In figure 9.21 above the function (9.44) is illustrated with $\eta_1 = 5 \cdot 10^{13} \text{Ns/m}^2$ and the value by Tabata on $\eta = 7 \cdot 10^{12} \text{Ns/m}^2$ and $V_b \approx 0.13$. It is recommended to use the dashed curve for pressure calculations or $\eta = 5 \cdot 10^{13}$.

9.74 A Rheological Model of Sea Ice

For the purpose of calculating ice pressure in columnar sea ice a simple Maxwell model will be used with a spring in series with a dashpot. Its deformation is described by the simple equation

$$\dot{\epsilon} = \dot{\sigma}/E_h + \sigma/\eta \quad \dots\dots(9.45)$$

- where E_h is the bulk elastic modulus, eq. (9.39)
- η is the bulk viscosity modulus, fig. 9.20
- σ is the stress
- $\dot{\epsilon}$ is the strain rate

As has been described in the preceding paragraphs the bulk moduli are, however, very difficult to evaluate. Furthermore, the whole

process of thermal expansion and brine volume variations with temperature is a complex matter to calculate, even if the elements described in paragraphs 2.53, 3.4 and 6.2 are fairly well verified. Each conclusion relies on many simplifying assumptions, why they taken together indicate that there is little to benefit from constructing a more complex model than (9.45) for the purpose of calculating thermal ice pressure. For the purpose of calculating the bearing capacity of ice covers, ice loads against structures, or ice breaking forces it may be of use to apply a more complex model. See for example Weeks and Assur (1967).

LIST OF TABLES		page
2.15	Composition of salts of sea water of the salinity 34.48 ‰	28
4.5	The thermal conductivity of snow as functions of its bulk density	59
7.6	Reflection coefficient for different types of ice at normal incidence. Generalized values found in literature and guessed values	87
7.11	Coefficient of extinction for different types of ice. Generalized values found in literature and guessed values	93
9.9	Ice monocrystals the stress at 45° to the basal planes. Values of the constants K and n in equation 9.11 for two ranges of temperature compensated creep rate	113
9.10	Ice monocrystals the stress parallel to the basal planes. Values of the constants K and n in equation 9.11	113
9.11	Snow ice (T1) Values of the constants K and n of equation (9.12) for different ranges of temperature-compensated creep rate.	115

LIST OF FIGURES		page
1.1	The bending and cracking of a floating ice cover due to a fast change of temperature in its upper surface.	2
1.2	Examples of expanding ice covers.	3
2.1	Schematic representation of the bonding and lone-pair orbitals in the water molecule.	8
2.2	A water dimer.	9
2.3	An ice-like water polymer.	9
2.4	Sketch of a part of an ice lattice showing the tetrahedral bond arrangement.	10
2.5	A "vertical" strip of tetrahedrons within an ice lattice. The direction perpendicular to the basal planes is called the c-axis.	10
2.6	A basal plane of ice.	11
2.7	A cut along the c-axis across two basal planes in an ice lattice.	12
2.8	A simplified model of a hexagonal prism unit and the process of plastic deformation under shear.	12
2.9	Simple types of dislocations.	14
2.10	A vertical section through columnar ice with drawn crystal boundaries. As some crystals with favourable crystal-axis orientation encroach on others there are fewer but courser crystals at the underside of the ice cover.	16
2.11	Preferred growth of crystals with inclined optic axes, resulting in gradual extinction of a vertically oriented crystal.	19
2.12	Some typical forms of snowflakes.	23
2.13	A vertical section through an ice cover before and after water has leaked onto it.	25
2.14	Examples of the growth and decay of lake ice covers.	26
2.16	The temperature of maximum density and the "freezing-point" temperature as functions of salinity.	29
2.17	Sections through columnar sea ice showing brine pockets at two different temperatures.	32

2.18	"Freezing-point curve" of sea-water brine showing the concentration of brine in equilibrium with ice versus temperature. The various solid salts are listed opposite the segment of the curve in which they are the dominant salt crystallizing.	34
2.19	Brine migration along the temperature gradient.	36
2.20	Phase relations, by volume, of sea ice of four typical salinities.	36
2.21	An idealized diagram of the shape of the brine inclusions in columnar sea ice and NaCl ice.	39
3.1	Compact density as a function of temperature for fresh-water ice.	42
3.2	The density of the snow cover in the winter of 1915/16, at Gåsbornshyttan and Gimo.	45
3.3	Mean course of density of snow cover in the winters of 1909/10 - 1917/18.	45
3.4	A comparison of the density of columnar sea ice with the salinity 20 ‰ as a function of temperature according to the relations in this chapter, and according to Anderson (1960) and Schwerdtfeger (1963).	48
3.5	The density of columnar sea ice without air inclusions as a function of temperature for different salinities.	49
3.6	Plots of density and of salinity as a function of depth. Annual sea ice in Hudson Bay near Churchill, Manitoba.	50
3.7	Coefficient of volume expansion versus temperature for three salinities for void free sea ice.	51
4.1	Thermal conductivity of ice as a function of temperature according to different authors.	53
4.2	The conductivity of porous fresh-water ice as a function of air content at 0°C.	54
4.3	Models of columnar sea ice to be used for calculating thermal conductivity in the vertical direction.	55
4.4	The bulk conductivity of columnar sea ice as a function of temperature for different salinities and air contents.	57
4.6	The thermal conductivity of snow as functions of its bulk density.	60
4.7	The "relative" conductivity of Anisimov in per cent.	61
5.1	The specific heat capacity of sea ice as a function of salinity and temperature.	65

5.2	The deficit of heat (negative enthalpy) of sea ice relative to its freezing point as a function of temperature for the salinities 3 and 20 ‰.	67
6.1	The temperature diffusivity of fresh-water ice as a function of temperature.	70
6.2	The temperature diffusivity of porous fresh-water ice as a function of its air content at 0°C.	71
6.3	The temperature diffusivity of columnar sea ice in the vertical direction as functions of temperature for the salinities 0.3 and 20 ‰.	72
6.4	The temperature diffusivity of snow as a function of its bulk density according to the relations for thermal conductivity of Abel, Bracht and Deveaux.	73
7.1	Spectra for solar and sky radiation at clear sky. Black-body radiation for 6000K and 270K.	78
7.2	Refraction of light.	80
7.3	The spherical and ellipsoidal vector surfaces for an optically uniaxial and positive crystal. The difference between the surfaces is exaggerated.	81
7.4	The reflection coefficient of a polished flawless ice surface at -3°C and $\lambda = 0.5 \mu\text{m}$.	84
7.5	Field measurements of reflection coefficient of snow.	86
7.7	Reflexion, refraction, scattering, and transmission of a beam of light in an ice cover.	88
7.8	Spectral curves of the ratio of transmitted light for samples of ice 2 cm thick.	89
7.9	Infrared absorption spectrum of ice in the range $1.4 \mu\text{m} \leq \lambda \leq 4 \mu\text{m}$.	90
7.10	Summary of results from Mellor's (1965) attenuation experiments.	91
8.1	Radiation fluxes on Feb. 28, 1962, clear day. Measured by Schwerdtfeger and Pounder (1963) on the ice of Hudson Bay (58°49' N, 94°14' W).	96
8.2	Temperatures in ice covers free from snow.	98
8.3	The temperature in a 0.10 m thick ice cover.	99
9.1	Dependence of properties of ice on its structure.	100

9.2	An idealized deformation-time curve for instantaneous loading and unloading of an ice sample.	102
9.3	A composite rheological model of ice.	103
9.4	A nonlinear rheological model of ice.	105
9.5	Typical creep curve in tension depicting three stages of creep using a constant load but at different temperatures.	109
9.6	Compression creep curves conditions obtained under constant strain rate.	110
9.7	Schematic diagrams representing types of bending of single crystals of ice under stress.	112
9.8	The deformation of two monocrystals with different orientation of crystal axes.	113
9.12	Temperature compensated creep rate as a function of the applied stress.	116
9.13	Hypothetical stress distributions in an ice specimen: b) during loading and c) shortly after unloading.	119
9.14	Causes of differences in compressive and tensile strength of ice.	124
9.15	Compressive strength of snow ice under increasing strain rates at -10°C .	124
9.16	Average ring tensile stress versus square root of the average brine volume, NaCl-ice.	129
9.17	An idealized diagram of the shape of the brine inclusions in columnar sea ice and NaCl-ice.	130
9.18	The compression of an ice specimen in G-axis direction. Vertical section through unit piece of the specimen.	132
9.19	A further simplification of the diagram of sea ice for the purpose of calculating its modulus of elasticity.	133
9.20	Dynamic modulus of sea ice versus brine.	136
9.21	The viscosity modulus of sea ice as a function of brine volume.	138

LIST OF NOTATIONS

A	coefficient of heat transfer	$W/(m^2 \cdot K)$
A	constants	
A_b	relative cross-sectional area of brine	--
A_i	relative cross-sectional area of ice	--
a	constants	
a	coefficient of thermal diffusion	m^2/s
$a(\theta)$ for compact ice	m^2/s
$a(\theta, \nu)$ for ice with air inclusions	m^2/s
$a(\theta, S)$ for saline ice	m^2/s
a	length of hydrogen bond in ice crystal	m
a_o	spacing of brine layers	m
a_s	bulk coefficient of thermal diffusion for snow	m^2/s
a_w	mass content of water vapour per unit volume of air	kg/m^3
B	horizontal direction along a basal plane	--
B	Bowen's ratio	--
b	Burger's vector	m
b	constants	
b	horizontal distance between two brine voids in the same layer	m
b_o	horizontal spacing between brine voids in the same layer	m
C	c-axis direction	--
$C(\theta, S)$	specific heat capacity of saline ice	$J/(kg \cdot K)$
C_i	specific heat capacity of ice	$J/(kg \cdot K)$
C_o	specific heat capacity of ice at $0^\circ C$	$J/(kg \cdot K)$
C_p	specific heat capacity (enthalpy)	$J/(kg \cdot K)$
C_s	cloudiness of the sky in eighths (octas)	--

C_w	specific heat capacity of water	J/(kg·K)
c, c_1, c_2	constants	
c	velocity of ordinary wave	m/s
c_e	velocity of extraordinary wave	m/s
c_o	speed of light in empty space	m/s
c_1, c_2	speed of light in different materials	m/s
D	coefficient of diffusion of gas or the molecules in ice	m ² /s
D_o	constant	m ² /s
d	differential operator	--
d	constants	
d	sample diameter	m
d_{cr}	crystal size, grain diameter	m
E	modulus of elasticity, static modulus of elasticity, bulk elasticity of saline ice	Pa
E_b	elastic modulus in bending	Pa
E_b	elastic modulus of brine layer	Pa
E_c	elastic modulus in compression	Pa
E_h	bulk modulus of sea ice for horizontal deformation	Pa
E_t	elastic modulus in tension	Pa
E_1	dynamic elasticity of pure ice	Pa
E_2	modulus of delayed elasticity	Pa
e_a	humidity, water vapour pressure	Pa
F	horizontal cross-sectional area of a brine void	m ²
F_g	vertical cross-sectional area of a brine void	m ²
$f(u)$	wind-speed function	m/s
$f(\sigma)$	creep function	s ⁻¹
G	vertical direction	--
g	vertical length of brine voids	m

g_o	vertical spacing between brine voids	m
h	thickness of ice cover	m
J	irradiation flux, solar irradiation	W/m^2
$J(t)$	creep compliance	Pa^{-1}
J_o	intensity of refracted radiation at $z=0$	W/m^2
J_z	intensity of radiation at depth z	W/m^2
J_λ	emitted effect per unit area and unit band-width at wave length λ	W/m^2
K	coefficient for viscous deformation	m^{-2}
K	" "	$m^{-2} Pa^{-n}$
K	compressibility of brine	Pa^{-1}
k	absorption coefficient	m^{-1}
L	specific latent heat of sublimation	J/kg
L_i	specific latent heat of fusion of water	J/kg
L_S	released latent heat of formation of a unit mass of sea ice	J/kg
l_a	side of rectangular brine void section in C-direction	m
l_b	side of rectangular brine void section in B-direction	m
m_b	mass of brine to mass of system	--
m_{bo}	mass ratio of brine at closure of brine voids	--
m_i	mass of ice (H_2O) to mass of system	--
m_{io}	mass ratio of ice at closure of brine voids	--
m_p	mass of precipitated salts to mass of system	--
n	exponent for viscous deformation	--
n, n_1, n_2	refractive indices	--
n_e	refractive index for extraordinary wave	--
n_o	refractive index for the ordinary wave	--

n_o	original number of dislocations per unit area	m^{-2}
P	load, force	N
p	mass of precipitated salt divided by mass of solvent	--
p	pressure parameter, pressure in brine voids	Pa
p	effect source per unit volume	W/m^3
Q	heat deficit per unit mass (enthalpy)	J/kg
Q_c	activation energy for creep	J/mol
Q_s	activation energy for self diffusion	J/mol
q	mass rate of sublimation per unit volume	$kg/(s\ m^3)$
q	heat flow per unit area	W/m^2
q_b	intensity of long-wave back radiation	W/m^2
q_c	convective (sensible) heat flux	W/m^2
q_e	rate of heat per unit area used for evaporation	W/m^2
q_l	intensity of incoming long-wave radiation	W/m^2
q_m	rate of heat per unit area used to melting	W/m^2
q_s	net incoming short-wave radiation flux	W/m^2
q_t	rate of change of stored heat per unit area due to change of temperature	W/m^2
r	reflexion coefficient, albedo	--
r_a	characteristic radius of brine void	m
r_b	characteristic radius of brine void	m
R	the universal gas constant	$J/(mol \cdot K)$
S	salinity, mass of salt to mass of solution	--
S	cross-sectional area of specimen	--
S_a	salinity of ambient sea water	--
S_b	salinity of brine	--
s	salt ratio, mass of salt in solution to mass of solvent	--

s_b	salt ratio of brine	--
T, T_1, T_2, T_3	absolute temperature	K
T_a	absolute temperature of air	K
t	time coordinate, point of time	s
u	wind speed	m/s
V_b	volume fraction of brine	--
V_{bo}	volume fraction of brine for which the sea-ice strength is nil	--
V	volume fraction of ice	--
x	coordinate	m
$Y(t)$	relaxation modulus	Pa
z	depth in ice or snow cover	m
α	angle of incidence	rad, degrees
α	linear coefficient of thermal expansion	K^{-1}
$\alpha, \alpha_1, \alpha_2$	constants	
β	coefficient for the mass of hydrated water	--
β	angle of refraction	rad, degrees
β	rate of increase of dislocations	m^{-2}
γ	volume coefficient of thermal expansion	K^{-1}
γ	psycrometric constant	Pa/K
γ	surface energy	J/m^2
Δ	difference operator	--
ϵ	emissivity	--
ϵ	strain, deformation per unit length	--
ϵ_a	emissivity of the atmosphere (air)	--
$\epsilon(t)$	deformation as a function of time	--
$\epsilon_0, \epsilon_1, \epsilon_2$ ϵ_3, ϵ_4	diverse amounts of deformation	--
η	viscosity modulus of sea ice	Ns/m^2
η_1	viscosity modulus	Ns/m^2

η_2	viscosity modulus	Ns/m^2
θ	temperature	$^{\circ}\text{C}$
θ_a	air temperature	$^{\circ}\text{C}$
θ_f	freezing point	$^{\circ}\text{C}$
θ_m	melting point	$^{\circ}\text{C}$
λ	specific thermal conductivity	$\text{W}/(\text{m}\cdot\text{K})$
λ	wave-length	m
$\lambda(\theta)$	conductivity of pure ice	$\text{W}/(\text{m}\cdot\text{K})$
$\lambda(\theta, S)$	conductivity of saline ice with air inclusions	$\text{W}/(\text{m}\cdot\text{K})$
$\lambda(\theta, \nu)$	conductivity of fresh-water ice with air inclusions	$\text{W}/(\text{m}\cdot\text{K})$
$\lambda(\theta, \nu, S)$	conductivity of saline ice with air inclusions	$\text{W}/(\text{m}\cdot\text{K})$
λ_o	$=\lambda(0^{\circ}\text{C})$ conductivity of ice at 0°C .	$\text{W}/(\text{m}\cdot\text{K})$
λ_a	thermal conductivity of air	$\text{W}/(\text{m}\cdot\text{K})$
λ_b	thermal conductivity of brine	$\text{W}/(\text{m}\cdot\text{K})$
λ_{max}	wave-length for maximum intensity of radiation	m
μ	imaginary part of the complex refractive index, extinction coefficient	--
ν	contents of air voids by volume	--
ν	Poisson's modulus	--
ξ	integration variable	$^{\circ}\text{C}$
ρ	density	kg/m^3
$\rho(\theta)$	compact density of ice	kg/m^3
$\rho(\theta, S)$	bulk density of saline ice without air inclusions	kg/m^3
$\rho(\theta, \nu)$	bulk density of fresh-water ice	kg/m^3
$\rho(\theta, S, \nu)$	bulk density of saline ice with air inclusions	kg/m^3
$\rho_b, \rho_b(\theta)$	density of brine at equilibrium temperature	kg/m^3

$\rho_i = \rho(\theta)$	compact density of ice	kg/m ³
ρ_p	density of precipitated salts	kg/m ³
ρ_s	bulk density of snow	kg/m ³
ρ_w	compact density of water	kg/m ³
$\rho_o = \rho(0^\circ\text{C})$	compact density of ice at 0°C	kg/m ³
σ	stress	Pa
σ	Stefan-Boltzmann's constant	W/(K ⁴ m ²)
$\sigma(t)$	stress as a function of time	Pa
σ_c	compressive strength	Pa
σ_f	strength of sea ice	Pa
σ_{max}	maximum yield strength of ice	Pa
σ_t	tensile strength	Pa
σ_o	strength of fictitious brine-free sea ice	Pa
σ_o	stress value	Pa
σ_1	stress in the ice phase	Pa
τ	integration help variable	s
τ_o	stress constant	Pa
ψ	plane porosity	--
∂	differential operator	--
\cdot	= $\partial/\partial t$ first derivative with respect to time	s ⁻¹
$\cdot\cdot$	= $\partial^2/\partial t^2$ second derivative with respect to time	s ⁻²

REFERENCES

- Ager, B. H:son, (1960): Studier över isförhållandena i Norrland, Dalarna och Värmland, Virkesavläggning på is. Statens Skogsforskningsinstitut, Avdelningen för arbetslära. Rapport 1960 Nr 10.
(Studies of the ice conditions in northern Dalecarlia and Värmland. The storing of timber on ice covers).
- Ager, B. H:son. (1963 a): Preparering av virkesavlägg på is. Skogshögskolan, Stockholm. 1963.
(Preparing places for the storage of timber on ice covers).
- Ager, B. H:son. (1963 b): Studies of the Density of Naturally and Artificially Formed Fresh-Water Ice. Journal of Glaciology, Vol. 1963, No. 32.
- Anderson, D.L. (1960): The physical constants of sea ice. Research applied in industry. Vol. XIII, No. 8, London 1960.
- Anisimov, M.I. (1961): Approximativ värdering av formler för snöns värmeledningsförmåga. Meteorologija i gidrologija, No. 9, Moskva 1961.
(An approximate evaluation of formulae for the thermal conductivity of snow. Translated into Swedish by SMHI).
- Armstrong, T., Roberts, B. and Swithinbank, C. (1966): Illustrated Glossary of Snow and Ice. Scott Polar Research Institute, Special publication, Number 4, University Printing House, Cambridge 1966.
- Assur, A. : (1958): Composition of Sea Ice and its Tensile Strength. National Academy of Sciences, National Research Council, Publ. 598, "Arctic Sea Ice", USA 1958.
- Bader, H. and Kuroiwa, D. (1962): The Physics and Mechanics of Snow as a Material, CRREL, Cold Regions Science and Engineering II-B.
- The Baltic Ice Code (1959): Östersjökoden för isunderrättelser. SMHI, Meddelanden, Serie E, nr 10, P.A. Norstedt och Söner, Stockholm 1959.
- Bengtsson, L. (1976): Snowmelt Estimated from Energy Budget Studies. Nordic Hydrology, 7, 1976, pp 3-18.
- Bennington, K.O. (1963): Some Crystal Growth Features of Sea Ice. Journal of Glaciology, Vol. 4, 1963, No. 36.
- Bergdahl, L. (1978): Thermal Ice Pressure in Lake Ice Covers. Department of Hydraulics, Chalmers University of Technology, Report Series A:2.
- Bergdahl, L. and Wernersson, L. (1977): Calculated and Expected Thermal Ice Pressures in Five Swedish Lakes. Department of Hydraulics, Chalmers University of Technology, Report Series B:7.

- Bergen, J. D. (1975): A Possible Relation of Albedo to the Density and Grain Size of Natural Snow Cover. *Water Resources Research*, Vol. 11, No 5, Oct. 1975.
- Brill, R. (1957): Structure of Ice. Snow Ice and Permafrost Research Establishment. Report No 33, July 1957.
- Brunt, D. (1944): *Physical and dynamical meteorology*. Cambridge 1944.
- Butiagin, I. P. (1966): Hållfasthet hos is och istäcke (naturundersökningar från Sibiriens floder). Sibiriska forskningsinstitutet för energetik. Novosibirsk 1966.
(Strength of ice and ice cover, field studies from the rivers of Siberia. Sibirian research institute for energetics. Translated into Swedish by SMHI, 1969).
- Butkovich, T. R. (1954): Ultimate Strength of Ice. SIPRE Res. Rep. 11, 1954.
- Butkovich, T. R. (1955): Density of Single Crystals of Ice from a Temperate Glacier. *Journal of Glaciology*, Vol. 2, p 553, 1955.
- Butkovich, T. R. (1957): Linear Thermal Expansion of Ice. SIPRE Research Report 40 (1957), US Army, Wilmette, Illinois.
- Carter, D. (1970): Brittle Fracture of Snow Ice, IAHR Ice Symposium, Reykjavik 1970.
- Carter, D. (1972): Brittle Fracture of Polycrystalline Ice under Compressive Loadings. IAHR Ice and Its Action on Hydraulic Structures, Leningrad 1972.
- Cherepanov, N. V. and Kamyashnikova, A. V. (1971): Sizes and Shapes of Congealed Ice Crystals. In Yakovlev 1971, pp 170.
- Cox, G. F. N. and Weeks, W. (1973): Salinity Variations in Sea Ice, Research Report 310, CRREL, Hannover, New Hampshire, 1973.
- Dietrich, G. and Kalle, K. (1967): *General Oceanography*, John Wiley and Sons Inc., New York 1967.
- Dorsey, N. E. (1940): *Properties of Ordinary Water-Substance*, New York: Reinhold Publishing Corp. 1940.
- Drouin, M. and Michel, B. (1971): Les poussées d'origine thermique exercées par les couverts de glace sur les structures hydrauliques. Rapport S-23 Génie Civil, Université Laval, Quebec 1971.
- Flügge, W. (1975): *Viscoelasticity*, Springer-Verlag, New York 1975.
- Frankenstein and Garner, (1967): Linear Relationship of Brine Volume and Temperature from -0.5 -- 22.9°C for Sea Ice. *Journal of Glaciology*, Vol. 6, No. 48, p 943-944.

- Fremling, S.(a): Grundläggande erfarenheter om is i sjöar och älvar. SMHI. Stencil. Stockholm. (Fundamental experience of ice in lakes and rivers).
- Fremling, S. (1968): Om istillväxt och isbärighet på sjöar. Föredrag vid SFM studiedagar i Arvidsjaur 1968-03-08. SMHI, HBI. (On the growth of ice and the carrying capacity of ice covers on lakes. A lecture in Arvidsjaur, March 8, 1968).
- Fremling, S. (1975): Nordic Ice Terms, Draft to Nordic IHD 1975. Continued under IHP, Stockholm.
- Frolov, A.D. and Slesarenko, Y.E. (1972): Characteristics of Elasticity of Sea Ice of Different Compositions. IAHR. Ice Symposium Leningrad 1972.
- Gaitskhoki, B.Y. (1970 a): Spectral Transmission of Snow and Some Ice Varieties. In Bogorodskij (1970).
- Gaitskhoki, B.Y. (1970 b): A Photometric Model of the Snow-Ice Cover. In Bogorodskij (1970).
- Glen, J.W. and Stephens, R.W.B. (1958): The Mechanical Properties of Ice. The Plastic Properties of Ice Advances in Physics. Vol. VII, No 25-28. London 1958.
- Gold, L.W. (1958): Some Observations on the Dependence of Strain on Stress for Ice. Canadian J. of Physics, Vol. 36, No 10, Oct 1958.
- Gold, L.W. (1958): Influence of Snow Cover on Heat Flow from the Ground. Some Observations Made in Ottawa Area. NRC of Canada Res. Paper No 63 of the Division of Building Research.
- Gold, L.W. (1965): The Initial Creep of Columnar-Grained Ice. Canadian J. of Physics. Vol 43 1965.
- Gold, L.W. (1968): Elastic and Strength Properties of Fresh-Water Ice. Ice Pressure against Structures. National Research Council (of Canada). Technical Memorandum No 92, Ottawa 1968.
- Gold, L.W. (1977): Engineering Properties of Fresh-Water Ice. J. of Glaciology, Vol. 19, No. 81.
- Harvey, H.W. (1966): The Chemistry and Fertility of Sea Waters, Cambridge University Press, London 1966.
- Hirayama, K., Schwarz, J. and Wu, H.C. (1973): Model Technique for the Investigation of Ice Forces on Structures. 2nd International Conference on Port and Ocean Engineering under Arctic Conditions, Reykjavik 1973.
- Hobbs, Peter V. (1974): Ice Physics, Clarendon Press, Oxford 1974.
- Janson, L.-E. (1963): Frost Penetration in Sandy Soil. Elanders Boktryckeri AB. Göteborg 1963.

- Johnson, P. R. (1972): The Modulus of Elasticity of Sea Ice Shown by Direct Tension and Compression Tests of Small Specimens. IAHR Symposium Ice and its action on hydraulic structures. Leningrad 1972.
- Jumppanen, P. (1973): Ice Thermal Loads against Walls of Water Reservoirs. 2nd Int. Conf. on Port and Ocean Engineering under Arctic Conditions. Reykjavik 1973.
- Kalle, K.: Fluchtentafeln zur Bestimmung der Dichte aus Salzgehalt und Temperatur des Meerwassers. Aus dem Archiv der Deutschen Seewarte etc. 60. Band Nr 2.
- Kalle, K. (1943): Der Stoffhaushalt des Meeres. Probleme der Kosmischen Physik Bd 23, Leipzig 1943.
- Kivisild, H. R. (1970): River and Lake Ice Terminology. IAHR. Ice Symposium, Reykjavik 1970.
- Knight, C. A. (1963): Studies of Arctic Lake Ice. Journal of Glaciology, Vol. 4 1963, No. 33.
- Krausz, A. S. (1968): Plastic Deformation of Fresh-Water Ice. In "Ice Pressure against Structures". National research council. Technical memorandum no. 92, Ottawa 1968.
- Lavrov, V. V. (1969): Deformation and Strength of Ice. Arctic and Antarctic Scientific Research Institute (Leningrad 1969), Israel Program for Scientific Translations, Jerusalem 1971.
- Lavrov, V. V. (1971): Scale Effect as an Indication of Ice-Breaking Mechanism. In Yakovlev 1971, pp 26.
- Lazier, S. S. and Metge, M. (1972): Observations on Thermal Cracks in Lake Ice. IAHR Ice Symposium, Leningrad 1972.
- Lewis, E. L. (1966): Heat Flow through Winter Ice. Conference on Low Temperature Science, Contribution, No. 62, Sapporo, Japan 1966.
- Lindgren, S. (1968): Istryck vid temperaturhöjningar. Institutionen för vattenbyggnad, KTH, Stockholm 1968. (Ice Pressure at Increases of Temperature).
- Lindgren, S. (1970): Thermal Ice Pressure, IAHR Ice Symposium, Reykjavik 1970.
- Liljequist, G. H. (1962): Meteorologi, Generalstabens litografiska anstalt, Stockholm.
- Lyons, J. B. and Stoiber, R. E. (1959 a): Crystallographic Orientation in Lake and Artificial Ice. Dartmouth College, Hanover, New Hampshire, 1959. Scientific Report No 2, Contract AF 19 (604) 2159.
- Lyons, J. B. and Stoiber, R. E. (1959 b): The Absorptivity of Ice, A Critical Review, Dartmouth College, Hanover, New Hampshire, Scientific Report No 3, Contract AF 19 (604) 2159.

- Lyons, J.B. and Stoiber, R.E. (1963): Orientation Fabrics in Lake Ice. *Journal of Glaciology*, Vol.4, 1963, No 33.
- Malmgren, F. (1927): On the Properties of Sea Ice. Norwegian North Polar Expedition with the "Maud" 1918-1925. Scientific Results, Vol 1, No 5, Bergen.
- Martinec, J. (1965): Snow Cover Density Changes in an Experimental Watershed. International Symposium on Scientific Aspects of Snow and Ice Avalanches. IUGG and IAHS, Davos 1965.
- Mellor, M. (1964): Properties of Snow. Report III-A1, Part III: Eng., Sect. A, Snow Engineering, C.R.R.E.L. 1964.
- Mellor, M. (1965): Some Optical Properties of Snow. International Symposium on Scientific Aspects of Snow and Ice Avalanches, Davos 1965. IUGG and IAHS.
- Mellor, M. (1977): Engineering Properties of Snow. *J. of Glaciology*, Vol. 19, No. 81
- Michel, B. and Ramseier, R.O. (1971): Classification of River and Lake Ice Based on Its Genesis, Structure and Texture. Département de Génie Civil, Section Mécanique des Glaces, Université Laval, Laval Canada.
- Muguruma, J. and Kikuchi, K. (1963): Lake Ice Investigations at Peter's Lake, Alaska. *J. of Glaciology*, Vol.4, 1963, No 36, sid. 689-708.
- Nilsson, B. (1971): Mätningar av snöns vertikala densitetsfördelning i Sverige. Nordic IHD, Report No 1, Lammi 1971. (Measurements of the Vertical Distribution of Snow Density in Sweden).
- Nord, M. and Taesler, R. (1973): Snötäcketets densitet och massa i Sverige. Byggeforskningen Rapport 21:1973. (The Density and Weight of the Snow Cover in Sweden).
- Ono, N. (1966): Specific Heat and Heat of Fusion of Sea Ice. Conference on Low Temperature Science, Contribution No 789, Sapporo, Japan 1966.
- Paily, P.P., Macagno, E.O. and Kennedy, J.F. (1974): Winter-Regime Surface Heat Loss from Heated streams. IAHR Report No 155, Institute of Hydraulic Research, University of Iowa, Iowa City, Iowa March 1974.

- Peyton, H.R. (1966): Sea Ice Strength, Geophysical Institute, University of Alaska, College, Alaska 99701.
- Perey and Pounder (1958): Crystal Orientation in Ice Sheets, Canadian Journal of Physics. Vol. 36, No 4, p 494-502.
- Peschanskii, I.S. (1971): Static Pressure of Sea Ice in Yakovlev 1971, pp 1-4.
- Pounder, E.R. (1965): The Physics of Ice. Pergamon Press 1965.
- Ramseier, R.O. (1967 a): Self-Diffusion of Tritium in Natural and Synthetic Ice Monocrystals. J. of Applied Physics, Vol. 38, No 6, USA 1967.
- Ramseier, R.O. (1967 b): Self-Diffusion in Ice Monocrystals, CRREL Research Report 232, Hanover, New Hampshire 1967.
- Ramseier, R.O. (1971): Mechanical Properties of Snow Ice. Proceedings the First International Conference on Port and Ocean Engineering under Arctic Conditions. NTH, Trondheim, Aug. 23-30 1971, POAC 1971.
- Ramseier, R.O. and Dickins, D.F. (1972): A New Approach to Field and Laboratory Tests of Tensile, Compressive and Flexural Strength of Polycrystalline Fresh Water Ice. IAHR Ice and its Action on Hydraulic Structures, Leningrad 1972.
- Schwarz, J. and Weeks, W.F. (1977): Engineering Properties of Sea Ice. J. of Glaciology, Vol. 19, No. 81.
- Schwerdtfeger, P. (1963): The Thermal Properties of Sea Ice. Journal of Glaciology, Vol. 4 1963, No. 36.
- Schwerdtfeger, P. and Pounder, E.R. (1963): Energy Exchange through an Annual Sea Ice Cover. International Association of Scientific Hydrology, Pub. No 61, 109.
- Seligman (1936): Snow Structures and Ski Fields, Edinburgh 1936.
- Sellers, W.D. (1965): Physical Climatology. University of Chicago Press, Chicago och London 1965.
- Shumskii, A.B. (1955): Principes de Glaciologie Structurale. 1955. Translation Annales du Centre d'Etudes et de decum Paleontologiques. 22 okt. 1957.
- SMHI (1961): Översiktligt utlåtande angående inverkan på isförhållandena inom Torne- och Kalix älv av olika alternativ för vattenkraftens utbyggnad. Avgivet på uppdrag av övre Norrbygdens Vattendomstol. (General opinion on the influence on the ice conditions in the rivers Torne and Kalix because of different schemes for the exploitation of the water power).

- Sulakvelidze (1959): The Equation of Heat Conduction of Porous Media Containing Saturated Vapour, Water, and Ice. The geophysical series No 2. Izvezdia Akademii Nauk SSSR. Moscow 1959. Translated into Swedish by SMHI, Stockholm 1961.
- Sweers, H. E. (1976): A Nomogram to Estimate the Heat-Exchange Coefficient at the Air-Water Interface as a Function of Wind Speed and Temperature; A critical survey of some literature. Journal of Hydrology 30: 375-401.
- Tabata (1958): Studies on Mechanical Properties of Sea Ice II-V. Low Temperature Science Ser. A. Vol. 17 p 147-66. Vol. 18 p 116-48. Vol. 19 p 187-201. 1958-1960.
- Thomas, C. W. (1963): On the Transfer of Visible Radiation through Sea Ice and Snow. Journal of Glaciology. Vol. 4, No 34.
- Uzunur, M. S. and Kennedy, J. F. (1974): Hydraulics and Mechanics of River Ice Jams, IIHR, Report No 161, Iowa City 1974.
- Weeks, W. F. (1963): Tensile Strength of NaCl Ice. Journal of Glaciology, Vol. 4 1963, No 31.
- Weeks, W. och Assur, A. (1967): The Mechanical Properties of Sea Ice. US Army, Cold Regions Research and Engineering Laboratory II-C3, Hanover 1967.
- Weibull, W. (1939 a): A Statistical Theory of the Strength of Materials. Ingeniörsvetenskapsakademiens handlingar Nr 151, Stockholm 1939.
- Weibull, W. (1939 b): The Phenomenon of Rupture in Solids. Ingeniörsvetenskapsakademiens handlingar Nr 153. Stockholm 1939.
- Williams, G. P. and Gold, L. W. (1958): Snow Density and Climate. NRC of Canada. Research Paper No. 60 of the Division of Building Research. Transactions Engineering Institute of Canada. Vol. 2 No 2, May 1958 p 91-94.
- WMO (1974): International Glossary of Hydrology, First Edition, UNESCO/WMO, WMO-No. 385-1974.
- WMO Sea-Ice Nomenclature (1970): Terminology, codes, and illustrated glossary. WMO - No. 259. TP. 145-1970. Secretariat of the World Meteorological Organization, Geneva, Switzerland.

Meddelanden

78. Cederwall, K.: Havet som recipient. Hydrodynamiska synpunkter.
Föredrag vid Sv. Havsforskningsföreningens årsmöte i Stockholm, mars 1975.
79. Sellgren, A.: Hydraulisk transport av fasta material i rör. 1975.
80. Andreasson, L. och Cederwall, K.: Rubbningar av grundvattenbalansen i urbana områden.
Hydrologisk konferens, Sarpsborg, 1975.
81. Cederwall, K.: Bräddning av avloppsvatten och effekten av utjämningsbassänger. "Världen, Vattnet och vi", Elmia 1975.
82. Cederwall, K.: Gross Parameter Solutions of Jets and Plumes. ASCE, HY5, May 1975.
83. Larsson, Sören och Lindquist, Per: Kalkning av försurade sjöar. Del I: Problembeskrivning samt utvärdering av kalkningen av Östra Nedsjön. Ex.arb. 1974:5.
84. Cederwall, K. och Svensson, T.: "Sediment flusing after dredging in tidal bays". 1975.
85. Göransson, C-G. och Svensson, T.: Strömkorsmätningar. Datorprogram för utvärdering inkl. korrektion för avdrift. Mars 1976.
86. Rahm, L. och Häggström, S.: Oskarshamns Kärnkraftverk. Modellstudier avseende kylvattenspridning vid framtida utbyggnad. Maj 1976. Del I Huvudrapport. Del II Bilagedel.
87. Sjöberg, A.: Beräkning av icke stationära flödesförlopp i reglerade vattendrag och dagvattensystem. Aug. 1976.

Slut på Meddelande-serien.

Institutionen för Vattenbyggnad

CHALMERS TEKNISKA HÖGSKOLA

Report Series A

- A:1 Bergdahl, L.: Physics of ice and snow as affects thermal pressure. 1977
- A:2 Bergdahl, L.: Thermal ice pressure in lake ice covers. 1978

Reports Series B

1. Bergdahl, L.: Beräkning av vågkrafter. 1977.
2. Arnell, V.: Studier av amerikansk dagvattenteknik. 1977.
3. Sellgren, A.: Hydraulic Hoisting of Crushed Ores. A feasibility study and pilot-plant investigation on coarse iron ore transportation by centrifugal pumps. 1977.
4. Ringesten, B.: Energi ur havsströmmar. 1977.
5. Sjöberg, A. och Asp, Th.: Brukar-anvisning för ROUTE-S. En matematisk modell för beräkning av icke-stationära flöden i floder och kanaler vid strömmande tillstånd. 1977.
6. Annual Report 76/77.
7. Bergdahl, L och Wernersson, L.: Calculated and Expected Thermal Ice Pressures in Five Swedish Lakes. 1977.
8. Göransson, C-G. och Svensson, T.: Drogue Tracking-Measuring Principles and Data Handling.
9. Göransson, C-G.: Mathematical Model of Sewage Discharge into confined, stratified Basins - Especially Fjords